



**THE EFFECTS OF BOAT MOORING SYSTEMS ON SQUID EGG BEDS DURING
SQUID FISHING**

by

VUTLHARI ABSALOM MALULEKE

Thesis submitted in fulfilment of the requirements for the degree

Master of Technology: Mechanical Engineering

in the Faculty of Engineering

at the Cape Peninsula University of Technology

Supervisor: Prof GJ Oliver

Co-supervisor: Prof MJ Roberts

Bellville

2017

CPUT copyright information

The dissertation/thesis may not be published either in part (in scholarly, scientific or technical journals), or as a whole (as a monograph), unless permission has been obtained from the University

DECLARATION

I, Vuthari Absalom Maluleke, declare that the contents of this dissertation/thesis represent my own unaided work, and that the dissertation/thesis has not previously been submitted for academic examination towards any qualification. Furthermore, it represents my own opinions and not necessarily those of the Cape Peninsula University of Technology.

Signed

Date

ABSTRACT

In South Africa, squid fishing vessels need to find and then anchor above benthic squid egg beds to effect viable catches. However, waves acting on the vessel produce a dynamic response on the anchor line. These oscillatory motions produce impact forces of the chain striking the seabed. It is hypothesised that this causes damage to the squid egg bed beneath the vessels. Different mooring systems may cause more or less damage and this is what is investigated in this research. The effect of vessel mooring lines impact on the seabed during squid fishing is investigated using a specialised hydrodynamic tool commercial package *ANSYS AQWA* models.

This study analysed the single-point versus the two-point mooring system's impact on the seabed. The *ANSYS AQWA* models were developed for both mooring systems under the influence of the wave and current loads using the 14 and 22 m vessels anchored with various chain sizes. The effect of various wave conditions was investigated as well as the analysis of three mooring line configurations.

The mooring chain contact pressure on the seabed is investigated beyond what is output from *ANSYS AQWA* using *ABAQUS* finite element analysis. The real-world velocity of the mooring chain underwater was obtained using video analysis. The *ABAQUS* model was built by varying chain sizes at different impact velocities. The impact pressure and force due to this velocity was related to mooring line impact velocity on the seabed in *ANSYS AQWA*.

Results show the maximum impact pressure of 191 MPa when the 20 mm diameter chain impacts the seabed at the velocity of 8 m/s from video analysis. It was found that the mooring chain impact pressure on the seabed increased with an increase in the velocity of impact and chain size.

The *ANSYS AQWA* impact pressure on the seabed was found to be 170.86 MPa at the impact velocity of 6.4 m/s. The two-point mooring system was found to double the seabed mooring chain contact length compared to the single-point mooring system. Both mooring systems showed that the 14 m vessel mooring line causes the least seabed footprint compared to the 22 m vessel.

ACKNOWLEDGEMENTS

I wish to thank:

- Professor Graeme J. Oliver, Cape Peninsula University of Technology for his guidance throughout this research.
- Professor Michael J. Roberts for giving me an opportunity to do this project, his contribution and for making funds available.
- Bayworld Centre for Research and Education (BCRE) for financial and logistical support during my studies.
- South African Squid Management and Industrial Association (SASMIA) for financial assistance with the field research at Port Elizabeth.
- Cape Peninsula University of Technology for their financial contribution in support of my attendance to The 10th South African Conference on Computational and Applied Mechanics (SACAM).
- Mr Rob Cooper for his assistance and contribution.
- Dr Jean Githaiga-Mwicigi for assistance with the Port Elizabeth Trip.
- Dr Tamer Abdalrahman for his contribution on *ABAQUS* simulations.
- Mr Kevin Sack for his input on the whole project.
- Lastly, my friends and family. Thank you for believing in me and encouraging me every step of the way.

DEDICATION

This thesis is dedicated to my loving grandmother (Ndaheni Maria Chouke) who has been patiently waiting for me to finish my MTech.

TABLE OF CONTENTS

DECLARATION.....	ii
ABSTRACT.....	iii
ACKNOWLEDGEMENTS.....	iv
DEDICATION.....	v
LIST OF FIGURES.....	viii
LIST OF TABLES.....	xii
GLOSSARY.....	xiii
CHAPTER ONE.....	1
1. Project introduction.....	1
1.1. Introduction.....	1
1.2. Background of mooring systems.....	3
1.3. Typical fishing vessels on site.....	5
1.4. Problem statement.....	6
1.5. Aim and objectives.....	6
1.6. Research methodology overview.....	7
1.7. Dissertation structure.....	8
CHAPTER TWO.....	9
2. Literature review.....	9
2.1. Mooring line impact on the seafloor studies.....	9
2.2. Mooring line analysis studies.....	17
2.3. Single-point and two-point mooring systems.....	23
CHAPTER THREE.....	24
3. Methods and mathematical formulations.....	24
3.1. ANSYS AQWA and ABAQUS introduction.....	24
3.1.1. ANSYS AQWA background.....	24
3.1.2. ABAQUS background.....	25
3.2. Mathematical formulations of the moored vessel.....	26
3.2.1. Governing equations of the chain mooring line in time-domain.....	26
3.2.2. Governing equations for the fishing vessel in time domain.....	32
3.3. Environmental loading.....	36
3.3.1. Description of waves.....	36
3.3.2. Currents.....	37
3.3.3. Winds.....	37
3.4. Underwater video analysis: Experimental.....	38
3.4.1. Tracker video analysis.....	38
CHAPTER FOUR.....	42
4. Results and discussions.....	42
4.1. ABAQUS model for the mooring chain impact on the seabed.....	44

4.1.1.	Geometry of the model.....	44
4.1.2.	Material property definition	45
4.1.3.	Mesh	46
4.1.4.	Contact	47
4.1.5.	Boundary Conditions and Loading	48
4.1.6.	Results.....	50
4.1.7.	Studless chain link seabed contact forces comparison with the slender rod method	65
4.2.	ANSYS AQWA model description and setup.....	68
4.2.1.	ANSYS AQWA simulation procedure description	68
4.2.2.	ANSYS AQWA model setup.....	75
4.3.	ANSYS AQWA model simulation results	79
4.3.1.	ANSYS AQWA model correlation with underwater chain velocity.....	79
4.3.2.	Effect of wave height and period on the 22 m single-point moored vessel...	83
4.3.3.	Mooring system results using three configurations.....	95
4.4.	Summary of results: ANSYS AQWA and ABAQUS models.....	116
4.4.1.	Single-point mooring system result overview.....	121
4.4.2.	Two-point mooring system result overview.....	123
	CHAPTER FIVE	127
5.	Conclusion	127
6.	Recommendations and future work	131
	REFERENCES.....	133
	APPENDIX/APPENDICES	139
	APPENDIX A: Chain specification data	140
	APPENDIX B: Steel and sand properties	141
	APPENDIX C: Vessel drawings.....	143
	APPENDIX D: Vessel hydrostatic results	145
	APPENDIX E: Studless chain drawings.....	147
	APPENDIX F: Calculations.....	149
	

LIST OF FIGURES

Figure 1.1: A chokka squid fishing vessel (a) anchored above an active egg bed (b) .	2
Figure 1.2: Schematic of the mooring system.....	3
Figure 1.3: Photographs of the anchor system used by squid fishing vessels.....	5
Figure 2.1: Photograph of a swing mooring showing typical damage caused by the mooring chain to the seagrass meadow	9
Figure 2.2: Schematic representation of a typical (A) ‘screw’ mooring system, (B) ‘swing’ mooring system and (C) ‘cyclone’ mooring system	11
Figure 2.3: Aerial photograph of the mooring area at Callala Bay showing characteristic round areas stripped of seagrass	12
Figure 2.4: Anchor arcs based on AIS (Automatic Identification System) vessel tracking data near the Port of Newcastle acquired from the Australian Maritime Safety Authority (AMSA)	13
Figure 2.5: Mean number of shoots uprooted/broken by the three anchor types (Hall in black; Danforth in grey; Folding grapnel in white)	15
Figure 2.6: Stud-Link (a) and Studless Chain (b).....	19
Figure 2.7: Diagram of large scale test setup	20
Figure 2.8: Suspended catenary mooring mount.....	21
Figure 2.9: Two-dimensional line configuration for forced oscillation tests.....	21
Figure 2.10: Mooring line touchdown points resulting in time-varying boundary condition.....	22
Figure 3.1: Modelling of a dynamic mooring line using a cable connection.....	27
Figure 3.2: Forces on a Cable Element	27
Figure 3.3: Local Tube Axis System	31
Figure 3.4: Vessel 6-DOF rotations and translations	33
Figure 3.5: Original underwater video image of the chain movement experiment	38
Figure 3.6: Underwater video analysis using Tracker	40
Figure 3.7: Discrete point vertical displacement	41
Figure 3.8: Discrete point underwater vertical velocity	41
Figure 4.1: CAD geometry of the 20 mm diameter chain	44
Figure 4.2: Seabed geometry	45
Figure 4.3: Single chain link meshed (stud link).....	46
Figure 4.4: Elastic foundation mesh	47
Figure 4.5: Linear and Quadratic Solid elements.....	47
Figure 4.6: Chain link and seabed contact surfaces	48
Figure 4.7: Chain-Seabed boundary conditions and loading.....	49

Figure 4.8: Chain velocity scatter plot.....	49
Figure 4.9: Chain velocity radar plot	50
Figure 4.10: Chain link-seabed contact stresses, pressures and forces at 1 m/s for the 20 mm diameter chain.....	51
Figure 4.11: Chain link-seabed contact stresses, pressures and forces at 3 m/s for the 20 mm diameter chain.....	52
Figure 4.12: Chain link-seabed contact stresses, pressures and forces at 5 m/s for the 20 mm diameter chain.....	52
Figure 4.13: Chain link-seabed contact stresses, pressures and forces at 6 m/s for the 20 mm diameter chain.....	53
Figure 4.14: Chain link-seabed contact stresses, pressures and forces at 8 m/s for the 20 mm diameter chain.....	53
Figure 4.15: Chain link-seabed contact stresses, pressures and forces at 10 m/s for the 20 mm diameter chain.....	54
Figure 4.16: Chain link-seabed contact stresses, pressures and forces at 1 m/s for the 16 mm diameter chain.....	55
Figure 4.17: Chain link-seabed contact stresses, pressures and forces at 3 m/s for the 16 mm diameter chain.....	56
Figure 4.18: Chain link-seabed contact stresses, pressures and forces at 5 m/s for the 16 mm diameter chain.....	56
Figure 4.19: Chain link-seabed contact stresses, pressures and forces at 6 m/s for the 16 mm diameter chain.....	57
Figure 4.20: Chain link-seabed contact stresses, pressures and forces at 8 m/s for the 16 mm diameter chain.....	57
Figure 4.21: Chain link-seabed contact stresses, pressures and forces at 10 m/s for the 16 mm diameter chain.....	58
Figure 4.22: Chain link-seabed contact stresses, pressures and forces at 1 m/s for the 14 mm diameter chain.....	59
Figure 4.23: Chain link-seabed contact stresses, pressures and forces at 3 m/s for the 14 mm <i>diameter chain</i>	60
Figure 4.24: Chain link-seabed contact stresses, pressures and forces at 5 m/s for the 14 mm diameter chain.....	60
Figure 4.25: Chain link-seabed contact stresses, pressures and forces at 6 m/s for the 14 mm diameter chain.....	61
Figure 4.26: Chain link-seabed contact stresses, pressures and forces at 8 m/s for the 14 mm diameter chain.....	61

Figure 4.27: Chain link-seabed contact stresses, pressures and forces at 10 m/s for the 14 mm diameter chain.....	62
Figure 4.28: Seabed contact forces by the 20 mm chain	63
Figure 4.29: Seabed contact forces by the 16 mm chain	64
Figure 4.30: Seabed contact forces by the 14 mm chain	64
Figure 4.31: Chain link-seabed contact forces (showing the 20, 16 and 14 mm chain links)	65
Figure 4.32: 36 mm diameter slender rod (a) 1 m long, (b) 0.12 m long	66
Figure 4.33: Contact pressure and force at 8 m/s on seabed using (a) & (b) 1 m rod, (c) & (d) 0.12 m rod and (e) & (f) studless chain link.....	67
Figure 4.34: ANSYS AQWA Hydrodynamic Simulation Procedure.....	68
Figure 4.35: ANSYS AQWA Workbench project schematic.....	69
Figure 4.36: Axes Systems.....	69
Figure 4.37: Fishing vessel cut at the waterline (vessel Lower Hull in yellow and Upper Hull in grey).....	70
Figure 4.38: Vessel centre of mass	71
Figure 4.39: Meshed vessel (22 m vessel)	72
Figure 4.40: Quadrilateral Panel element (QPPL)	72
Figure 4.41: Triangular Panel element (TPPL)	73
Figure 4.42: The DISC Element.....	73
Figure 4.43: The TUBE Element.....	74
Figure 4.44: Single-point moored 22 m vessel.....	75
Figure 4.45: Single-point moored 14 m vessel.....	76
Figure 4.46: Mooring line profile of the 22 m vessel single-point for 1200 s simulation duration.....	80
Figure 4.47: Mooring line profile of the 14 m vessel single-point for 1200 s simulation duration.....	81
Figure 4.48: ANSYS AQWA video analysis using <i>Tracker</i>	82
Figure 4.49: Mooring chain profile for 1 m and 7 s wave height and period	88
Figure 4.50: Mooring chain profile for 1 m and 10 s wave height and period	89
Figure 4.51: Mooring chain profile for 2 m and 7 s wave height and period	90
Figure 4.52: Mooring chain profile for 2 m and 10 s wave height and period	91
Figure 4.53: Mooring chain profile for 2.5 m and 7 s wave height and period	92
Figure 4.54: The effect of wave conditions on tension	93
Figure 4.55: The effect of wave conditions on chain laid length.....	94
Figure 4.56: The effect of wave conditions on anchor uplift forces.....	94

Figure 4.57: Configuration 1 - Single-point mooring system with anchor in line with waves and current (top view).....	95
Figure 4.58: Configuration 2 - Single-point mooring system with anchor at an angle with incoming waves and current, (a) top view & (b) isometric view	95
Figure 4.59: Configuration 3 - Two-point mooring system with 'V' shaped anchoring, (a) top view & (b) Isometric view.....	96
Figure 4.60: Horizontal displacements (X-direction) of the vessels in three configurations.....	101
Figure 4.61: Lateral displacements (Y-direction) of the vessels in three configurations	103
Figure 4.62: Vessel vertical displacements for all three configurations	105
Figure 4.63: Frequency distribution of the mooring chain laid length on the seabed for Configuration 1.....	106
Figure 4.64: Frequency distribution of the mooring chain laid length on the seabed for Configuration 2.....	107
Figure 4.65: Mooring chain laid length for all 3 configurations	108
Figure 4.66: Mooring chain laid length for all three configurations on the 22 m vessel	109
Figure 4.67: Tension time-history at Fairlead - Configuration 1 and 2.....	112
Figure 4.68: Tension time-history of the two-point mooring system – Configuration 3	114
Figure 4.69: Anchor uplift forces for the all three Configurations.....	115
Figure 4.70: Single-point moored 22 m vessel overview (Tension (a), Laid chain length on the seabed (b), Mooring chain-seabed contact forces (c) & Anchor uplift forces (d))	121
Figure 4.71: Single-point moored 14 m vessel overview (Tension (a), Laid chain length on the seabed (b), Mooring chain-seabed contact forces (c) & Anchor uplift forces (d))	122
Figure 4.72: Two-point moored 22 m vessel overview (Tension on Cable 1 (a) & 2(b), Laid chain length on the seabed on Cable 1 (c) & 2(d))	123
Figure 4.73: Two-point moored 22 m vessel overview (Mooring chain-seabed contact forces (a) and Anchor uplift forces on Cable 1 (b) & 2(c))	124
Figure 4.74: Two-point moored 14 m vessel overview (Tension on Cable 1 (a) & 2(b), Laid chain length on the seabed on Cable 1 (c) & 2(d))	125
Figure 4.75: Two-point moored 14 m vessel overview (Mooring chain-seabed contact forces (a) and Anchor uplift forces on Cable 1 (b) & 2(c))	126

LIST OF TABLES

Table 4.1: Description of various models used for mooring line analysis	43
Table 4.2: Steel chain properties of 20 mm chain	45
Table 4.3: Seabed soil properties	46
Table 4.4: Element types in ANSYS AQWA	72
Table 4.5: 22 m vessel properties.....	75
Table 4.6: Single-point mooring anchor coordinates for the 22 m vessel	76
Table 4.7: 14 m vessel properties.....	76
Table 4.8: Single-point mooring anchor coordinates for the 14 m vessel	76
Table 4.9: Mooring chains mechanical properties.....	77
Table 4.10: Ocean environment data	78
Table 4.11: Wave conditions used for motion correlation.....	82
Table 4.12: Effect of wave height and period results	83
Table 4.13: Seabed contact Pressure and Force due to various contact points velocities	84
Table 4.14: Single-point mooring with 'Anchor 2' coordinates for the 22 m vessel (anchor at angle)	96
Table 4.15: Single-point mooring with Anchor 2 coordinates on the 14 m vessel.....	96
Table 4.16: Two-point mooring anchor coordinates on the 22 m vessel	97
Table 4.17: Two-point mooring anchor coordinates on the 14 m vessel	97
Table 4.18: Result summary of the 22 m moored vessel	117
Table 4.19: Result summary of the 14 m moored vessel	118

GLOSSARY

Abbreviations

BCRE	- Bayworld Centre for Research and Education
FEA	- Finite Element Analysis
TD	-Time-Domain
FD	- Frequency-Domain
LMM	- Lumped Mass Method
PDEs	- Partial Differential Equation
ODEs	- Ordinary Differential Equations
FEM	- Finite Element Method

Symbols

A	: area
\mathbf{A}	: added mass matrix
\vec{a}_j	: acceleration of the cable at node j
\mathbf{B}	: added mass matrix
C_a	: added mass coefficient
C_d	: drag coefficient
C_m	: inertia coefficient
\mathbf{C}	: added mass matrix
D	: line diameter
ΔD_e	: diameter of the element
EA	: axial stiffness
\mathbf{F}_d	: drag force on the mooring line element
$\mathbf{F}_{Inertia}$: inertial force
$F_{Chain\ max\ tension}$: maximum tension force
$F_{Minimum\ break\ load}$: minimum breaking force of a chain
$F_{Chain\ link\ force}$: chain link impact force
F_y	: hydrodynamic force in the y-direction
F_z	: hydrodynamic force in the z-direction
\vec{F}	: hydrodynamic loads
\vec{F}_h	: element external hydrodynamic loading vectors per unit length
g	: gravitational constant
H	: wave height.

j	: node of an element (notation)
(j)	: element (notation)
\mathbf{K}	: impulse response functions
K_{xx}	: radius of gyration on xx plane
K_{yy}	: radius of gyration on yy plane
K_{zz}	: radius of gyration on zz plane
L_B	: laid length
M_y	: bending moment in in the y -direction
M_z	: bending moment in in the z -direction
m	: structural mass per unit length
m_a	: cable element added mass matrix
\mathbf{M}	: the inertia matrix
\vec{M}	: bending moment vector
\vec{P}_{bot}	: bottom location of the cable attachment point
\vec{P}_{top}	: top location of the cable attachment point
ρ	: sea water density
p	: hydrodynamic pressure
\vec{r}	: position vector with respect to the centre of gravity
\vec{q}	: distributed moment load
\vec{R}	: cable element position vector
S_j	: the unstretched cable length from the anchor point
ΔS_e	: length of the element
S_0	: mean wetted surface of the vessel
T_0	: peak period
T_1	: mean wave period
T	: mean wave period
\vec{T}	: tension force vector
\dot{u}	: fluid acceleration vector
u_f	: directional fluid particle velocity
u_s	: transverse directional structure velocity
u_{cj}	: current velocity along the j -th
u_{sj}	: structure motion velocity along the j -th
\vec{V}	: is the cable element shear force vector
V	: flow velocity

v_{impact}	: chain link velocity impact
\vec{X}	: vessel displacement vector in six degrees of freedom
$\vec{\dot{X}}$: the vessel velocity vector
$\vec{\ddot{X}}$: vessel acceleration vector
ω	: wave frequency
ϕ	: velocity potential
\vec{w}	: element weight
∇	: gradient "del"

CHAPTER ONE

1. Project introduction

1.1. Introduction

The South African chokka squid fishery is based in the Eastern Cape between Plettenberg Bay and Port Alfred, and is a major source of foreign revenue as the entire catch, on average some 8000 t, is exported to Europe. Squid fishing is considered as one of South Africa's most valuable fisheries. Most of the catch is exported generating approximately R500 000 000 in foreign revenue (Krusche et al., 2014). Despite South Africa's efforts and progress over the past decade to improve the state of its marine resources, significant challenges remain. A report by the World Wide Fund for Nature indicated that many of South Africa's inshore marine resources are overexploited and some have collapsed (World Wide Fund South Africa, 2011). Starting in 2012 the squid industry has consecutively experienced 3 of its least productive years for a 20-year period pushing the industry to the verge of collapse (Blignaut, 2012).

Observations by South African marine and coastal management departments have found that the collapse possibly correlates with a change in the squid boat mooring systems. The squid boats changed from a single-point mooring system to a two-point mooring system which is now considered the industry standard. Divers from the South African Department of Environmental Affairs have noticed an interaction between the mooring chain and squid eggs (MJ Roberts 2015, personal communication, 2 July).

Commercial squid fishing is only viable when the vessels are above spawning aggregations formed in the water column above egg beds on the seafloor (Figure 1.1 (b)). Egg beds comprise hundreds of thousands of translucent, slim and slimy egg capsules about 15 cm in length that are glued to the bottom substrate forming massive mats often spanning tens of meters. Hatching occurs about 3 weeks from spawning on average. Traditionally, the fishing vessels position themselves above an egg bed using a single-point mooring system with the anchor dropped upwind of the egg bed. A significant part of the chain lies on the seafloor over eggs.

The fleet comprises 138 vessels ranging between 11 and 22 m in length on average (Figure 1.1 (a)). Each vessel carries about 22 fishermen who land the squid using hand-held jigs on fishing line. This number excludes the number of crew who are not allowed to fish. Waves acting on the vessel set up dynamic behaviour in the mooring line which

rapidly lifts the chain off the seabed, dropping it back with considerable force on the bottom (Sarkar & Eatock Taylor, 2002), and possibly damaging squid eggs. As sea and wind conditions change daily, vessels regularly pick up anchor and relay the anchor chain. In 2010, a new 'double anchor system' (two-point mooring system) was introduced and used by about 10 vessels. This 'V' shaped anchor line configuration offers vessels greater position control over the egg beds but potentially doubles the impact of the chain on the eggs (MJ Roberts 2015, personal communication, 2 July).

In 2013, the chokka squid fishery crashed and has not fully recovered. Concern has been raised by both fisheries managers and boat owners that the chain impact - especially from the two-point mooring system (double anchor system) - maybe causing excessive damage to the squid eggs reducing recruitment.



Figure 1.1: A chokka squid fishing vessel (a) anchored above an active egg bed (b)

These egg masses can extend over an area as large as $10\,000\text{ m}^2$. This study is the first part of an investigation into the impact of anchor chains on the seabed; it focuses on the mechanical impact of the mooring chain system on the single and two-point mooring systems when the 14 and 22 m squid fishing vessels are analysed. The second part of the investigation is beyond the scope of this thesis, which will be done after the results from the first part of the investigation are available. The results are going to be used for studying the damage and consequences of the chain impact on the egg beds and hatching success. The numerical investigation of the behaviour of the mooring chain and seabed interaction in this thesis is performed using *ANSYS AQWA* software to obtain structural displacement, dynamic contact length and mooring forces in the time domain, and by *ABAQUS* finite element software to determine the impact forces on the seabed.

1.2. Background of mooring systems

Mooring lines are useful in securing a structure against environmental forces. The predominant environmental forces are the wind, current and wave. Ebbesen (2013) described the primary function of a mooring system as to impose the floater (boat or vessel) with a horizontal stiffness to limit its horizontal motion (Ebbesen, 2013). The design of a mooring system is such that it will resist the vessel movements and environmental forces (Chrolenko, 2013). This is achieved by the mooring systems' ability to provide the vessels' required restoring forces to maintain the equilibrium position when the environmental loads are exerted on it (Balzola, 1999).

A basic mooring system is made up of three components which are chain/rope, anchor, and a flotation device. The stiffness of the mooring system depends on the anchor holding capacity, anchor embedment depth and the seabed soil properties (Vineesh et al., 2014).

Figure 1.2 is an illustration of the mooring line anchoring system using a catenary chain. Catenary shape provides slackness for vessel horizontal excursions. The mooring line is made up of steel chain. The chain mooring line is designed to have a degree of slack which allows the anchor to be locked on the seabed. When the wave conditions become severe, the slack mooring line usually prevents the anchor from dragging on the seabed and reduces tension on the mooring chain. The slack mooring chain imposes high mooring line stiffness on the vessel by absorbing the energy generated and dissipates it.

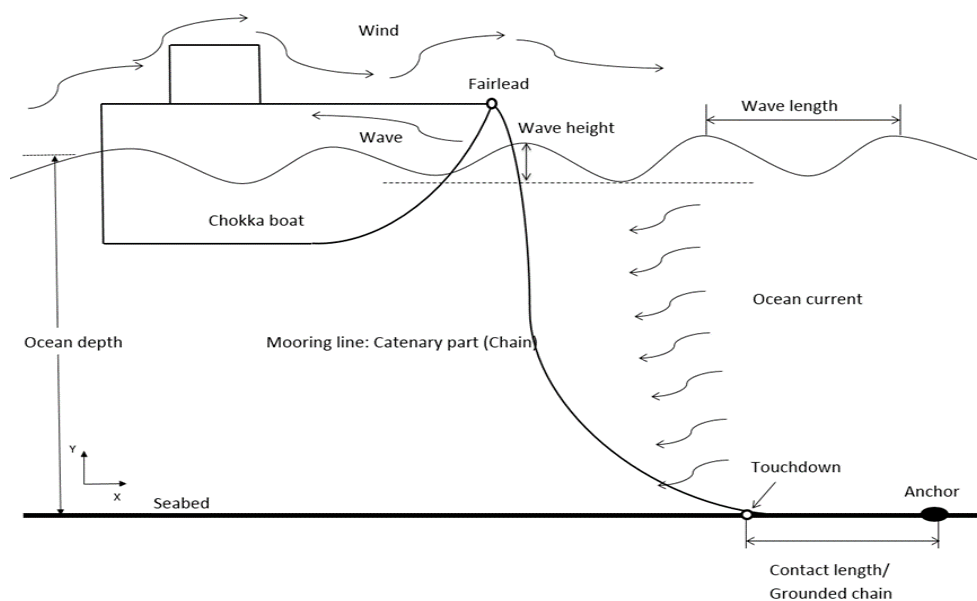


Figure 1.2: Schematic of the mooring system

The Klusman 100–250 kg anchor mass is mostly used by the squid fishery with about 80 – 160 m of chain length using 14 – 20 mm link diameter steel chain. Catenary moorings mainly use drag embedment anchor or the horizontal anchor. This anchor type can only resist horizontal loads (Miedema et al., 2006). The anchor is deployed for positioning the fishing vessel and pulled up either for re-deployment to a new location or when the vessel goes back to the harbour. The steel chain weight ranges between 4.36 and 10 kg/m. The chain is controlled by a winch on the vessel's foredeck that feeds chain through the fairlead on the vessel's bow. Two types of chain links are used - studless and studded.

The studded chain link is designed to prevent knot formation but is more susceptible to fatigue failure than the studless link (ABC Moorings, 2015). Note that the description of the studless and stud link chain is in section 2.2. In mechanics, the chain component is characterised by the catenary stiffness (effect), low elasticity, high non-breaking strength and mass. As shown in the previous figure, the mooring system is subjected to varying wind, waves and current, all of which introduce dynamic behaviour into the mooring line.

In Figure 1.2 shown, the part of the mooring line that lies on the seabed is termed grounded chain while that suspended in the water column is the catenary. The touchdown point is a position along the mooring where the chain begins lifting off the seabed. This point varies as a result of the dynamic sea conditions. Pellegrino and Ong, (2003) demonstrated that when the mooring chain is excited due to wave loading, the chain dynamically interacts with the seabed; which creates a boundary condition that varies in time and in space. The dynamic excitation causes a significant change in the mooring line's catenary profile resulting in part of the chain to lift off and drop back down on the seabed (Yu & Tan, 2006). This is illustrated in Figure 2.10 in Chapter 2 and can be modelled using a dynamic simulation which accounts for the application of loads on the system over time with the consideration of wave inertia forces and structural damping.

The mooring system's ability to provide a connection between the squid fishing vessel and the seafloor by means of an anchor chain enhances squid catches and thus plays an important role in the squid fishing industry. Ocean waves induce hydrodynamic loads on the squid fishing vessel. These excited wave forces acting on the vessel causes dynamic behaviour on the mooring chain which is anchored to the seafloor.

This is evident by the apparent unstable oscillatory motions of the mooring chain. When the above phenomena take place, a significant part of the chain lying on the seafloor lifts up and drops back down under dynamic conditions (Sarkar & Eatock Taylor, 2002). This phenomenon was also noticed by divers by from the South African Department of Environmental Affairs. This study will investigate and analyse the motion and the impact force of the mooring chain on the seabed (seafloor) on the single and two-point mooring systems.

1.3. Typical fishing vessels on site

To ensure that the problem is clearly understood, a site visit to Port Elizabeth was undertaken to gather practical information on the mooring systems. Figure 1.3 below shows varying inspections of the double (two-point) and single anchor (single-point) configurations.

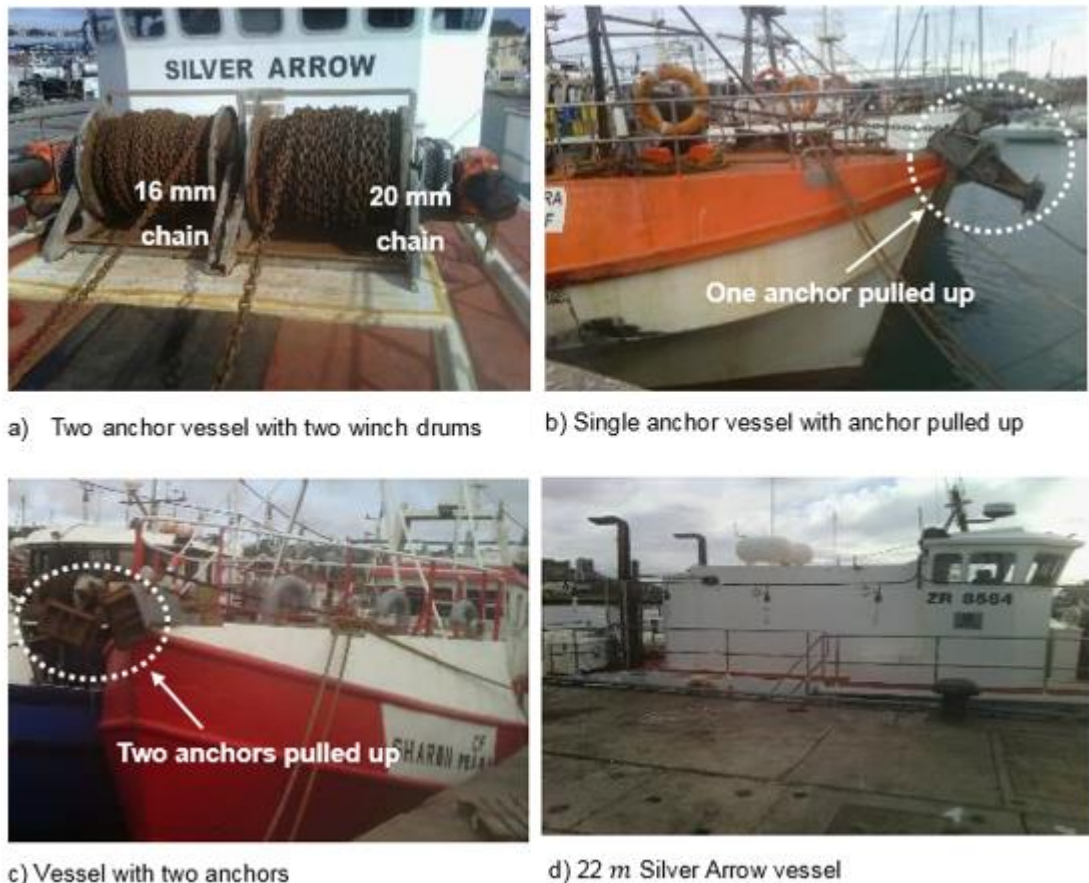


Figure 1.3: Photographs of the anchor system used by squid fishing vessels

Specific objectives of the site visit included:

1. Familiarity with the squid fishing vessels, anchor systems and anchor deployment methods.

2. To gather information on chain specifications (chain mass per unit length, chain length and diameter)
3. To obtain actual vessel dimensions (obtain vessel engineering drawings for accurate modelling and vessel mass)

The information on mooring systems obtained include:

1. The chain mooring line specifications are shown in Appendix A supplied by McKinnon Chain (PTY) LTD.
2. Vessels on-site are in the range of between 11 and 22 m.
3. The vessel operators or skippers provided enough information on the anchor deployment methods and conditions at sea.
4. Anchor deployment: the anchor is dropped below the bow of the vessel; when the anchor reaches the seabed, the anchor chain is then increased as the vessel moves away from the anchor position, as this happens. The anchor drags on the seabed until it is locked on the seabed.
5. The mooring chain length depends on the fishing depth and sea conditions.
6. Obtained vessel specific information. This consisted of knowing the steel chain sizes of 13, 14, 16 and 20 mm in diameter which are commonly used depending on the vessel size. The 20 mm chain is the heaviest of all the four chain sizes and is used to anchor a vessel when the sea conditions are harsh; while the 16 mm used in conjunction with the 20 mm for two-point mooring to provide more stability. The 20 mm and the 16 mm are commonly used in the squid fishing industry. The single anchor vessel either uses 20, 16, 14 or 13 mm chain based on the skippers' discretion.

1.4. Problem statement

We will investigate the effect of different mooring line systems and types in terms of potential impact on squid egg beds.

1.5. Aim and objectives

The aim of this study is to develop numerical models for predicting the behaviour and impact of the single-point versus the two-point mooring system. The predictions will then be used to investigate the likelihood of the anchor chains damaging the squid eggs.

The main objectives are divided into the following sections in order to develop numerical models to quantify the impact force of the mooring chain on the seabed –

- Numerical models will be used to simulate single-point mooring system versus the two-point mooring system using the 14 and the 22 m long vessels.
- The impact force and frequency of the chain on the seabed will be analysed and quantified.
- The models will be used to analyse the dynamic tension on the mooring line and determine which mooring system has the greatest tension.
- The numerical models will also be used to quantify this dynamic tension based on various ocean conditions which best represent the real-world motion of the mooring chain underwater and impact on the seabed.
- The numerical models will be validated by video footage analysis obtained of the mooring chain impacting the seabed at a considerable velocity.
- The numerical models will be setup using methodologies from related studies and analyses of a moored vessel at sea; software packages user and theory guides will also be used for ensuring correct model setup.

1.6. Research methodology overview

The following methods of investigation were used in undertaking this study:

- Hydrodynamic analysis – this is the moored vessel’s response in the ocean environment; numerical simulations were performed by using a specialised hydrodynamic analysis commercial package *ANSYS AQWA* for analysing the moored vessel response. This software enables the analysis of the interaction between the chain and the motion of a moored vessel under the influence of ocean environment forces i.e. wave and current forces.
- Finite element analysis – *ABAQUS* finite element analysis software was used to determine the seabed contact forces under varying mooring chain diameter and the impact velocity.
- Video analysis – *Tracker* software was used to analyse the video footage captured by marine divers when capturing the mooring chain motion impacting the seabed. Video analysis was performed for determining the mooring chain underwater velocity. The velocity was used for validating and calibrating the numerical models in *ANSYS AQWA* and *ABAQUS*.

1.7. Dissertation structure

Chapter 2 reviews relevant literature on the impacts of the mooring lines; it also presents common approaches used for solving the dynamics of a mooring line. Chapter 3 presents the background of the *ANSYS AQWA* and *ABAQUS* modelling tools. It also presents the governing equations and loads acting on the moored vessel. Lastly, it also presents underwater video analysis of a video footage captured by marine divers. Chapter 4 presents both *ABAQUS* and *ANSYS AQWA* results. A table is also provided which lists and describes all the subsequent analysis conducted in this study. Chapter 5 presents conclusions that can be drawn from this study and also provides recommendations as well highlights main software limitations.

CHAPTER TWO

2. Literature review

This chapter reviews the literature on mooring systems; it reviews studies on mooring line impact and the seabed interaction highlighting numerical and experimental models used.

2.1. Mooring line impact on the seafloor studies

Boat and buoy anchoring can have a negative impact on the seabed habitat through its three stages (1) anchor laydown to the seabed, (2) anchor drag on the seabed and (3) pulling the anchor chain from the seabed. When the anchor and chain drag on the seabed, the seagrass is then cut and pulled from the seabed (Collins et al., 2010). Swinging mooring chain has been observed to be scrapping the seabed leading to coarser seabed surface. This reduced the number of seagrass species growing in the Medina estuary, Cowes, England area that has been affected by the swinging mooring chain (Herbert et al., 2009).

A study near Perth of Western Australia found that boat chain mooring lines produce round patches in seagrass meadows of the range between 3 to 300 m² (see Figure 2.1) (Walker et al., 1989). The study found that “Cyclone” boat moorings which are characterised by three anchors and a swivel causes less damage to seagrass meadows than “Swing” mooring lines which are characterised by a single anchor and chain. It was found that the swing mooring system caused scoured area 10 times more than the cyclone mooring system. This resulted in the total loss of seagrass meadow due moorings to be about 5.4 hectares in Rottnest Island (Walker et al., 1989).



Figure 2.1: Photograph of a swing mooring showing typical damage caused by the mooring chain to the seagrass meadow

(Adapted from Walker et al., 1989)

Contrary to the latter study, Hastings et al. (1995) argued that “Cyclone” mooring lines caused more damage on the seagrass meadows than “Swing” mooring lines. Their study was conducted by comparing areal coverages obtained using aerial photography of seagrasses and sand patches within seagrass beds taken between 1941 and 1992.

Seagrass loss was found to be caused due to the change from single anchor swing mooring lines to cyclone mooring lines which used three chains. Cyclone mooring lines were found to have produced three circular patches in the seagrass bed, these holes caused 5 m radius round patches on the seafloor. Hastings et al. (1995) stated that the study by Walker et al. (1989) only investigated the condition of seagrass meadows observed in 1987 which neglected the rate at which seagrasses were lost due to boat mooring lines. The two studies compared above both agree that boat chain mooring systems cause damage to the seagrass meadows on the benthic ecosystem.

In addition to the study conducted by Hastings et al. (1995), the temporal decline of seagrass beds was associated with the damage caused by permanent chain mooring systems. The study showed a decrease in seagrass beds area and an increase in sand patch area on the seafloor in relation to mooring lines; these findings were obtained in a period between 1941 and 1992 in Rocky Bay and Thomson Bay, Rottnest Island, Western Australia. More seagrass damage was found in Rocky Bay with 18% of seagrass area lost between 1941 and 1992, and 13% between 1981 and 1992 (Hastings et al., 1995).

The conclusion from the study by Hastings et al. (1995) was that the decline of seagrasses in Rocky Bay corresponds with the doubling of boat moorings and an increase in boat size and traffic between 1981 and 1992. This loss of seagrasses was also as a result of the change from a single anchor swing mooring line to a cyclone mooring line with three chains. The study highlighted that the single weighed swing mooring lines cause the least damage when compared to cyclone mooring lines as it covers less seagrass area. Both the swing and cyclone mooring systems were found susceptible for seafloor abrasion – a phenomenon where the seafloor surface is swept by the mooring chain.

A similar study to Hastings et al. (1995) was conducted by Demers et al. (2013) in Callala Bay, Australia; the study compared a ‘seagrass-friendly’ screw mooring, cyclone mooring and a standard single anchor swing mooring line types. It was found that ‘Swing’ mooring lines produced substantial seabed scour, stripping seagrass

patches of about 18 m diameter; whereas cyclone moorings produced extensive stripped patches of about 36 m diameter on average. The screw mooring was found to cause less seagrass scour amongst the three types of moorings on the latter studies; this was noticed by finding a small circular scar around most 'screw' mooring systems. The cyclone mooring system was found to cause the most damage which agrees with findings from the study by Hastings et al. (1995). The three types of mooring mentioned above are illustrated in Figure 2.2 below.

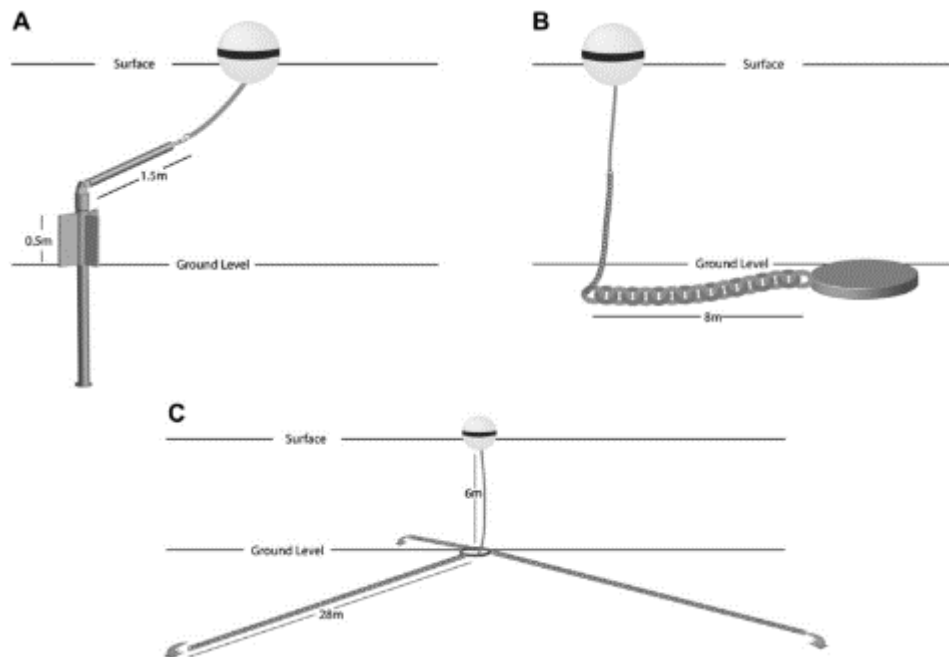


Figure 2.2: Schematic representation of a typical (A) 'screw' mooring system, (B) 'swing' mooring system and (C) 'cyclone' mooring system

(Adapted from (Hastings et al., 1995).

These studies by Walker et al. (1989), Hastings et al. (1995) and Demers et al. (2013) are all in agreement that the mechanical impact of boat mooring chains causes disturbance to seagrass meadows; this mechanical impact mostly produce stripped areas within seagrass meadows (Demers et al., 2013). The next Figure 2.3 shows distinctive round areas stripped of seagrass in Callala Bay mooring area obtained by an aerial photograph.



Figure 2.3: Aerial photograph of the mooring area at Callala Bay showing characteristic round areas stripped of seagrass

(Adapted from Demers et al., 2013)

Another study by Davis et al. (2016) was recently completed involving large vessels interaction with the marine environment with an emphasis on the impact of seafloor biota. The study investigated the impact of large vessels with the length of between 100 – 300 m and a single anchor chain link of about 60 – 200 kg. The study used a case study in South Eastern Australia to highlight the complex issues surrounding large vessel anchoring. The investigation involved exploring activities which interact with marine environments. The investigation placed an emphasis on the substantial ambiguity surrounding the impacts caused by large vessel anchoring on the seafloor organisms (Davis et al., 2016).

The outcomes from this study were that vessels at anchor pose a risk to the seafloor and its biota as a ship's anchor can shift, and its mooring chain swing across the seabed, causing abrasion of the seafloor and damage to the benthic ecosystems. The study stated that the mapping of the seafloor areas with high shipping activity can give more insight on which marine habitats may be at risk. This can be achieved by the use of remotely operated vehicles and cameras to compare marine life (fish and invertebrates) between the areas which are subject to heavy anchoring (Davis et al., 2016).

The next Figure 2.4 shows the impact of recreational and commercial vessels' mooring chains in shallow water environment of less than 50 m in depth (Davis et al., 2016). Automatic Identification System (AIS) was used to show vessels at anchor changing

positions due to changing current, wind and swell. The conditions at sea cause vessels to swing on their anchor chains. These changes in vessel position appeared as anchoring arcs.

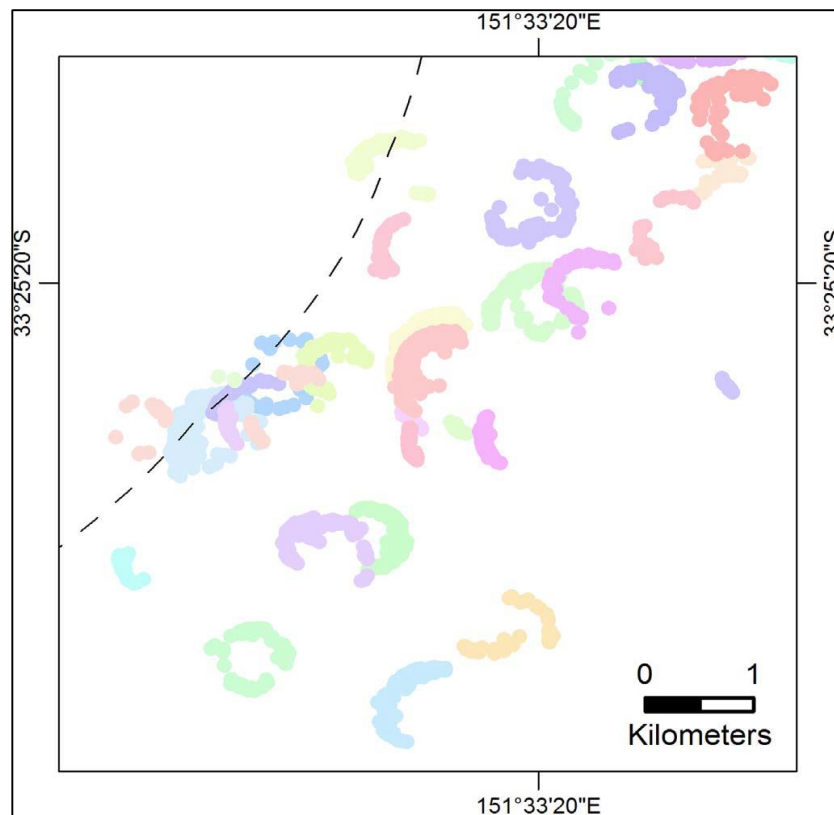


Figure 2.4: Anchor arcs based on AIS (Automatic Identification System) vessel tracking data near the Port of Newcastle acquired from the Australian Maritime Safety Authority (AMSA)

(Adapted from Davis et al., 2016)

A case study by Rajasuriya et al. (2013) investigated the effects of human-induced disturbances in Sri Lanka coral reefs. The study found that human activities such as sewage discharges, oil discharges, destructive fishing practices, land and mangrove destruction and tourism cause degradation of the coral reefs. Boat anchoring was found to be one of the human disturbance factors together with net fishing (Rajasuriya et al., 2013). Although boat moorings were found to cause damage to the coral reefs, however, the amount the damage was not quantified.

Milazzo et al., (2004) studied the effect of different anchor types in three anchoring stages on boats anchored on seagrass beds in a marine protected area. The study experimentally quantified the damage caused by boat anchoring by counting seagrass shoot density after the anchoring process. Various factors were tested to quantify the damage; these factors include the use of a chain or a rope, the use of different anchor types and the analysis of the three anchoring stages i.e. anchor laydown, anchor drag on the seabed and lock-in and anchor weighing. The pattern shown by each factor tested was checked for consistency in different locations of the seagrass meadows.

The mechanical destruction of seagrass species was attributed to human activities and boat moorings. Human activity impact was quantified to be on a large spatial scale from 1000 to 10 000 m, whereas on a smaller spatial scale, the seagrasses suffered from the chain mooring mechanical damage from the scale of 10 to 100 m. Human activities included sewage discharge, fish farming and construction of marinas. The mechanical damage mainly happens in coastal regions where frequent recreational activities takes place (Milazzo et al., 2004).

The findings from the study are summarised by the next Figure 2.5 which shows the number of shoots broken or uprooted caused by different anchor types on seagrass meadows. This figure clearly shows that more seagrass damage occurs during the 'weighing stage' whereby the anchor is pulled back to the vessel (Milazzo et al., 2004). During the weighing stage, the portion of the mooring chain lying on the seagrass bed drags on the seagrass bed before it is weighed causing abrasion to the seagrass meadows.

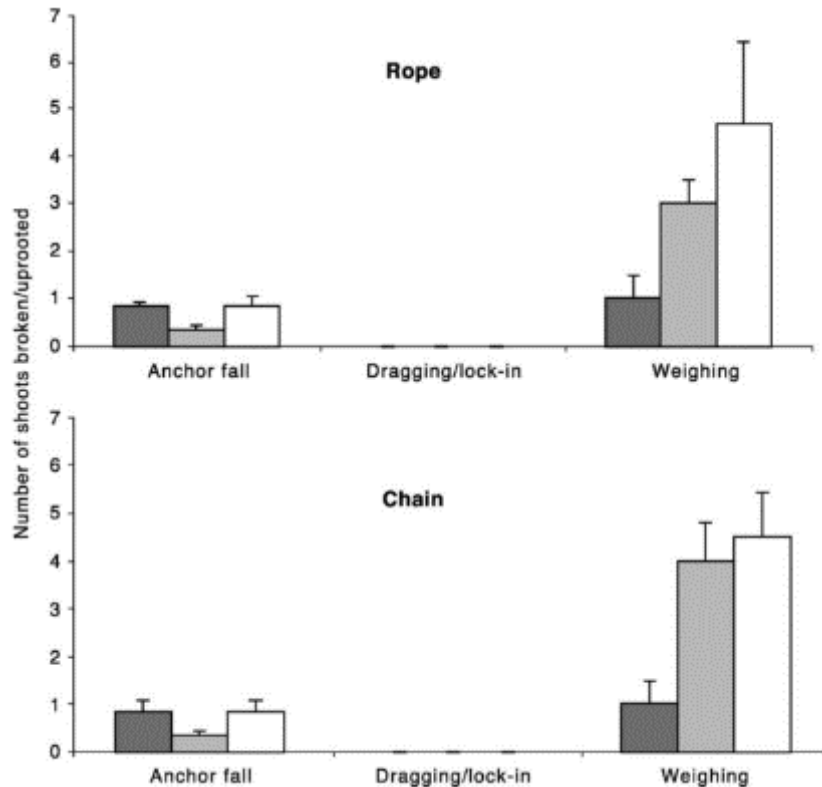


Figure 2.5: Mean number of shoots uprooted/broken by the three anchor types (Hall in black; Danforth in grey; Folding grapnel in white)

(Adapted from Milazzo et al., 2004)

Milazzo et al. (2004) also noticed that when studying boat moorings, more damage of seagrasses seemed to be caused by anchor drag which sweeps seagrass bed, during the forward and backwards motion of the boats (Milazzo et al., 2004). It should be noted that this study focused upon light anchor of 4 kg in mass and the boat of about 5.5 m in length; thus, results and conclusions made in this study are more likely to differ in regions where long vessels, with heavy anchors and chains are used. The study cited above clearly demonstrates that boat anchoring causes severe damage to seagrass beds due to the mechanical impact of the anchor chains.

Francour et al. (1999) “studied the direct effects of boat moorings on seagrass beds in the Port-Cros National Park”. The study revealed through field experiments 34 seagrass shoots destroyed on average during the boat anchoring process, especially when the seagrass mat compactness was weak. These experiments were carried in seven different sites; various factors which could have affected the number of uprooted

seagrass shoots were studied. They included the density of the root mat, the seagrass meadow density and the extent of rhizome exposure. The study noticed a clear direct effect of anchoring whereby 20 seagrass shoots were uprooted when the anchor digs into the seagrass bed. During the anchor weighing stage, 14 seagrass shoots on average were also observed to be uprooted whereby the anchor was retrieved to the boat with an electrical windlass (Francour et al., 1999).

Within the context of climate change, a study by Kininmonth et al. (2014) investigated the impact of anchor damage within the Great Barrier Reef World Heritage Area (GBRWHA) in Australia. The coral reefs and seagrass habitats were susceptible to human disturbances which included boat anchoring. This disturbance of the coral reefs seagrass habitats includes the anchor deployment, anchor retrieval and anchor chain-seabed interaction which potentially causes loss of the coral reefs and seagrasses (Kininmonth et al., 2014). Only 19% of approximately 20 000 km² GBRWHA was considered vulnerable to anchor damage. The study classified human activity such as anchoring as a small scale disturbance to the coral reefs and seagrasses. (Kininmonth et al., 2014).

In the study cited above, the assessment of the area exposed to anchor damage was found to be a challenging task due to the difficulty of the oceanic environment and the absence of real verifiable data. In GBRWHA five major ports, the deployment of the anchor and chain drag were found not to have a direct impact on coral reefs and seagrasses (Kininmonth et al., 2014).

It can be deduced from the literature cited above that large vessels seem to cause more damage on the seafloor than smaller vessels. This is because large vessels require heavy chain to be deployed for anchoring. In all cases studied here, the mooring chain caused considerable destruction to the benthic habitat in some regions, whereas in some regions no considerable destruction to the coral reef systems was found. Studies here suggest that more vessel activity is more likely to cause considerable damage to the benthic system. This view is also supported by Abadie et al. (2016) which states that severe boat anchoring in seagrass areas eventually leads to the destruction of seagrass meadows due to the mechanical damage of the anchoring process.

It is worth noting that this mechanical damage has various degrees of impact on seagrasses depending on the rate and type of the anchor used, as well as the depth of the sea and the boat size. The mechanical damage aforementioned also induce a

change in the nature of the seagrass substrate which generates round patches on the seabed (anthropogenic patches) (Abadie et al., 2016).

There seems to be no consensus on which fishing practices are seafloor “friendly” amongst boat/vessel owners as there is currently no boat anchoring standard during fishing. However, studies cited above indicate that mooring chains used for buoys and boats cause abrasion to the seafloor surface.

2.2. Mooring line analysis studies

Mooring line behaviour as a result of the wind, current and wave action, has received attention by numerous studies. For example, Sluijs & Blok (1977) first established a static analysis of mooring line forces; this was followed by a dynamic analysis which incorporated the dynamic effects such as inertia, dynamic loading, and geometric non-linearities and was solved mathematically by using finite difference method (Sluijs & Blok, 1977).

Masciola et al. (2014) outlined three approaches for solving dynamic mooring line behaviour - (1) line representation from the finite-element analysis (FEA), (2) finite-difference method (FD), and (3) lumped-mass (LM) method. These approaches can achieve similar results as long as an adequate fine discretisation is used; however, simplifications have to be introduced into these models in order to reduce computational cost which includes the omission of bending, torsion, and shear stiffness (Masciola et al., 2014). The fact that these approaches can yield similar results was established by Ketchman & Lou (1975) who demonstrated that LM approach gives the same results as FEA representations when a sufficient fine discretisation is used (Ketchman & Lou, 1975).

In alignment with these findings, Boom (1985) found that by assuming the mooring line to be composed of an intersected set of discrete elements, that the system of partial differential equations which is used to describe the variables along the mooring line can be replaced by the equation of motion. This was achieved by employing the lumped-mass and finite element methods. These methods were found to be more applicable in the general approaches of analysing various underwater systems such as chains and cable (Boom, 1985).

Ha (2011) describes the lumped-mass method as a continuous distribution of the mass mooring line where a discrete distribution of lumped masses is replaced by a finite

number of points. The replacement of mooring line mass leads to idealising the system as a set of non-mass linear springs and concentrated masses. Therefore, the line is idealised into a number of lumped masses connected by a massless elastic line taking drag and elastic stiffness into account (Ha, 2011). This “involves the grouping of all effects of mass, external forces and internal reactions at a finite number of nodes along the mooring line. A set of discrete equations of motion is derived from applying the equations of dynamic equilibrium and continuity (stress/strain) to each mass”. These equations are solved using finite difference techniques in time-domain (Boom, 1985).

The finite element method utilises interpolation functions to describe the behaviour of a given variable internal to the discretised mooring line element in terms of the displacements of the nodes defining the element. The equations of motions for a single element are obtained by applying the interpolation function to kinematic relations (strain or displacement), constitutive relations (strain or displacement) and the equations of dynamic equilibrium. The solution procedure of the finite element method is similar to the lumped-mass method (Boom, 1985); the study by Boom (1985) concluded that computer codes based on FEM were proven to be less computer time efficient when compared with the LM algorithms. The study then used the lumped-mass method to analyse the dynamic mooring line behaviour. The model was built with a special attention on the maximum mooring line tension. Results from the study were then validated from oscillation model tests.

Several models were developed using the FEM approach for analysing mooring line response to hydrodynamic forces. Vineesh et al. (2014) used the FEA approach for solving the dynamics of a buoy anchored by a mooring chain and a spar platform under wave, current and wind environmental forces using FEA package *ANSYS 10.0* (Vineesh et al., 2014), however, this study did not consider the mooring line interaction with the seabed.

Jameel et al. (2011) modelled mooring lines in *ABAQUS* as 3D tensioned beam elements. Hybrid beam elements were used to model the mooring line; these hybrid elements accounted for 6 DOF including displacements and axial tension as nodal degrees of freedom of the mooring line. The axial tension of the mooring was found to maintain the catenary’s shape. The choice of hybrid beam elements was due to their easy convergence; linear or nonlinear truss elements can also be implemented in the *ABAQUS* model, however, they have their own limitations (Jameel et al., 2011).

Yu & Tan (2006) developed an efficient 2D finite element model to numerically analyse the interaction of the mooring lines with the seabed. The model was developed in the time domain using *ABAQUS*. Hybrid beam elements and the Newton-Rhapson iteration procedure were implemented. The seabed was represented by using elastic and soil constitutive models; the coulomb model used the contact friction coefficient of 0.4. The hydrodynamic forces acting on the mooring line were simulated using the wave height of 3 m and period of 4 s for the simulation duration of 800 s.

The mooring line pretension was set to 36 kN and a vertical force of 3000 kN was applied at the fairlead point. One of the outcomes from the study was that, the environmental forces influence the mooring line predominantly on its longitudinal profile, while the transversal profile response can be ignored in the dynamic analysis (Yu & Tan, 2006). Kim (2003) also modelled the seafloor as an elastic foundation between the single-point chain mooring line and multi-body floating platform (Kim, 2003).

Yang (2007) conducted a “hydrodynamic analysis of mooring lines based on optical tracking experiments” using free and forced oscillation tests. These tests were implemented to verify the numerical results of moored body motion. Owing to the lack of experimental data available, the drag coefficients for chains were typically assumed to be the same as for a rod, but with an equivalent diameter equal to twice the bar size of the chain link. The study emphasised the difficulty of determining studless chain drag coefficients since the chain has a complex shape which complicates experiments.

Figure 2.6 below show an example of a stud and studless chain.

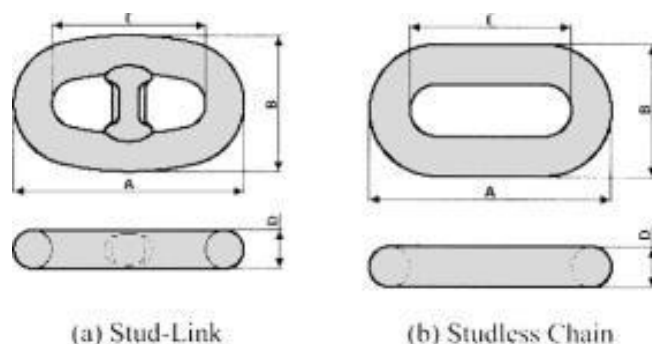


Figure 2.6: Stud-Link (a) and Studless Chain (b)

Since the chain comprises of interconnected links which have the shape of oval rings, the direct force measurement on the body (i.e. the chain link) using a force gauge is

difficult. The chain links are free to rotate at the interconnections to a certain extent, the torsional motion of the chain might be a consideration in the analysis even for small lengths of chain. Also, as compared to simple body shapes, the complex geometry of chain links causes more complex wake flow kinematics. For these reasons, predicting the hydrodynamic loading on moving chain is quite challenging (Yang, 2007).

The optical tracking experiments were conducted using a high-speed video camera which provided an opportunity for exploring the feasibility of deducing Morison drag and inertia coefficients from measured trajectories of chain and cable elements undergoing controlled free or forced oscillations in calm water (Yang, 2007). Figure 2.7 shows the setup of the large-scale optical testing experiment conducted in a 3D wave basin. The basin was 45 m long, 30 m wide and 6 m deep (Yang, 2007).

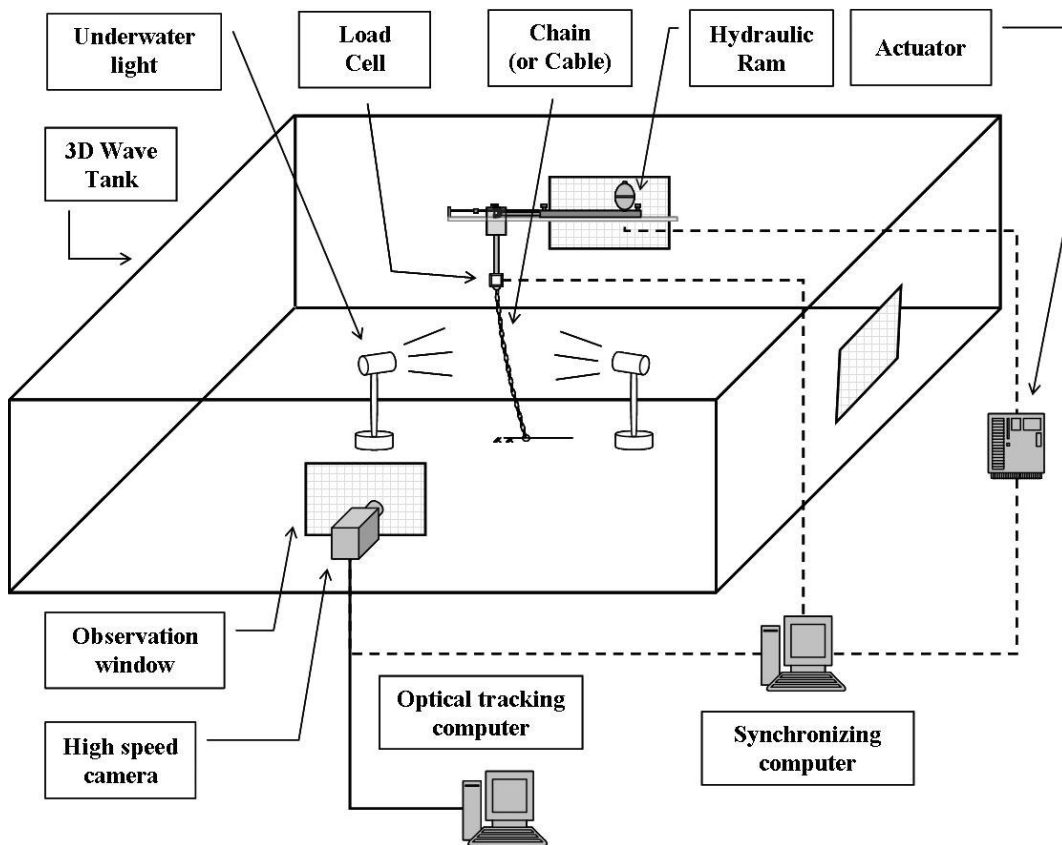


Figure 2.7: Diagram of large scale test setup

(Adapted from Yang, 2007)

The next Figure 2.8 below shows a suspended catenary mooring line with white markers for optical computer tracking. These experiments took place in a small 3D

wave basin whose sides were made of glass, which allowed direct measurement of line kinematics by optical tracking. The video footage recorded by the optical tracking camera was processed to extract time-histories of the position for all markers (Yang, 2007).

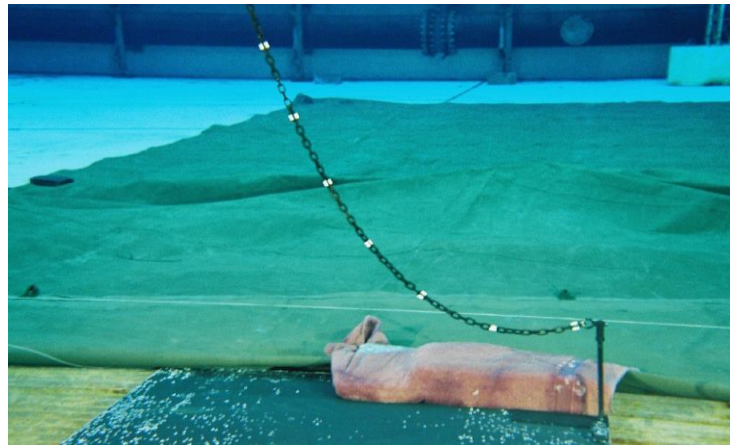


Figure 2.8: Suspended catenary mooring mount
(Adapted from Yang, 2007)

Figure 2.9 shows 2D mooring line configuration for forced oscillation tests for semi-taut catenary mooring.

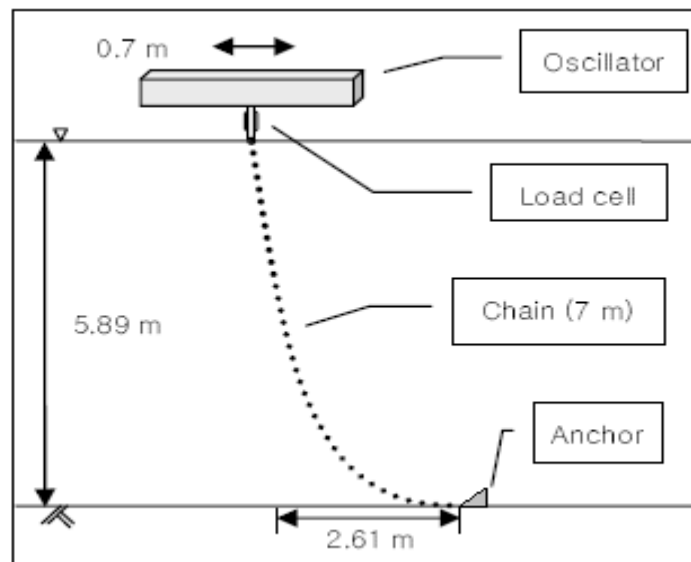


Figure 2.9: Two-dimensional line configuration for forced oscillation tests
(Adapted from Yang, 2007)

Wang et al. (2010) investigated the 3D interaction between the mooring chain and the seabed; they described the interaction between the chain and the seabed as a very complex process which has not been thoroughly understood yet (Wang et al., 2010). This interaction was found to cause a significant effect on the dynamic behaviour of the mooring chain. The interaction was as a result of the mooring chain excitation due to the action of wave loads. This interaction created a boundary condition that varied in time and in space (Pellegrino & Ong, 2003). The change in the mooring chain's longitudinal profile resulted in a significant amount of the chain length lying on the seafloor to lift off and drop back down; the amount of the mooring chain length dropping back on the seafloor varied with time (Yu & Tan, 2006). The following Figure 2.10 illustrates various touchdown points of the mooring line.

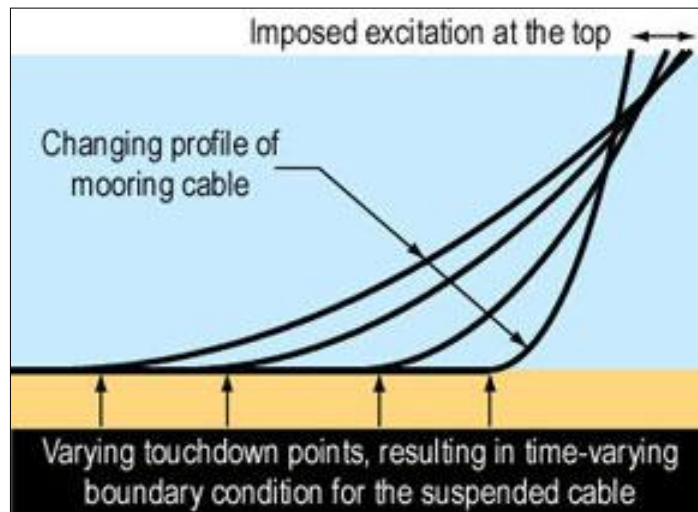


Figure 2.10: Mooring line touchdown points resulting in time-varying boundary condition

(Adapted from Pellegrino & Ong, 2003)

This problem can be solved in both frequency and time domain analysis. The frequency domain analysis approach was first presented by Pellegrino & Ong (2003) on modelling of seabed interaction of mooring cables (Yu & Tan, 2006). However, Frequency-domain analysis neglects the “non-linear hydrodynamic load effects and non-linear interaction effects between” the vessel, the mooring line and the seabed. Time-domain simulations are preferred since they best predict the mooring line dynamics, although they are time-consuming in nature and are mostly carried for about 3600 s (DNV, 2011).

2.3. Single-point and two-point mooring systems

As stated in the introduction, the “double anchor i.e. two-point mooring system, was introduced into the South African squid fishery. Currently, there is no available literature dedicated on the comparison of the single-point and two-point mooring systems used in the squid fishing industry between Plettenberg Bay and Port Alfred in Eastern Cape. The subsequent damage each mooring system type causes has not been quantified. However, studies reviewed in this thesis shows that the mooring chain interaction with the seafloor caused abrasion to the seafloor and its species.

As cited by Demers et al. (2013) single-point mooring systems are prone to dragging on the seabed causing a radial contact zone. However, the dynamic behaviour of a two-point mooring has not been given much attention by researchers. Two-point mooring systems require more deployment area than single-point mooring systems which can cause concerns for fishermen as each of their boats is competing for the limited resources. Single-point mooring system is easy to deploy and has less seabed footprint in general compared to the two-point mooring system.

CHAPTER THREE

3. Methods and mathematical formulations

This chapter describes the methods and theory of the research problem, the way this was modelled, and the software packages used to obtain the quantitative description of the behaviour of squid fishing vessel anchor lines.

3.1. ANSYS AQWA and ABAQUS introduction

Two primary numerical simulation programs have been used to investigate the dynamic response of the moored squid fishing vessels interaction with the seabed. The first is ANSYS AQWA which was used to model the wave and current forces acting on the moored vessel. The second is ABAQUS which was used for determining contact forces on the seabed *since ANSYS AQWA does not have this functionality*. The secondary software package used was *Tracker* which was used for analysing the acquired video footage from divers on analysis the motion of the chain underwater. This section gives the general background of ANSYS AQWA and ABAQUS software

3.1.1. ANSYS AQWA background

ANSYS AQWA has been used as the primary investigative tool in this project. It is a toolset used for investigating effects hydrodynamic loads on marine structures. It provides an environment for investigating the effects of the wave, wind and current loads on floating or fixed offshore structures. This includes ships, tension leg platforms (TLPs), semi-submersibles, renewable energy systems and breakwater design. ANSYS AQWA uses potential flow solver, the wave loads on a structure are calculated through a panel method which is based on potential flow theory (ANSYS AQWA, 2015).

ANSYS AQWA uses a Boundary Element Methods (BEM), or Panel Methods, or Boundary Integral Methods (BIM) to calculate the pressures and forces on the floating vessel. It can also conduct time-domain simulation with mooring lines attached to the vessel. When this is done, mooring line tension forces and vessel displacement in different wave conditions can be obtained.

ANSYS AQWA can simulate the wind, wave and current loading on the floating structure. This can be achieved by employing 3D radiation/diffraction theory and Morison's equation for slender structures in regular waves in the frequency or time-domain. The static and dynamic stability characteristics of the moored floating structure

under steady or unsteady environmental loads can be estimated (ANSYS AQWA, 2015).

The software simulates mooring, stability, vessel motions in regular and irregular waves within time and frequency-domain by solving the governing equations (Eder, 2012). This is achieved by using diffracting and non-diffracting panels; Morison elements (TUBE, STUB and DISC) are used for slender structures i.e. the mooring line etc. While Panel elements (QPPL and TPPL) are used for the rigid bodies i.e. the vessel hull, defined by point masses (PMAS), fenders, articulations and elastic catenaries.

ANSYS AQWA can generate time-history of the simulated motions of floating structures, arbitrarily connected by articulations or mooring lines, under the action of the wind, wave and current forces. The positions and velocities of the structures are determined at each time step by integrating the accelerations due to these forces in the time domain, using a two-stage predictor-corrector numerical integration scheme (ANSYS AQWA, 2015).

3.1.2. ABAQUS background

The ABAQUS software was used to simulate the contact between the chain mooring line and the seabed. This is a finite element numerical technique used to solve structural problems such as dynamic vibration problems, thermal connections and non-linear statics and contact problems. In the finite element model, the entire structure acts as a continuum. The model can handle all nonlinearities, loading and boundary conditions.

The finite element method utilises interpolation functions to describe the behaviour of a given variable internal to the discretised mooring line element in terms of the displacements of the nodes defining the element. The equations of motions for a single element are obtained by applying the interpolation function to kinematic relations (strain/displacement), constitutive relations (stress/displacement) and the equations of dynamic equilibrium (Allan, 2008).

ABAQUS provides an environment for pre-processing and post-processing the behaviour of the mooring line contact with the seabed in 2D and 3D.

3.2. Mathematical formulations of the moored vessel

This section presents the mathematical formulations of the chain mooring line and the fishing vessel when subjected to sea conditions. The equations of motion are used to achieve this objective; these equations are based on the basic Newton's second law of motion which provides a tool for studying the relationship of the response to the parameters governing that response. The equations of motion are modified in order to represent the time-dependent (dynamic) terms and the nonlinear behaviour of the vessel-mooring interaction.

3.2.1. Governing equations of the chain mooring line in time-domain

The nonlinear chain mooring line is represented by a catenary section in ANSYS AQWA; the catenary section is assumed to have a circular profile which is represented by a nonlinear dynamic catenary cable. The catenary section also allows the mooring line to be made up of different section properties. The cable which represents the mooring line is connected between the anchor and vessel Fairlead point. The dynamic response of the catenary cable is characterised by its large axial stiffness in the longitudinal direction compared to the lateral stiffness (transverse stiffness). When the catenary section data is defined, ANSYS AQWA internally converts all the mooring lines sections to a two-dimensional load/extension database with the maximum of 600 points (ANSYS AQWA, 2015).

The cable connection is modelled using Morison-type line elements subjected to external loads – the wave, wind and current loads. Figure 3.1 shows the configuration of a dynamic chain mooring line model discretised into a number of finite elements by lumping each mass of an element into a corresponding node using the Lumped-Mass method. The variables $\hat{a}_j = (a_1, a_2, a_3)$ indicate the unit axial vector from a node j -th to node $(j + 1)$ -th, while the unstretched mooring line length from the anchor point to the j -th node is represented by S_j . The seabed is assumed to be a simple plane which is flat and horizontal. The mud line springs shown at each node are used for modelling the reaction force of the seabed. The springs are chosen for reducing discontinuities and energy losses at the touchdown point of the node in the discretized chain mooring line (ANSYS AQWA, 2015).

The depth of the mud layer shown in Figure 3.1 is indicated by \hat{z} which is located above the seabed. The laid length denoted by L_B of a dynamic chain mooring line interacting

with the seabed is measured from the anchor point to the touchdown point of a node. The touchdown point is defined as $0.28\hat{z}$ above the seabed (ANSYS AQWA, 2015).

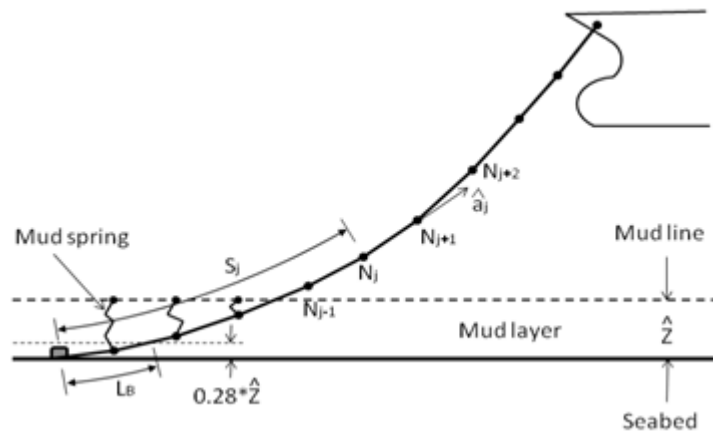


Figure 3.1: Modelling of a dynamic mooring line using a cable connection

(Adapted Aqwa Theory Manual, 2015)

Various forces which act on a mooring line represented by a cable connection are described by Equation 3.2-1 below. The single cable element is subjected to external hydrodynamic loadings and structural inertial loading (ANSYS AQWA, 2015):

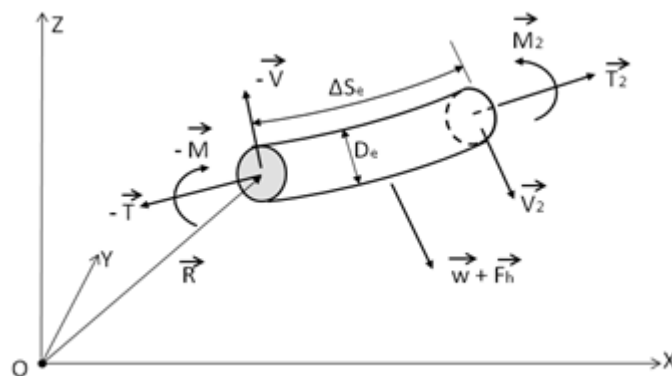


Figure 3.2: Forces on a Cable Element

(Adapted from ANSYS AQWA Theory Manual, 2015)

The motion equation of this cable element is obtained from the general Newton's second law of motion:

$$\mathbf{F} = m\mathbf{a}$$

where \mathbf{F} represents all the forces acting the cable element which are cable tension, shear, weight and hydrodynamic forces which are due to forces acting on a cable element immersed in water with its relative motion. These terms acting on the cable element can be written as vectors which account for the direction of the chain element, if vectors are ignored, this will lead to an inaccurate solution, vectors are represented by the arrow (\rightarrow) and are placed on top of each term on the equation below:

$$\frac{\partial \vec{T}}{\partial s_e} + \frac{\partial \vec{V}}{\partial s_e} + \vec{w} + \vec{F}_h = m \frac{\partial^2 \vec{R}}{\partial t^2} \quad \text{Equation 3.2}$$

$$\frac{\partial \vec{M}}{\partial s_e} + \frac{\partial \vec{R}}{\partial s_e} \times \vec{V} = -\vec{q}$$

m – represents the structural mass per unit length

\vec{q} – represents the moment distribution loading per unit length

\vec{R} – represents the position of the first node of the cable element using vector representation

ΔS_e – is the length of the cable element

ΔD_e – is the diameter the cable element

\vec{w} – is the weight of the cable element

\vec{F}_h – represent the external hydrodynamic forces per unit length using vector representation. \vec{F}_h is formulated using a modified drag force equation called the Morison's equation which is used for calculating the wave loads on slender structural members.

\vec{T} – represent the tension force at the first node of the cable element using vector representation

\vec{M} – represent the bending moment at the first node of the cable element using vector representation

\vec{V} – represent the shear force at the first node of the cable element using vector representation

t – represents time

∂ – shows the partial derivative

The terms $\frac{\partial \vec{T}}{\partial s_e}, \frac{\partial \vec{V}}{\partial s_e}, \vec{w}, \vec{F}_h$ from the left hand-side of the Equation 3.2 are summed up to incorporate all the forces acting on the cable element; the term $m \frac{\partial^2 \vec{R}}{\partial t^2}$ is mass and acceleration product.

The tension and bending moment of the cable element are related to the bending stiffness EI and the axial stiffness EA of the cable material properties shown by the following relations:

Equation 3.3

$$M = EI \frac{\partial \vec{R}}{\partial s_e} \times \frac{\partial \vec{R}}{\partial s_e^2}$$

$$T = EA \varepsilon$$

where ε is the axial strain of the element.

The following boundary conditions are applied at the fairlead and anchor point:

Equation 3.4

$$\vec{R}(0) = \vec{P}_{bot}$$

$$\vec{R}(L) = \vec{P}_{top}$$

$$\frac{\partial^2 \vec{R}(0)}{\partial s_e^2} = \vec{0}$$

$$\frac{\partial^2 \vec{R}(L)}{\partial s_e^2} = \vec{0}$$

where $\vec{P}_{bot}, \vec{P}_{top}$ represents the discretised mooring line attachment points; L represents the total length of the unstretched mooring line.

The motion equation given in Equation 3.2 can be integrated to obtain Equation 3.5 in matrix form below:

Equation 3.5

$$\begin{bmatrix} -\vec{T} \hat{a}_j^T \\ \vec{T}_{j+1} \hat{a}_j^T \end{bmatrix} + \begin{bmatrix} -[V_j] \\ -[V_{j+1}] \end{bmatrix} + \frac{L_j}{2} \begin{bmatrix} [\vec{w} + \vec{F}_h]^T \\ [\vec{w} + \vec{F}_h]^T \end{bmatrix} = \frac{mL_j}{2} \frac{\partial^2}{\partial t^2} \begin{bmatrix} \vec{R}_j^T \\ \vec{R}_{j+1}^T \end{bmatrix}$$

In which $[V_j] = [V_{(j-1)}] - [V_{(j)}]$ is the shear force at node j , which is determined from the two adjacent elements.

The excitation force due to the wave on the nonlinear dynamic cable is ignored. Therefore, in Equation 3.5 the hydrodynamic force \mathbf{F}_h acting on a mooring line cable element consists of the drag force, the buoyant force, and the added mass related force, the relation is shown by:

Equation 3.6

$$\mathbf{F}_h = \mathbf{F}_b + \mathbf{F}_d - \mathbf{m}_a[\widehat{\mathbf{a}}_j, \widehat{\mathbf{a}}_{j+1}]^T$$

where \mathbf{m}_a is the added mass matrix of the cable element and $\widehat{\mathbf{a}}_j$ represents the acceleration vector of cable element at node j .

The drag force with respect to time on the cable element is conveyed in the basic form shown as

Equation 3.7

$$\mathbf{F}_d(t) = \left\{ \mathbf{f}_d(j) - \frac{1}{2} C_d S_c \rho_w |\mathbf{U}_j(t) - \mathbf{V}_j(t)| \{\mathbf{U}_j(t) - \mathbf{V}_j(t)\} \right\}$$

The dynamic response of the discretised mooring line shown by Equation 3.2, Equation 3.3, and Equation 3.4 is solved by using the discrete Lump-Mass method in ANSYS AQWA.

The Morison-type elements of the discretised mooring line are solved by Morison's equation. The Morison's equation approach is used for slender structures when the diameter of a structural element is less than 1/5th of the shortest wavelength. It can be applied on mooring lines, 3D buoys and floating vessels. The Morison's equation is given by Equation 3.2-8 below:

Equation 3.8

$$\mathbf{F} = \mathbf{F}_{Inertia} + \mathbf{F}_{Drag}$$

The inertial forces (due to the motion of the fishing vessel) are predominant than the drag forces. The inertia forces can be identified by considering a spectrum of waves interacting with the ship. In this case this is represented by irregular waves and are fully described in

$\mathbf{F}_{Inertia}$ is the sum of the Froude–Krylov force $\rho \mathbf{V} \mathbf{u}$ and the he hydrodynamic mass force $\rho C_m \mathbf{V} \dot{\mathbf{u}}$ and the \mathbf{F}_{Drag} is defined by the basic drag equation.

This can be written as:

Equation 3.9

$$F = \underbrace{\rho \frac{\pi}{4} D^2 C_m \dot{u}}_{\text{Inertia force term}} + \underbrace{\frac{1}{2} \rho C_d D u |u|}_{\text{Drag force term}}$$

since $\frac{\pi}{4} D^2 = A$,

This equation is further expanded for a moving body in an oscillatory flow as follows:

Equation 3.10

$$\begin{aligned} dF &= \rho A C_m \dot{u}_f - \rho A (C_m - 1) \dot{u}_s + \frac{1}{2} \rho D C_d |u_f - u_s| (u_f - u_s) \\ &= \rho A (1 + C_a) \dot{u}_f - \rho A C_a \dot{u}_s + \frac{1}{2} \rho D C_d |u_f - u_s| (u_f - u_s) \end{aligned}$$

where D is the drag diameter, C_d is the drag coefficient, u_f is the fluid particle velocity in the lateral direction, u_s is the structure velocity in the transverse direction, $C_m = C_a + 1$ represents the inertia coefficient, and A is the cross-sectional area.

The definition of the directional dependent forces and moments of the discretised element is shown in Figure 3.3 below.

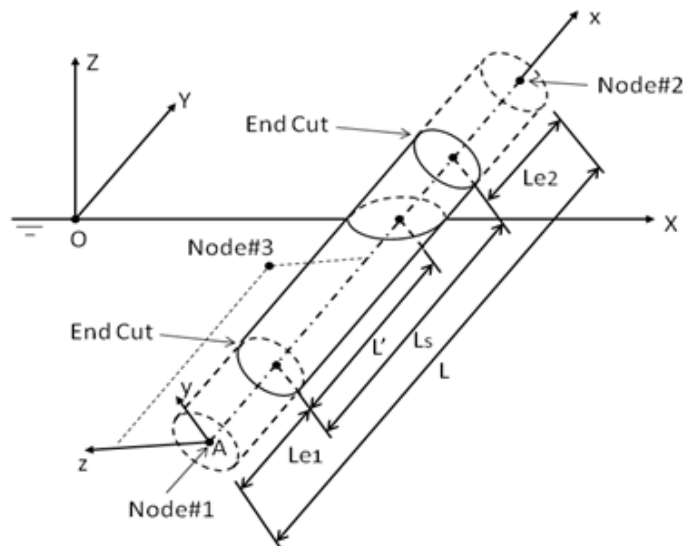


Figure 3.3: Local Tube Axis System

(Adapted from ANSYS Aqwa Theory Manual, 2015)

The hydrodynamic forces and moments acting on an element are determined “with reference to the local tube axis system by the integration of the cross-sectional over the submerged length of L' ,”

Equation 3.11

$$F_y = \int_{L_{e1}}^{L'+L_{e1}} \left\{ \frac{1}{2} \rho D_y C_{dy} |\vec{u}_f - \vec{u}_s| (u_{fy} - u_{sy}) + \rho A C_{my} \dot{u}_{fy} - \rho A (C_{my} - 1) \dot{u}_{fy} \right\} dx$$

$$F_z = \int_{L_{e1}}^{L'+L_{e1}} \left\{ \frac{1}{2} \rho D_z C_{dz} |\vec{u}_f - \vec{u}_s| (u_{fz} - u_{sz}) + \rho A C_{mz} \dot{u}_{fz} - \rho A (C_{mz} - 1) \dot{u}_{fz} \right\} dx$$

$$M_y = \int_{L_{e1}}^{L'+L_{e1}} \left\{ \frac{1}{2} \rho D_z C_{dz} |\vec{u}_f - \vec{u}_s| (u_{fz} - u_{sz}) + \rho A C_{mz} \dot{u}_{fz} - \rho A (C_{mz} - 1) \dot{u}_{fz} \right\} x dx$$

$$M_z = - \int_{L_{e1}}^{L'+L_{e1}} \left\{ \frac{1}{2} \rho D_y C_{dy} |\vec{u}_f - \vec{u}_s| (u_{fy} - u_{sy}) + \rho A C_{my} \dot{u}_{fy} - \rho A (C_{my} - 1) \dot{u}_{fy} \right\} x dx$$

“In AQWA, a three-point Gaussian integration scheme is employed to estimate the integral forms given by Equation 3.11” (ANSYS AQWA, 2015).

“The forces and moments on each tube element are then transformed to the fixed reference axes (FRA) and, in addition, the moments are with respect to the centre of gravity of the structure. The total fluid load is the summation of forces on all the tube elements and the panel elements” (ANSYS AQWA, 2015).

3.2.2. Governing equations for the fishing vessel in time domain

To obtain the hydrodynamic response the fishing vessel at sea, the most common approach used is the 3D panel method which is based on fluid potential theory. The panel method is a technique for solving incompressible potential flow over thick 2D and 3D geometries (for external flow); it is used to determine the fluid velocity and the pressure distribution, on an object (Mason, 2015). The panel method is based on the potential flow theory assumption that the fluid is inviscid (negligible viscosity.), incompressible, irrotational and steady. The motion of the fishing vessel is represented by six degrees of freedom (6-DOF) rigid body translational and rotational motions which are categorised into two – Translation (heave, sway, and surge) and Rotational (yaw, pitch and roll) as shown in Figure 3.4 below.

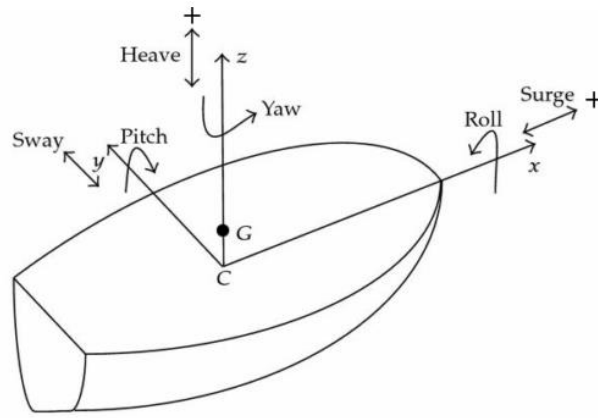


Figure 3.4: Vessel 6-DOF rotations and translations

(Adapted from Ibrahim & Grace, 2010).

The solution flowfield (fluid domain) is found by representing the fishing vessel surface by a number of panels, and solving a linear set of algebraic equations which satisfies the Laplace's equation to determine unknown variables. The potential flow panel method is incorporated in the Bernoulli's equation to find the fluid pressure at a given point on the surface of the fishing vessel. The fishing vessel surface is discretised into number panels called a mesh. Finer meshed geometries tend to yield more accurate results. The panels below the vessel waterline are called 'diffracting panels', these panels are subject to the three-dimensional panel method based on fluid potential theory. The panels above the waterline are called 'non-diffracting panels'.

The hydrodynamic loads are mainly caused by the interactions between the vessel and the waves. The hydrodynamic loads acting on the fishing vessel are the drag, the wave, and the inertia loads. Drag loads (viscous forces) on the hull of the vessel are important when structural members are slender and wave amplitude is large and are obtained using Morison's equation. This is the net force opposing the vessel's forward movement due to the pressure and shear forces acting on the wetted surface of the vessel (ANSYS AQWA, 2015).

Equation 3.12

$$[F_{dmj}] = C_{dm} [|\mathbf{u}_j| |\mathbf{u}_j|] \text{ where } j=1,6$$

“where $[F_{dmj}]$ is the 6×1 matrix which consists of the three Morison hull drag force components and three Morison hull drag moment components, C_{dm} is a 6×6 Morison drag coefficient matrix, and $\mathbf{u}_j (j = 1, 6)$ is the relative translational or rotational velocity component in the structure local axis frame. The translational relative velocity ($j=$

1,3) in Equation 3.12 is the difference between the steady fluid velocity (current speed only without fluid particle velocity due to waves) and the structural motion velocity” (ANSYS AQWA, 2015),

Equation 3.13

$$\mathbf{u}_j = \mathbf{u}_{cj} - \mathbf{u}_{sj}$$

where \mathbf{u}_{cj} and \mathbf{u}_{sj} represents the current and structure velocity.

The wave exciting load, in small amplitude waves, consists of the diffraction force and first order wave force – the Froude-Krylov force. The diffraction force is due to wave disturbance which is caused by the presence of the vessel. Both the diffraction and Froude-Krylov forces are the active forces acting on the vessel.

The wave exciting load and the wave inertia load on the vessel are solved using the fluid potential theory. This can be formulated from the basic potential flow equation which used to determine flow around an object and is given by:

Equation 3.14

$$V = \nabla\phi$$

where V represents the flow velocity, ϕ velocity potential and ∇ is the gradient “del” which based on vector calculus, it represents the rate of change of a function with directions or components.

When radiation and diffraction waves are taken into account, the fluid flow field that surrounds the floating vessel through the application of the velocity potential from Equation 3.14 then becomes:

Equation 3.15

$$\phi(\vec{X}, t) = a_w \phi(\vec{X}) e^{-i\omega t}$$

where the incident wave amplitude is represented by a_w and the wave frequency is represented by ω . V is replaced by (\vec{X}, t) for keeping the notation consistent.

The term $\phi(\vec{X})$ is has contributions from the radiation waves due to the six degrees of freedom of the vessel motion, the diffracted and the incident wave.

The potential due to wave contributions in the vessel 6-DOF may therefore be written as:

Equation 3.16

$$\varphi(\vec{X})e^{-i\omega t} = \left[(\varphi_1 + \varphi_d) + \sum_6^{j=1} \varphi_{rj} X_j \right] e^{-i\omega t}$$

The potential functions derived above enable the resultant physical quantities such as fluid pressure and vessel motions in time-domain to be determined.

The term $X_j = u_j(1,3)$ and $X_j = \theta_{j-3}, (j = 4, 6)$, φ_1 represents the first order wave potential, the diffraction wave potential is represented by φ_d , the radiation wave potential is represented by φ_{rj} .

The first order hydrodynamic pressure on the vessel hull is calculated by using the linearized Bernoulli's equation below after obtaining the wave velocity potentials,

Equation 3.17

$$p^{(1)} = -\rho \frac{\partial \phi(\vec{X}, t)}{\partial t} = i\omega \rho \varphi(\vec{X}, t) e^{-i\omega t}$$

The nonlinear response of the fishing vessel under hydrodynamic loads is obtained by integrating the equation of motion with respect to time in the form as proposed by Cummins, 1962:

Equation 3.18

$$(\mathbf{M} + \mathbf{A})\ddot{\vec{X}}(t) + \mathbf{B}\dot{\vec{X}}(t) + \mathbf{C}\vec{X}(t) + \int_0^\infty \mathbf{K}(\tau)\ddot{\vec{X}}(t-\tau)d\tau = \vec{F}(t)$$

where \mathbf{M} represents the inertia matrix. \mathbf{A} is the added mass matrix, \mathbf{B} is the viscous damping and \mathbf{C} , which are the viscous damping matrix and \mathbf{C} is the hydrostatic restoring matrix. \mathbf{K} contains the impulse response functions. The added mass (\mathbf{A}) of the structure occurs due to the water displaced by the structure in motion. \vec{X} is the 6-DOF vessel displacements vector, $\dot{\vec{X}}$ is the vessel velocity vector and $\ddot{\vec{X}}$ vessel acceleration vector. The 6 degrees of freedom (DOF) vessel displacements are represented by \vec{X} and the dot symbolises differentiation with respect to time. The first dot shows differentiation vessel displacements which gives the velocity shown by $\dot{\vec{X}}$, likewise, the second dot shows the vessel displacements differentiated twice which gives us $\ddot{\vec{X}}$ which is the acceleration of the vessel. The external force is denoted by \vec{F} which is the hydrodynamic loads contributions of both linear and nonlinear forces; these include the

consideration of the nonlinear properties of mooring line characteristics as well as the irregular wave load on the fishing vessel. The irregular wave load represents the wave theory which realistically represents the water particle kinematics to estimate the drag and inertia for all the six degrees of freedom (6-DOF) of the structure (ANSYS AQWA, 2015).

The equation of motion described above is solved using an iterative time-domain numerical integration scheme which calculates the solution quickly and efficiently. To achieve this, a three-point Gaussian integration scheme is used in ANSYS AQWA.

3.3. Environmental loading

The moored vessel experiences the wave, current and wind ocean environment loads. In ANSYS AQWA, the fishing vessel is modelled as a rigid body, and the wind loads and wave forces acting on the rigid body are described in this section. This section also gives the theory description of the ocean environment hydrodynamic loads.

3.3.1. Description of waves

According to DNV (2011), “ocean waves are irregular and random in shape, height, length and speed of propagation”. A random wave model is required for describing a real sea state. Sea waves can be classified as irregular (random) waves which are specified in terms of height and period, and direction of propagation. They are predominantly generated by the wind and appear to be irregular in character (Haritos, 2007).

The fishing vessel is assumed to be under the influence of irregular waves. This wave type is defined by the Pierson-Moskowitz spectrum in ANSYS AQWA. The wave spectrum is formulated by the significant wave height and the average wave period parameters. The Pierson-Moskowitz spectrum is given by:

Equation 3.19

$$S(\omega) = 4\pi^3 \frac{H^2}{T_z^4} \frac{1}{\omega^5} \exp\left(-\frac{16\pi^3}{T_z^4} \frac{1}{\omega^5}\right)$$

where $S(\omega)$ represent the Pierson-Moskowitz spectrum

The following relationship exists between T_z , T_1 and T_0 :

$$T_0 = 1.408.T_z$$

$$T_1 = 1.086.T_z$$

where T_1 is the average wave period and T_0 is the maximum period, ω is the wave frequency, T is the average wave period and H is the wave height.

3.3.2. Currents

Currents create significant loads on marine structures, particularly on moored vessels and offshore structures. Currents are based on the assumption that they move in a horizontal direction but may vary depending on the depth of water. The interaction of currents and waves is crucial in the simulation of offshore structures. The combined fluid particle velocity of currents and waves may increase the fluid drag force on smaller components such as risers and mooring lines. Ocean currents contribute to the drag force on the hull of the fishing vessel as well as increasing drag forces on the chain mooring. Currents can be defined with a uniform or a non-uniform profile (ANSYS AQWA, 2015).

The Agulhas Current has been described as one of the fast-flowing currents in any ocean and reaches an estimated top speed of 2.6 m/s . Its velocity depends on variations in the equatorial current velocity, which in turn change with location, depth, and season. It is present between Plettenberg Bay and Port Alfred region with an estimated average flow rate of 0.2 to 0.6 m/s (The Editors of Encyclopædia Britannica, 2009).

3.3.3. Winds

Wind loads not only create wind-induced waves but also directly generate drag loads on the fishing vessel upper hull portion. The wind with a constant direction over time, the frequency distribution of the wind speed fluctuations can be described by means of a wind spectrum (ANSYS AQWA, 2015). However, the effects of wind loads will be ignored in this study. This because ocean waves are wind dependent and therefore the results of the analysis in this study remain valid. Additionally, adding the wind will increase the number of parameters to be evaluated which will increase the number of analysis to be done.

Thus, only the effects of the waves and currents will be considered. The wind direction is assumed to be in the same direction as the waves and currents for simplifying the analysis.

3.4. Underwater video analysis: Experimental

As stated in the introduction, scuba scientist divers have long observed anchor chain movement across squid egg beds. This was captured using underwater video camera; the chain was marked with a white plastic bag. Vertical and horizontal measuring sticks with white markers were used for calibration. Analysis of this video footage was performed using an open source software called *Tracker*. This motion analysis of the chain is later used to calibrate *ANSYS AQWA* and *ABAQUS* models ultimately to determine the chain contact forces on the seabed. Various ocean conditions will be evaluated for making correlations with the output from the following video analysis.

3.4.1. Tracker video analysis

A total of four video footage were obtained, the three were recorded on the double anchor mooring and one was recorded on the single-point mooring. One of the video footage obtained had better stability than others and thus was selected for video analysis.

Figure 3.5 below shows an example of the original video image with labels. The mooring chain shown has a diameter of 20 mm. The video footage analysed was obtained from the double anchored (two-mooring) vessel.

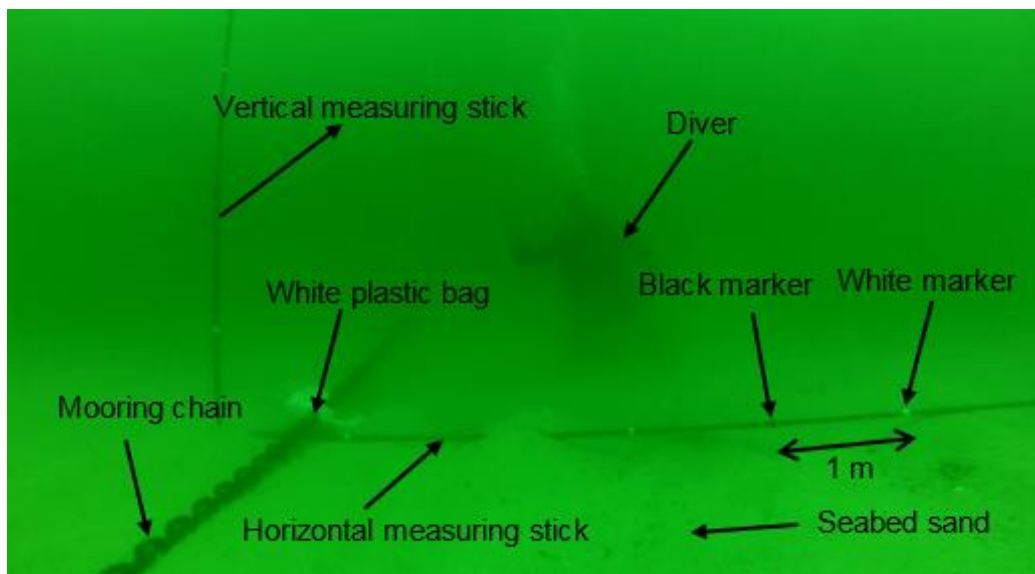


Figure 3.5: Original underwater video image of the chain movement experiment

For this experiment, a high definition video camera was used to record the 9 minutes and 47 seconds long video footage. The portion of the video that was analysed starts from

3 minutes and 10 seconds to 4 minutes and 3 seconds. This portion was extracted due to better visibility and video camera stability for analysing the 2D motion of the chain. One video camera was used, hence only the 2D motion of the chain could be analysed.

The frame rate of 50 frames per second was used for capturing the rapid motion of the chain underwater. The frame-rate is defined as the acquisition frequency of the video camera; high frame has a better resolution which can record the smallest detail of the chain motion. Generally, higher frame-rates are required for tracking objects moving at high speeds (Paredes & Taveira-Pinto, 2016).

(The original video footage of the recorded chain motion has been stored on the following website: <https://www.youtube.com/watch?v=8DB56jq1HG0&t=18s>).

The video analysis, in accordance with Paredes & Taveira-Pinto (2016), was done in three stages (i) video linearization where the optical distortions were corrected or minimized; (ii) calibration to match the pixel coordinates with the real world coordinates; and (iii) video footage acquisition of the chain motion underwater.

Since all video and photo cameras have imaging distortions, video enhancement techniques were required to improve the quality of the video footage. The large thickness of water and suspended particulate matter between the camera and the chain lessened the contrast of the footage as a result of light absorption and scattering by the suspended particles in the water column. One of the techniques used to enhance the video quality was to reduce video noise by conversion of the video image from RGB to 8-bit grayscale. This greatly improved the contrast between the chain markers and the background allowing for easy analysis.

A margin of error is expected and thus the measurements of the video analysis discarded as outliers. An accurate error analysis will require cameras with higher optical quality and the optimisation of procedures used for calibration which are objectives not pursued in this work (Paredes & Taveira-Pinto, 2016).

Figure 3.6 below shows an example of the *Tracker* video analysis user interface. The video is in grayscale to improve contrast between the chain, discrete (white plastic bag) tracking point and the background. *Tracker* uses a colour-based tracking technique. The region where the colour-based operation is going to be performed is highlighted in red. During analysis, the program searches for white colours on the selected region for each frame of the video sequence.

Tracker also allows for the video image angle to be adjusted perpendicular to the 2D plane movement of the mooring chain. This was done by adjusting the angle of the origin such that it fits perpendicularly with the reference point of the video image.

About 2 m of the chain in the figure below was observed to have lifted off and dropped back down on the seabed in sequence.

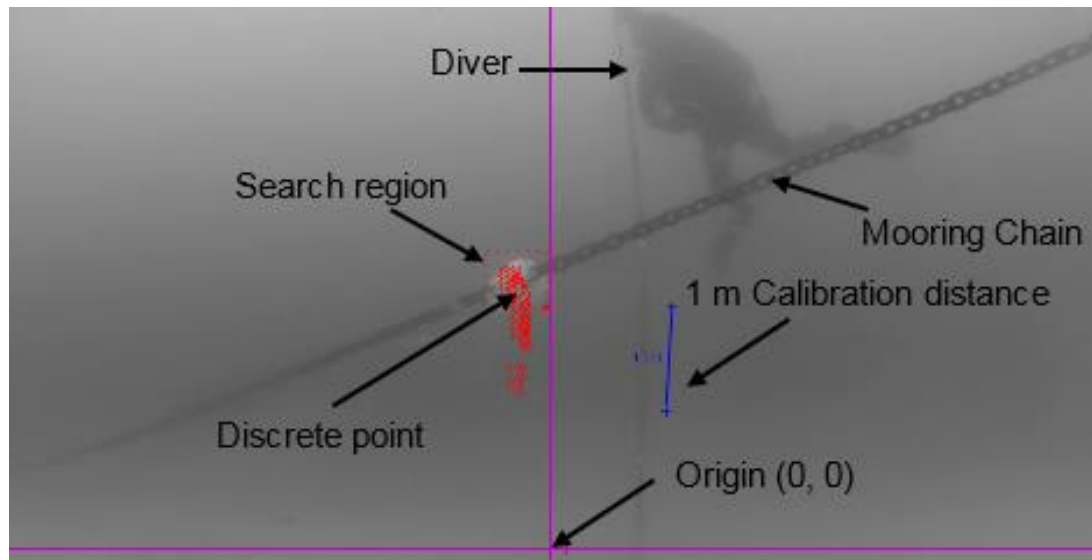


Figure 3.6: Underwater video analysis using Tracker

Figure 3.7 below show the vertical displacement of the tracked discrete point. This vertical motion of the discrete point was as observed to be more dominant than the horizontal motion. This was the expected result which was also observed in the video footage showing the mooring chain lifting off and dropping back down at a different frequency and speed. The velocities associated with this vertical displacement will be used to calibrate the *ANSYS AQWA* model as well as to determine the seabed contact forces using the *ABAQUS* model.

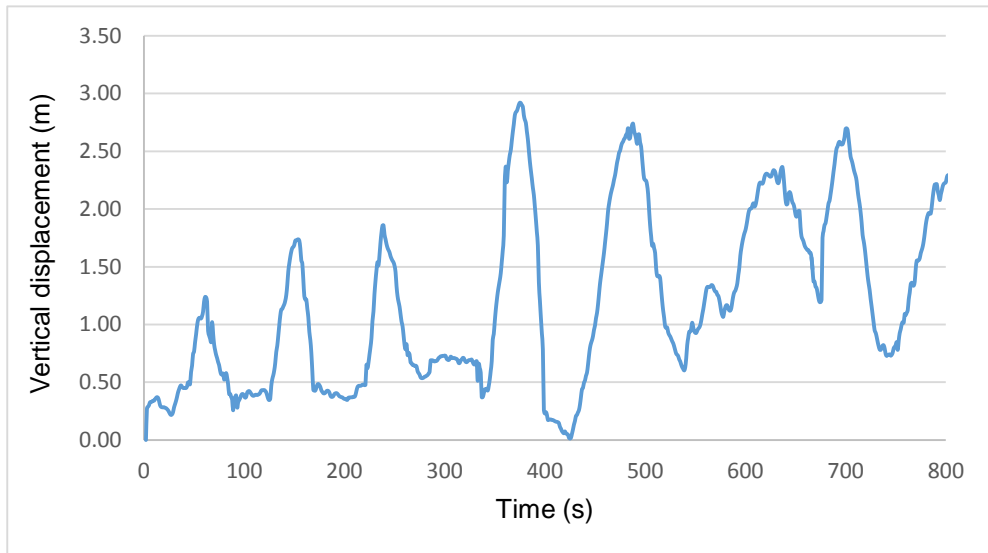


Figure 3.7: Discrete point vertical displacement

Figure 3.8 below shows the velocity of the discrete tracking point in the vertical direction where the tracked values fell within the range of -8.01 and 8.14 m/s. As can be seen, most values fall between ± 4 and 5 m/s.

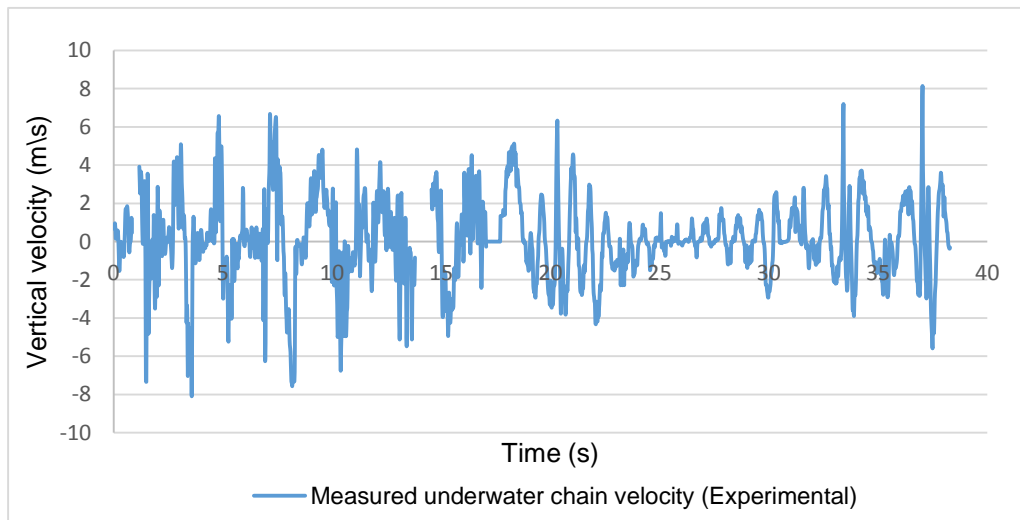


Figure 3.8: Discrete point underwater vertical velocity

CHAPTER FOUR

4. Results and discussions

The results obtained in this study were reported in two parts. The first part was the *ABAQUS* simulation model based on the measured chain velocity obtained from video analysis. The impact forces and pressures of a single chain link were investigated on the 14, 16 and 20 mm diameter chains. The second part of the investigation was the *ANSYS AQWA* simulation of both the single-point and the two-point mooring systems.

ABAQUS results are first presented for correlating them to the expected chain velocity in *ANSYS AQWA* simulations. This is because of the *ANSYS AQWA* software limitation which does not account for the mooring chain impact pressure and force on the seabed. The software only considers the dynamic mooring line length laid on the seabed, anchor uplift forces and the dynamic mooring line tension. Hence, *ABAQUS* models were used for estimating seabed impact pressure and forces of the dynamic mooring chain.

Table 4.1 gives a summary of the types of analysis conducted in this thesis.

Table 4.1: Description of various models used for mooring line analysis

Analysis	Description
<p>1:</p> <p>The model was developed for investigating the seabed effect of three mooring chain sizes at different velocities. The velocities were obtained from the underwater video analysis.</p>	<p><i>ABAQUS</i> chain-seabed impact</p> <ul style="list-style-type: none"> • Varied chain link sizes of 14, 16 and 20 mm at 1, 3, 5, 6, 8 and 10 m/s • OUTPUT parameters: Contact force and contact pressure
<p>2:</p> <p>The model was developed for investigating seabed impact forces based on the slender rod method.</p>	<p><i>ABAQUS</i> chain-seabed impact</p> <ul style="list-style-type: none"> • Used 0.12 and 1 m slender rod length • Used circular 3D solid equivalent section • Varied maximum velocities of 5 and 8 m/s. • OUTPUT parameters: Contact force and contact pressure • Made correlations with a single chain link
<p>3:</p> <p>The model was developed for studying the effect of wave height and period.</p> <p>The model was also used for investigating the wave condition which correlates to the observed chain impact motion.</p>	<p><i>ANSYS AQWA</i> time domain simulations:</p> <ul style="list-style-type: none"> • Varied wave conditions: <ul style="list-style-type: none"> ○ 1 m wave height with 7 s period ○ 1 m wave height with 10 s period ○ 2 m wave height with 7 s period ○ 2 m wave height with 10 s period ○ 2.5 m wave height with 7 s period • Used 22 m single-point moored vessel • Used constant chain diameter of 20 mm with 160 m length • OUTPUT parameters: Tension, Laid length and Anchor uplift forces and seabed contact pressure
<p>4:</p> <p>The model was developed for investigating the effects of three mooring configurations on the seabed.</p>	<p><i>ANSYS AQWA</i> time domain simulations:</p> <ul style="list-style-type: none"> • Used constant wave conditions: 2.5 m wave height and 7 s period • Used three mooring line configurations on the 14 and 22 m vessels (single and two-point mooring) • Used constant chain diameter of 20mm with 160 m length • OUTPUT parameters: Tension, Laid length and Anchor uplift forces
<p>5:</p> <p>The model was developed for investigating the effect of three chain sizes on the seabed.</p>	<p><i>ANSYS AQWA</i> time domain simulations:</p> <ul style="list-style-type: none"> • Constant wave conditions: 2.5 m wave height and 7 s period • Constant mooring line length of 160 m • Varied chain diameter of 14, 16 and 20 mm • OUTPUT parameters: Tension, Laid length and Anchor uplift forces

4.1. ABAQUS model for the mooring chain impact on the seabed

The impact force of the mooring chain on the seabed was modelled using *ABAQUS 6.14-1* finite element analysis software. In this study, a single chain link was simulated at different chain velocities of impact. Since *ANSYS AQWA* uses a flexible slender rod (cable) to model the mooring line as most mooring line analysis tools do, the single chain link (3D studless chain link) impact simulations are compared to those using a 3D flexible slender rod in *ABAQUS*. The impact forces and pressures due to different velocities will later be related to the *ANSYS AQWA* model mooring line velocities at different points of contact along the mooring line. The velocities used in this analysis were obtained from the underwater video analysis in Chapter 3.4.

4.1.1. Geometry of the model

The 20 mm diameter studless chain CAD geometry is shown in Figure 4.1 below. To save computational time, only a single link of chain was simulated in *ABAQUS*. The contact force of a single chain link well represents all mooring chain links in contact with the seabed when impact velocity is the same. Results presented in Section 4.1.7 show that the seabed impact pressure and force due to the impact velocity are the same for 0.12 and 1 m long rods (both rods with the same diameter). The simulated short rod (0.12 m long) represents a single link rod that makes up the entire mooring line. The 1 m rod represents a series of 0.12 m short rods that makes up 1 m rod. Therefore, a single chain link impact pressure and force shown in Figure 4.1 below will be the same as long as the impact velocity is the same.

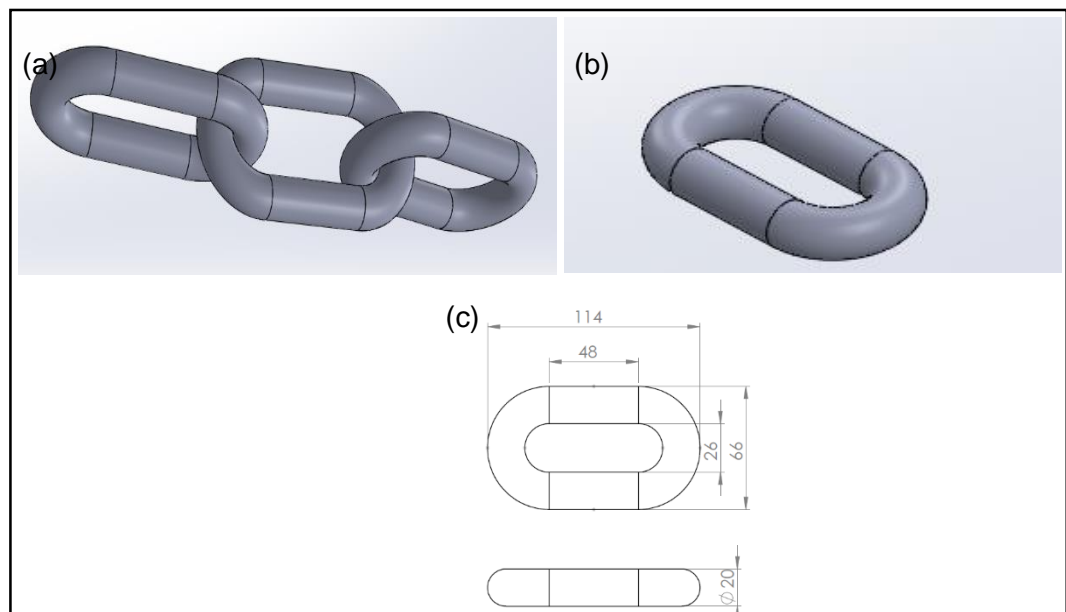


Figure 4.1: CAD geometry of the 20 mm diameter chain

The seabed geometry is shown in the next Figure 4.2. The dimensions of the seabed geometry are 0.08 x 0.15 x 0.25 m. The region where the chain link contacts the seabed was meshed with a fine mesh and is shown by the partitioned region.

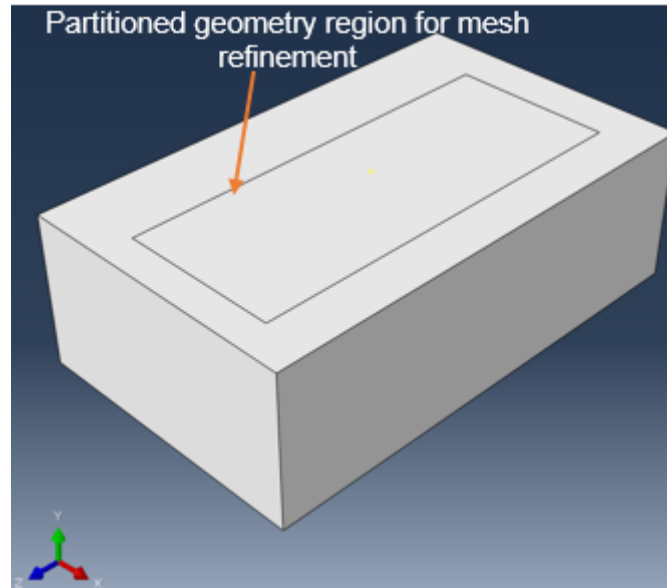


Figure 4.2: Seabed geometry

4.1.2. Material property definition

The mooring chain link was modelled as a 3D homogenous solid using steel properties shown in Table 4.2 below. Appendix E shows the dimensions of the 14 and 16 mm diameter studless chain links.

Table 4.2: Steel chain properties of 20 mm chain

Chain Mooring Line properties			
Parameter	Value	Units	References
Nominal diameter	14, 16 & 20	mm	Appendix E
Steel density, ρ	7800	kg/m^3	Appendix B
Poisson's ratio, ν	0.3		Appendix B
Young's modulus, E	200E9	Pa	Appendix B

The seabed was modelled as an elastic foundation using soil properties with the contact friction coefficient of 0.74 for sand recommended by Taylor & Valent (1984). The elastic foundation makes a simplifying assumption of neglecting cohesion and adhesion effects of the seabed soil. Yu & Tan, (2006) used elastic and elastic-plastic models for modelling the mooring chain-seabed contact using *ABAQUS/Standard* contact algorithms. Yu & Tan also stated that “The elastic foundation can be used for the

calculation of cable/seabed interaction with adequate accuracy”. The following Table 4.3 shows the seabed soil properties used for the elastic foundation model. (See Appendix B for the seabed sand properties).

Table 4.3: Seabed soil properties

Seabed dense sand properties			
Parameter	Value	Units	Reference
Sand density, ρ	1922	kg/m^3	Appendix B
Poisson's ratio, ν	0.3	-	Appendix B
Young's modulus, E	1440 000 000	Pa	Appendix B
Friction coefficient	0.74	-	(Taylor & Valent, 1984)

4.1.3. Mesh

Figure 4.3 below show the 3D chain link meshed with quadratic tetrahedral elements of type C3D10M. *ABAQUS* has four types of solid elements which are hexahedral, Hex-dominated, tetrahedral and wedge elements (see Figure 4.5). The tetrahedral element type selected is described as C3D10M. C3D10M stands for a 10-node modified quadratic tetrahedron by using an explicit element type. C3D stands for a three-dimensional continuum and 10 stands for a 10-node quadratic tetrahedral. “Quadratic elements provide more accurate results than linear elements, but increase the computational time as well” (Bjørnsen, 2014).

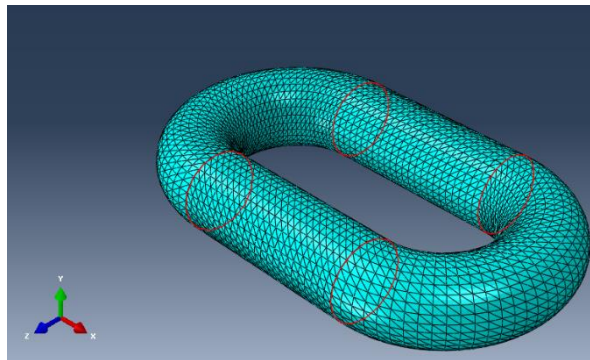


Figure 4.3: Single chain link meshed (stud link)

For the elastic foundation, linear hexahedral element type C3D8R was selected and is described as an 8-node linear brick element with reduced integration and hourglass control. “Hourglass control prevents mesh instability due to spurious deformation mode of a Finite Element Mesh” (Belytschko et al., 1984).

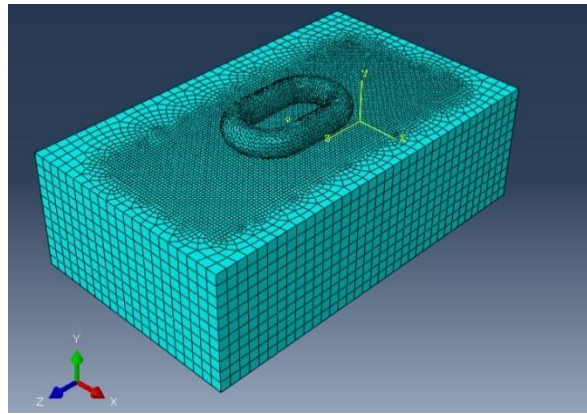


Figure 4.4: Elastic foundation mesh

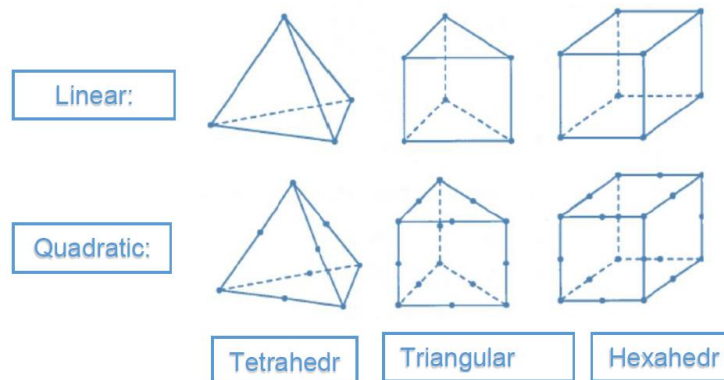


Figure 4.5: Linear and Quadratic Solid elements

(Adapted from Bjørnsen, 2014)

4.1.4. Contact

The chain link-seabed impact was modelled using *ABAQUS/Explicit* general contact. The contact region between the chain link and the seabed is shown in Figure 4.6. The “Explicit General contact” interaction property between the chain link and the seabed was defined by the “normal behaviour” and “tangential behaviour” contact properties. The “tangential behaviour” penalty contact friction coefficient of 0.74 was set.

In *ABAQUS /Explicit*, the solution for a particular time step is solved based on the history of the previous step. At the end of each time step, the updated system matrices is executed and the new system of equations is solved without iteration. If the increments are small enough accurate results will be computed, otherwise the solution

will diverge. This is due to the fact that the equilibrium is not strictly enforced (ABAQUS, 2012).

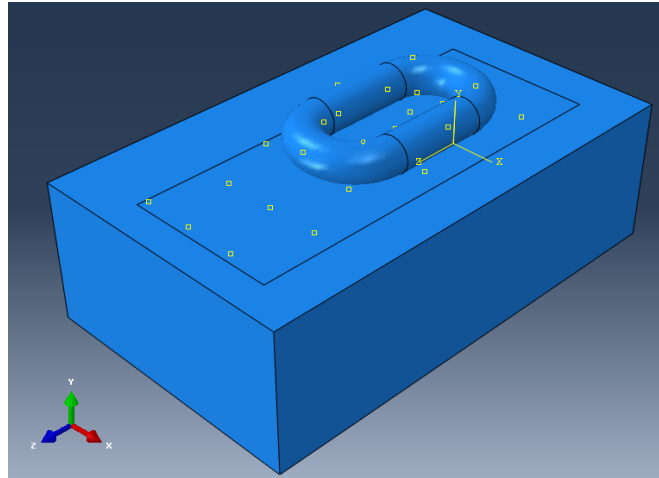


Figure 4.6: Chain link and seabed contact surfaces

4.1.5. Boundary Conditions and Loading

The loading on the chain link was defined using “velocity field” option; velocities of 1, 3, 5, 6, 8 and 10 m/s were varied. These velocities were selected based on the measured underwater chain velocity time-history shown in Figure 4.8. The seabed elastic foundation was fixed on all sides except the top side where the chain link impacts the seabed. Figure 4.7 shows boundary conditions regions and the chain-link velocity field. The elastic foundation sides were fixed with “Encastre” boundary condition as shown.

The ANSYS AQWA software ignores the friction of the mooring section lying on the seabed. In reality, the seabed experiences (1) friction due to the vertical contact force of the mooring chain, (2) friction in the longitudinal direction of the chain (when the chain drags along its axis) and (3) friction in the transverse direction (when the mooring chain sweeping across the seabed). Due to the complexity of analysing the mooring chain movement in the longitudinal and transverse directions in ABAQUS, this study this focuses on the assessment of the vertical impact of the mooring chain.

Furthermore, the underwater video footage obtained of the mooring chain impacting the seabed showed the vertical movement of the mooring chain predominant than the longitudinal and transverse movements. Last of all, the vertical impact assessment of the mooring chain on the seabed was also requested by marine biologist who noticed

an interaction between the mooring chain and the seabed as stated in the introduction of this thesis.

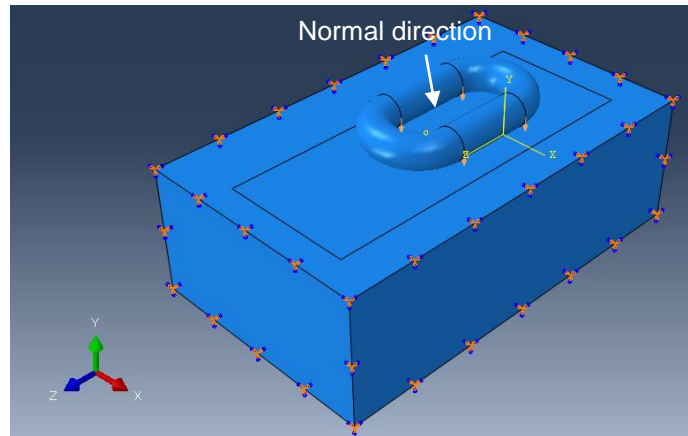


Figure 4.7: Chain-Seabed boundary conditions and loading

Figure 4.8 shows the scatter plot of the measured chain velocity from *Tracker* in Chapter 3.4. This figure shows that the most expected maximum values fall in the range -8.01 and 8.14 m/s.

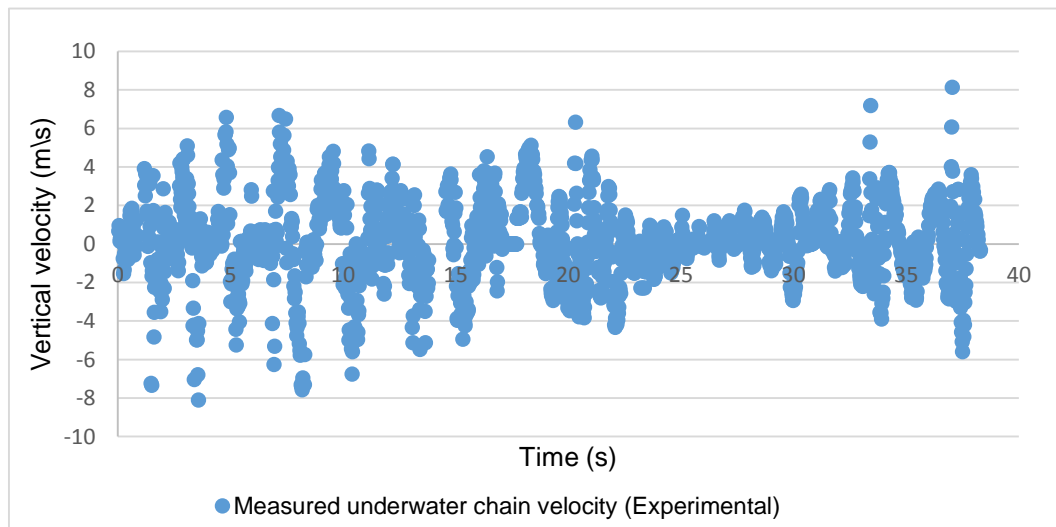


Figure 4.8: Chain velocity scatter plot

The radar plot clearly shows how the velocity is distributed in the next Figure 4.9.

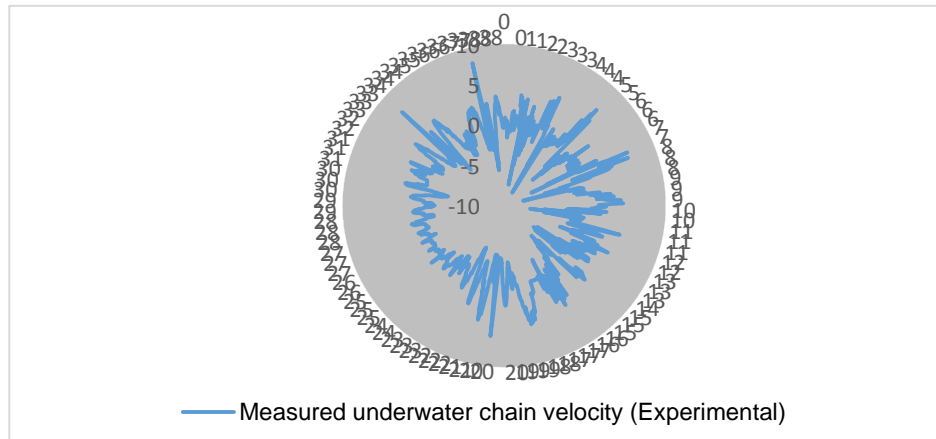


Figure 4.9: Chain velocity radar plot

4.1.6. Results

The results of the analyses are presented as CNORM (Normal Contact force), CPRESS (Contact Pressure) and S (von Mises) stress. The stresses as a result of the chain-link impacting the seabed at 1 and at 10 m/s are shown respectively in all three chain-link sizes; while the stresses, contact pressures and contact forces on the seabed for the 20, 16 and 14 mm chain links is shown by evaluating the impact at 1, 3, 5, 6, 8, and 10 m/s.

4.1.6.1. 20 mm chain results

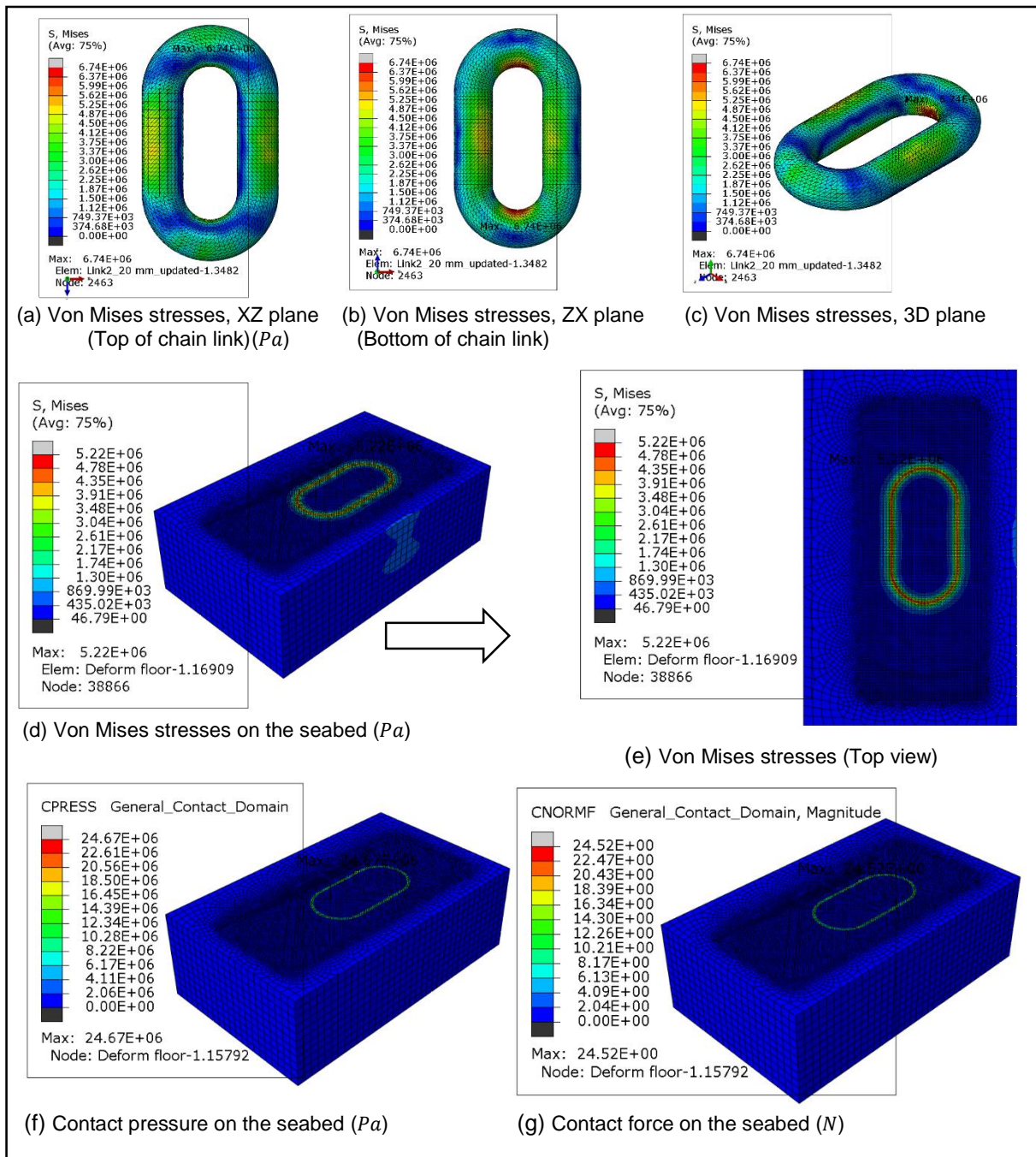


Figure 4.10: Chain link-seabed contact stresses, pressures and forces at 1 m/s for the 20 mm diameter chain

Figure 4.10 above show the seabed contact forces when the 20 mm chain link impacts the seabed at 1 m/s. The average contact force at this velocity was found to be 19.41 N; while the Von Mises stress on the 20 mm chain link was found to be 6.74 MPa. It was noticed that the Von Mises stresses on the seabed are higher than those on the chain link. This is because the seabed is made of soil which has low elastic modulus compared to the high elastic of steel chain link.

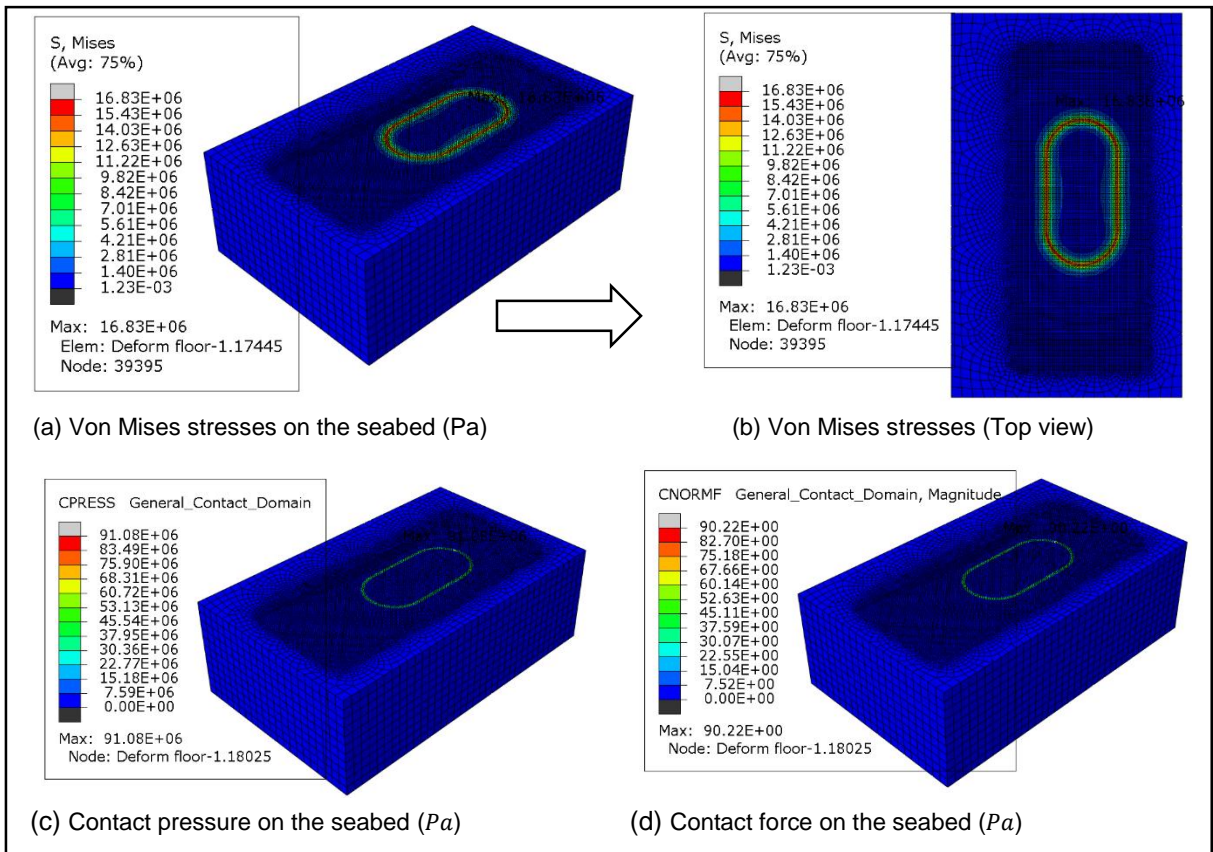


Figure 4.11: Chain link-seabed contact stresses, pressures and forces at 3 m/s for the 20 mm diameter chain

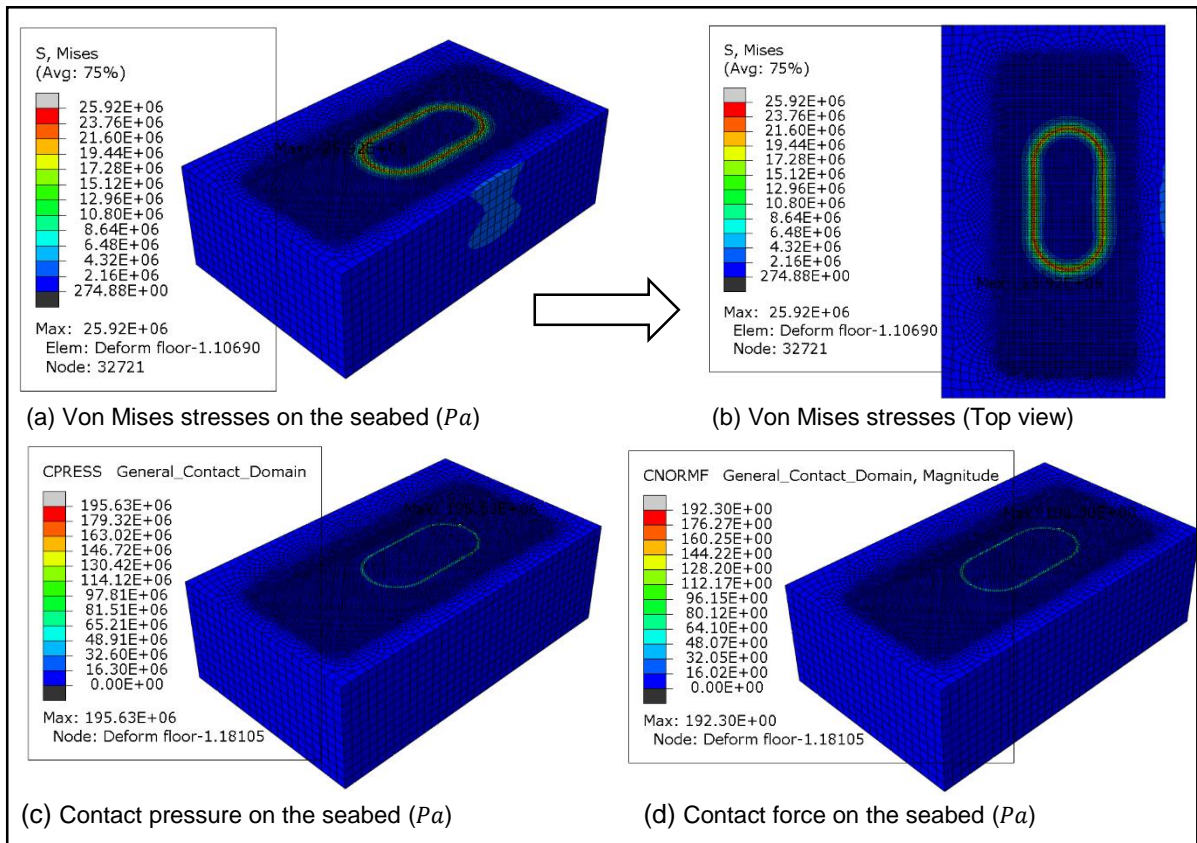


Figure 4.12: Chain link-seabed contact stresses, pressures and forces at 5 m/s for the 20 mm diameter chain

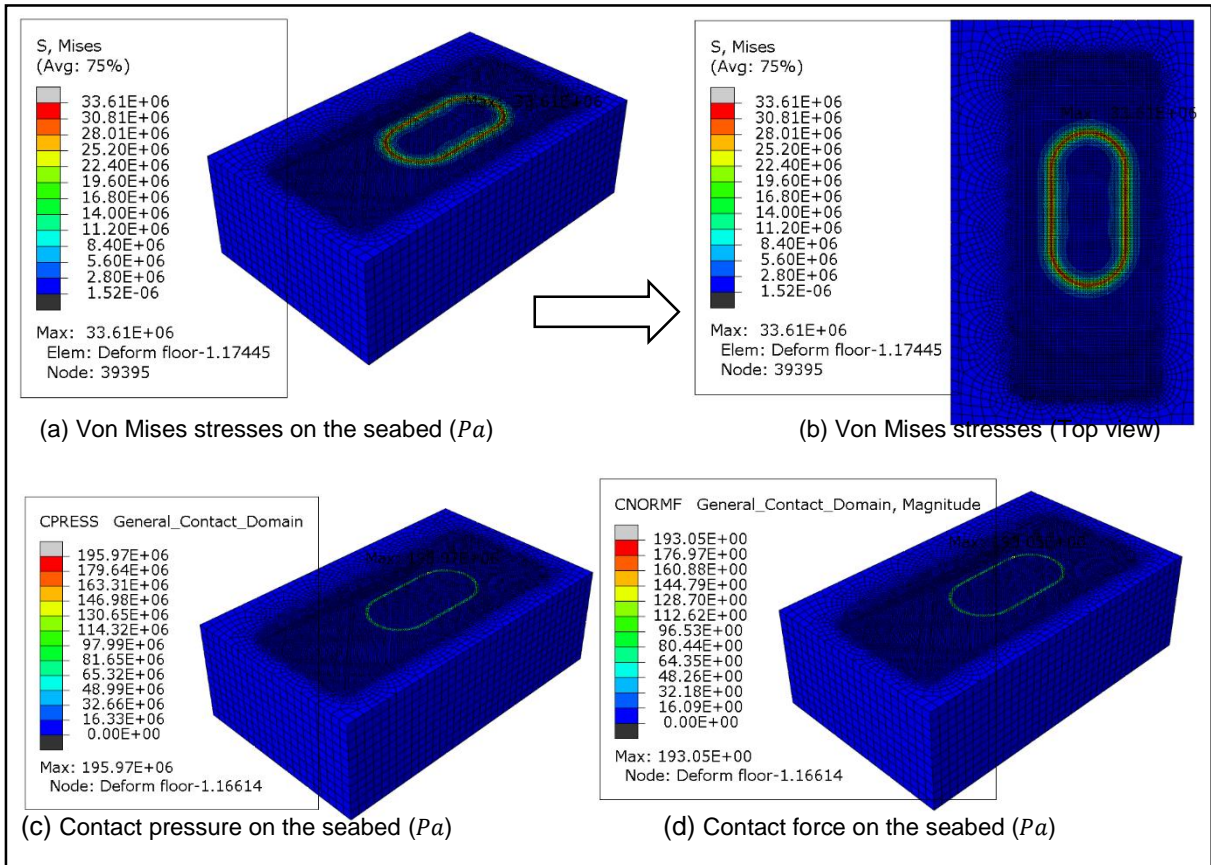


Figure 4.13: Chain link-seabed contact stresses, pressures and forces at 6 m/s for the 20 mm diameter chain

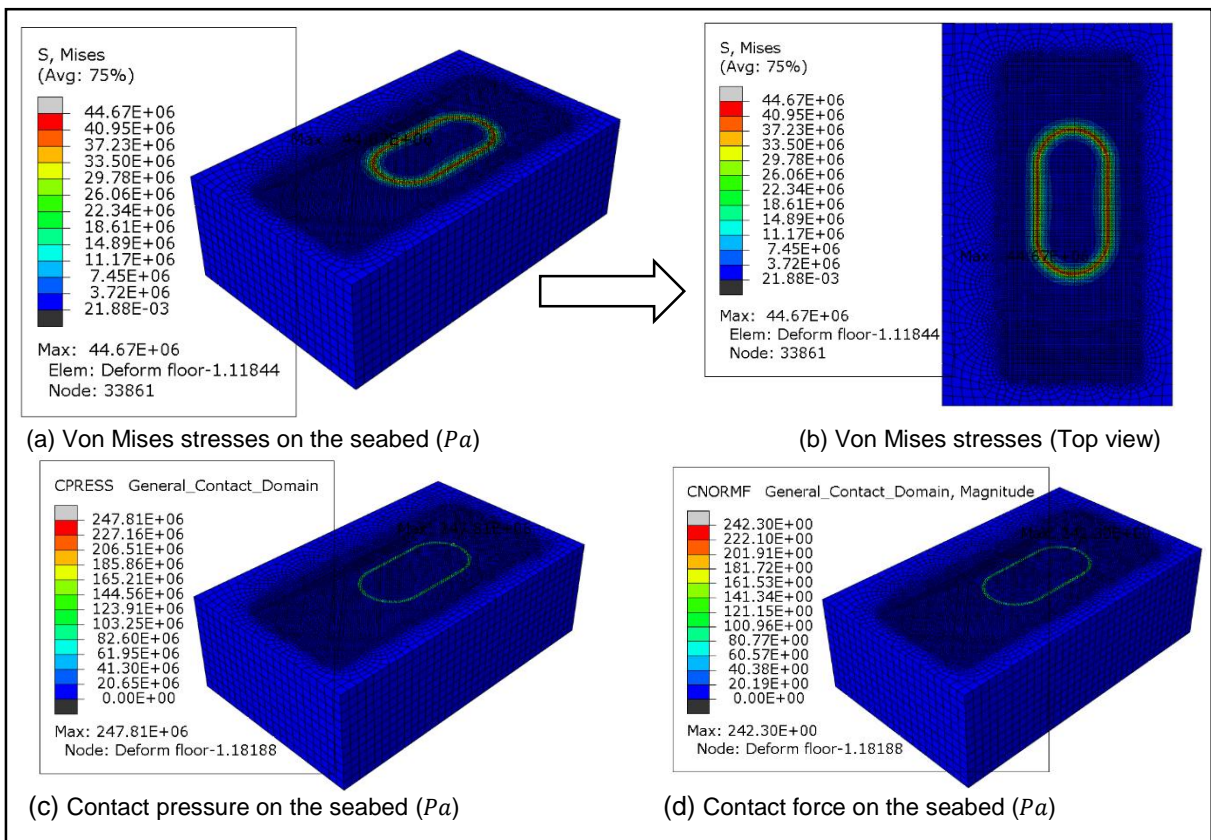


Figure 4.14: Chain link-seabed contact stresses, pressures and forces at 8 m/s for the 20 mm diameter chain

Figure 4.15 below show the maximum contact forces on the seabed when the chain link impacts the seabed at 10 m/s. The maximum contact forces were averaged by only considering the first four maximum contact forces. The average contact force was found to be 385.44 N (Figure 4.15 (a)), the corresponding contact pressure was found to be 499 MPa (Figure 4.15 (b)). The chain link stresses are shown by (Figure 4.15 (a) & (b)). The maximum contact stress on the chain is shown to be 38.41 MPa. This is below the 400 MPa steel yield strength, this shows that the chain has insignificant deformation as it impacts the seabed.

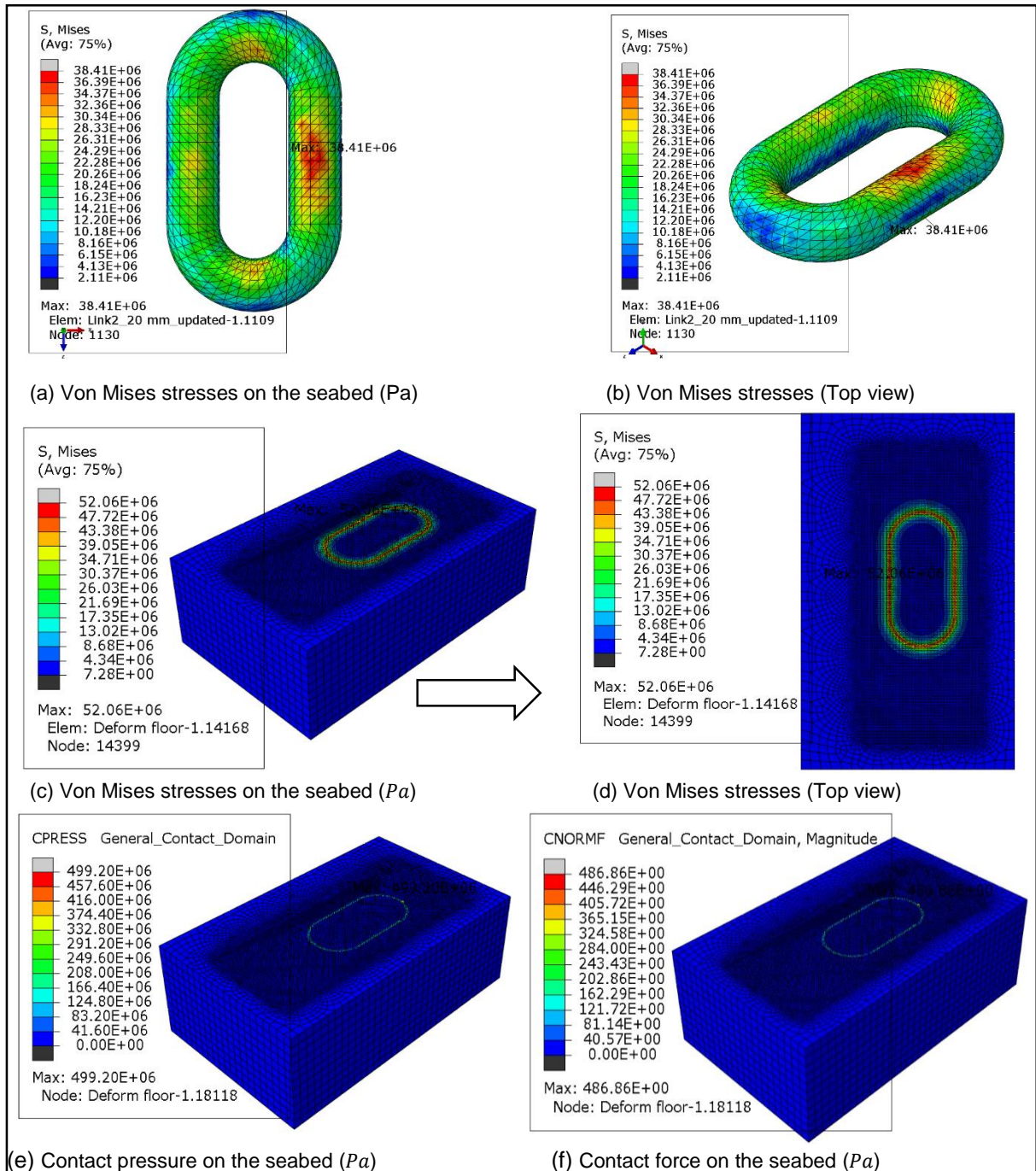


Figure 4.15: Chain link-seabed contact stresses, pressures and forces at 10 m/s for the 20 mm diameter chain

4.1.6.2. 16 mm chain results

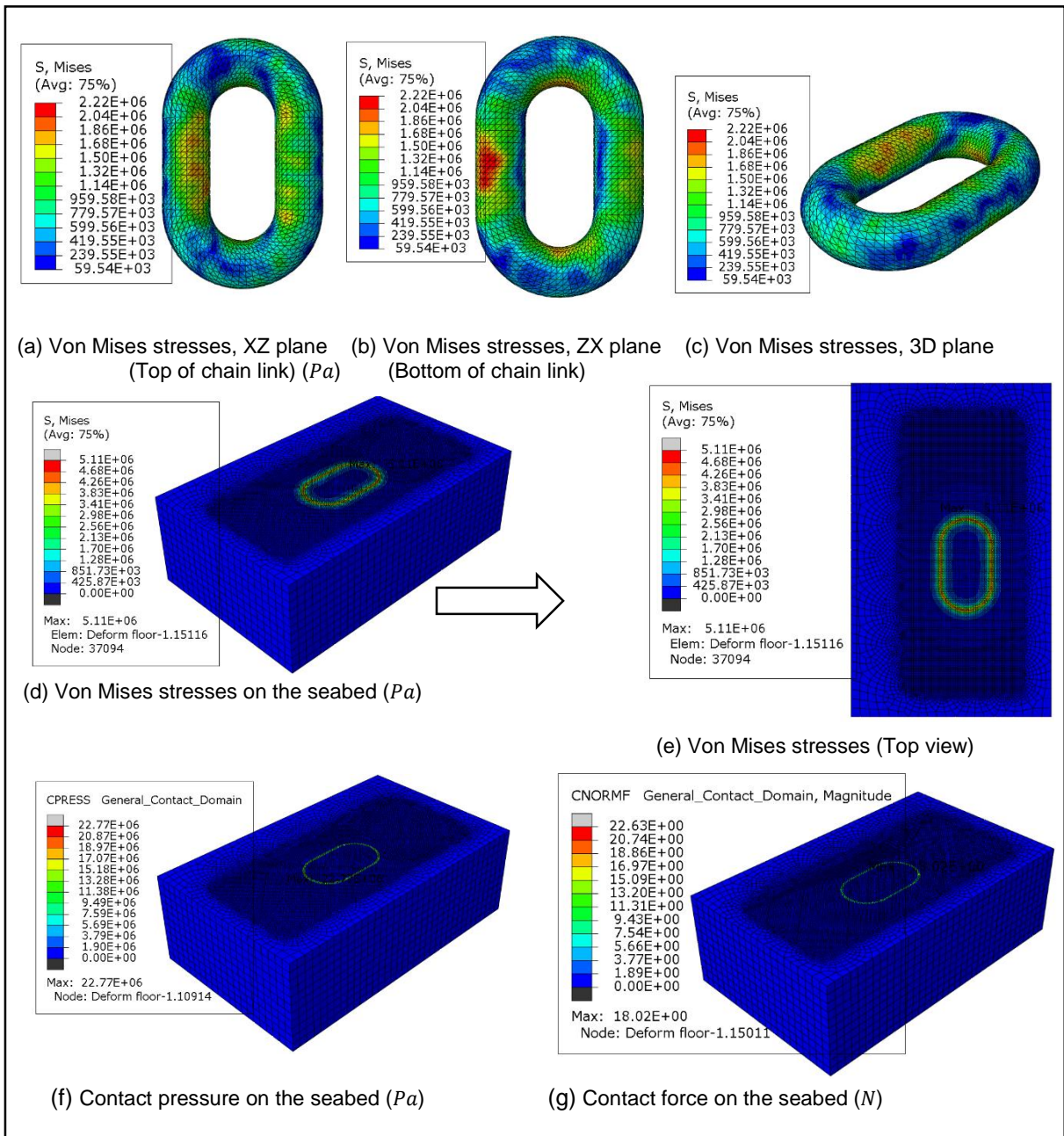


Figure 4.16: Chain link-seabed contact stresses, pressures and forces at 1 m/s for the 16 mm diameter chain

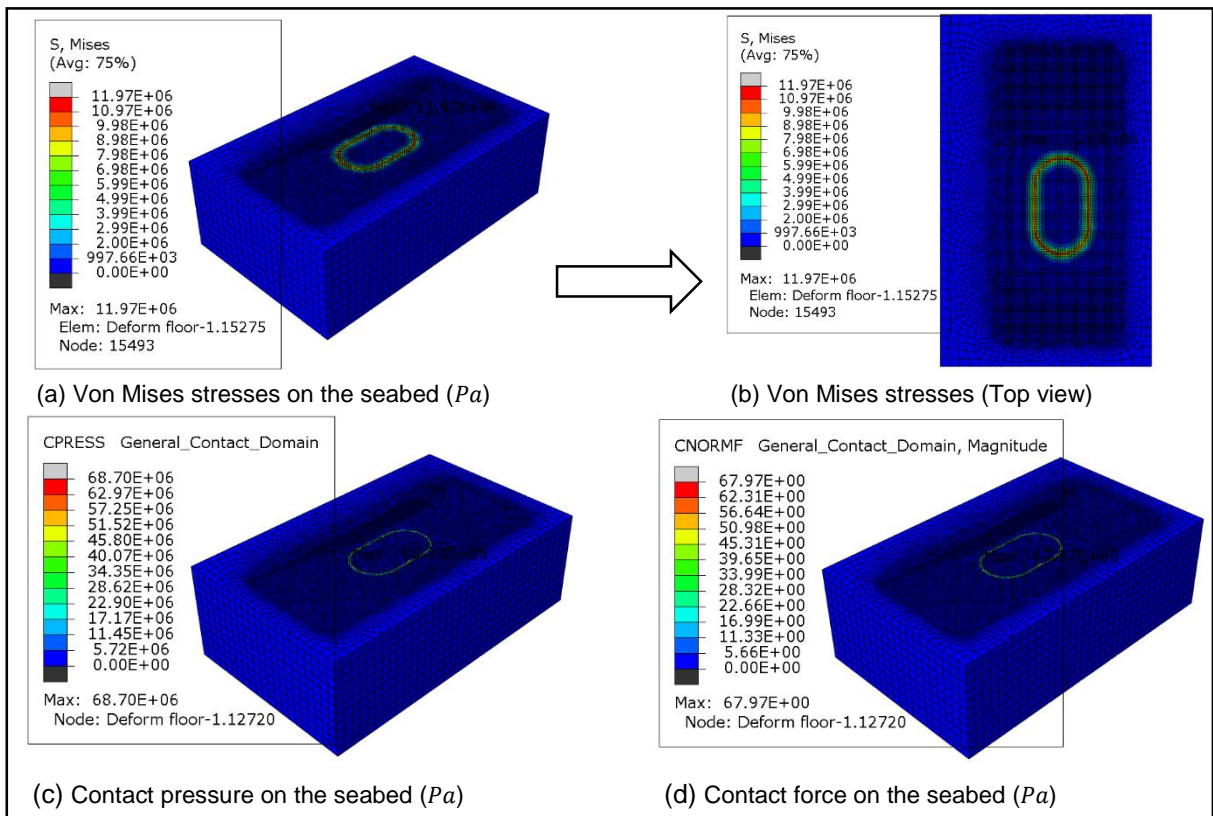


Figure 4.17: Chain link-seabed contact stresses, pressures and forces at 3 m/s for the 16 mm diameter chain

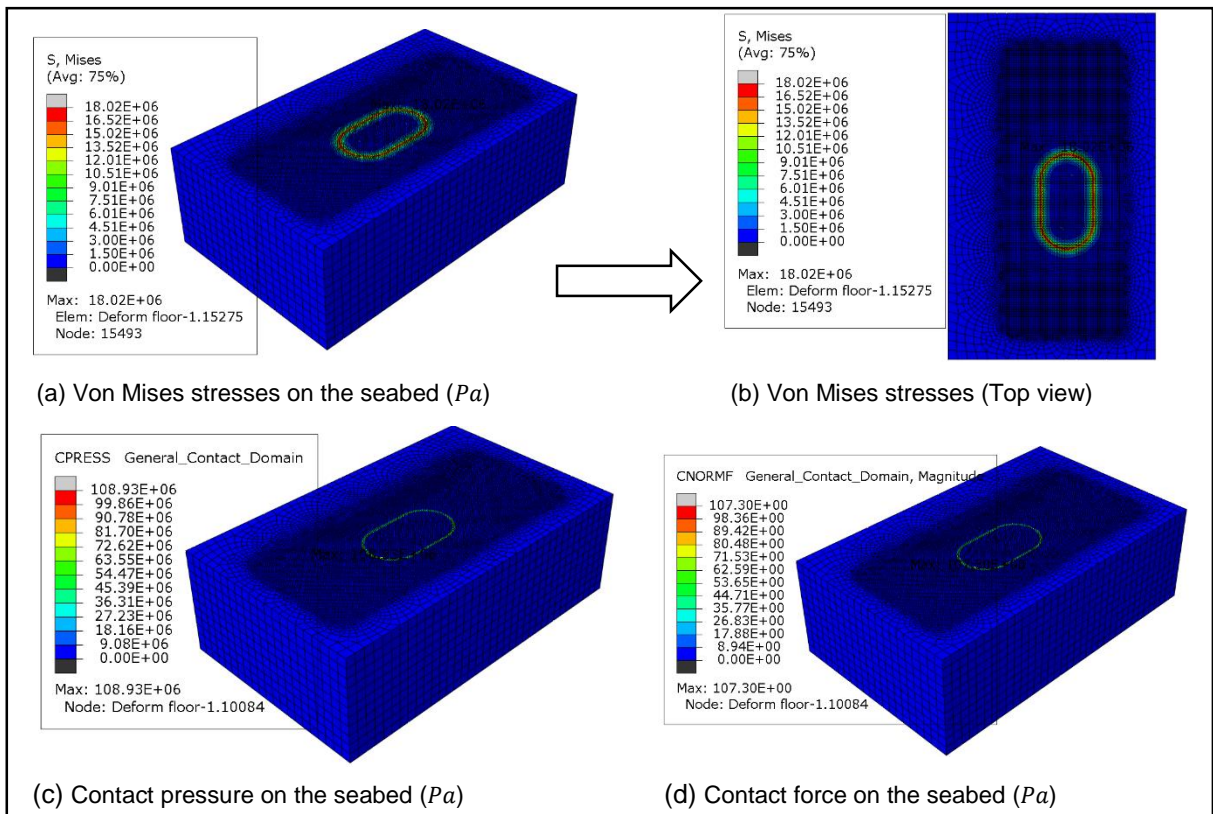


Figure 4.18: Chain link-seabed contact stresses, pressures and forces at 5 m/s for the 16 mm diameter chain

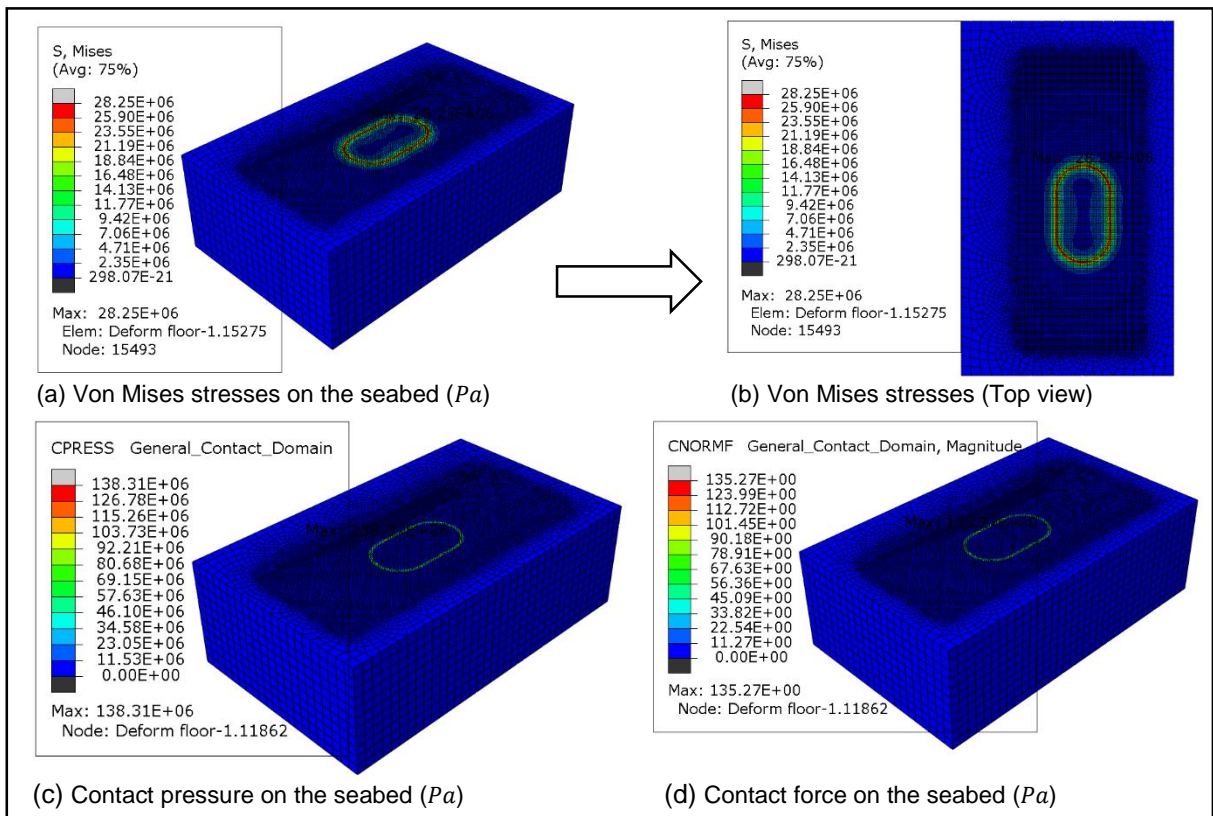


Figure 4.19: Chain link-seabed contact stresses, pressures and forces at 6 m/s for the 16 mm diameter chain

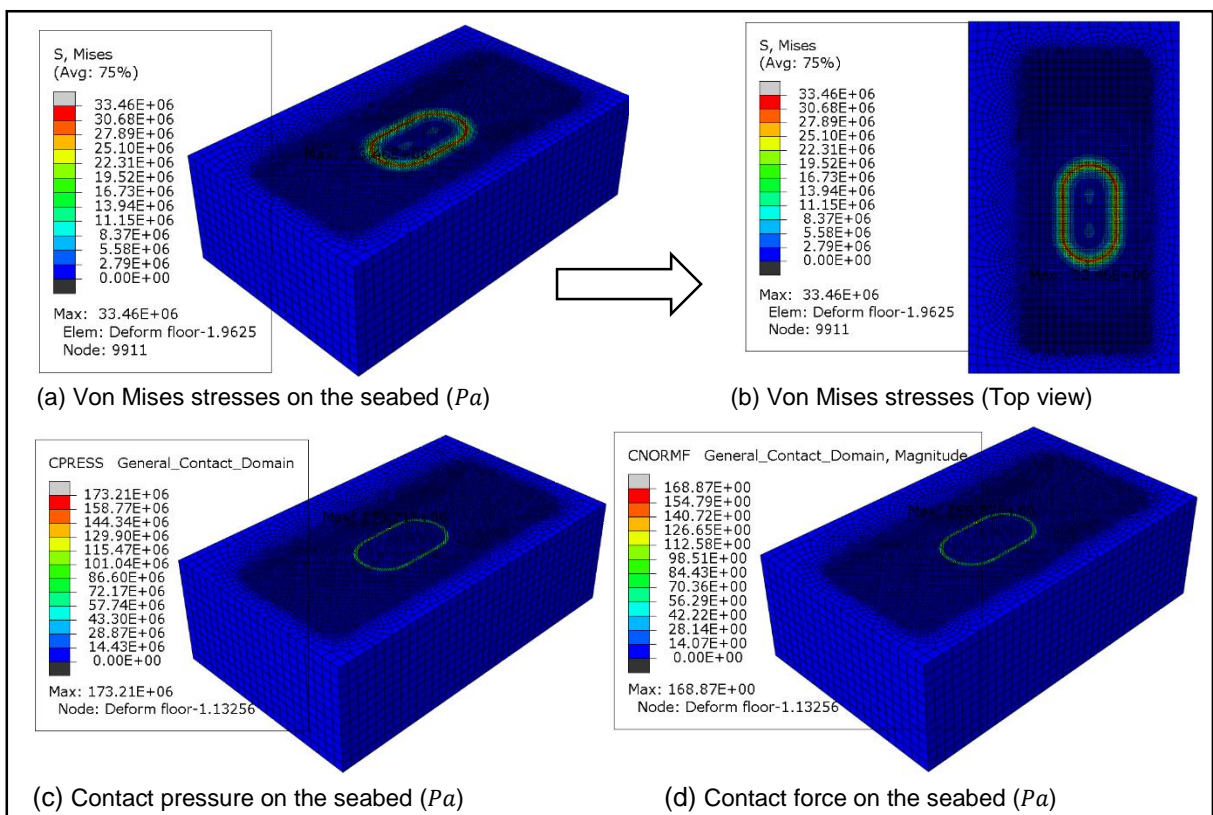


Figure 4.20: Chain link-seabed contact stresses, pressures and forces at 8 m/s for the 16 mm diameter chain

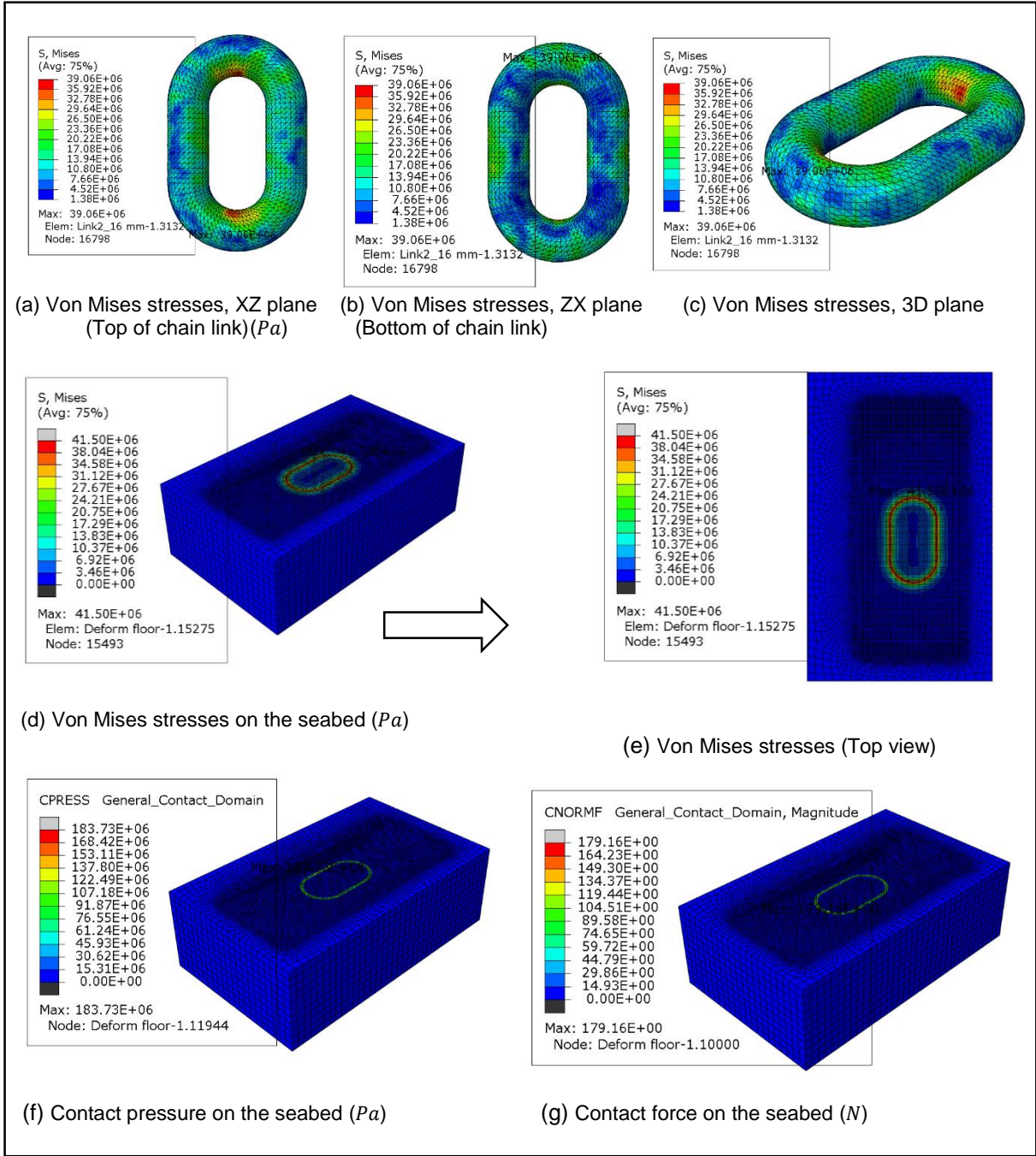


Figure 4.21: Chain link-seabed contact stresses, pressures and forces at 10 m/s for the 16 mm diameter chain

4.1.6.3. 14 mm chain results

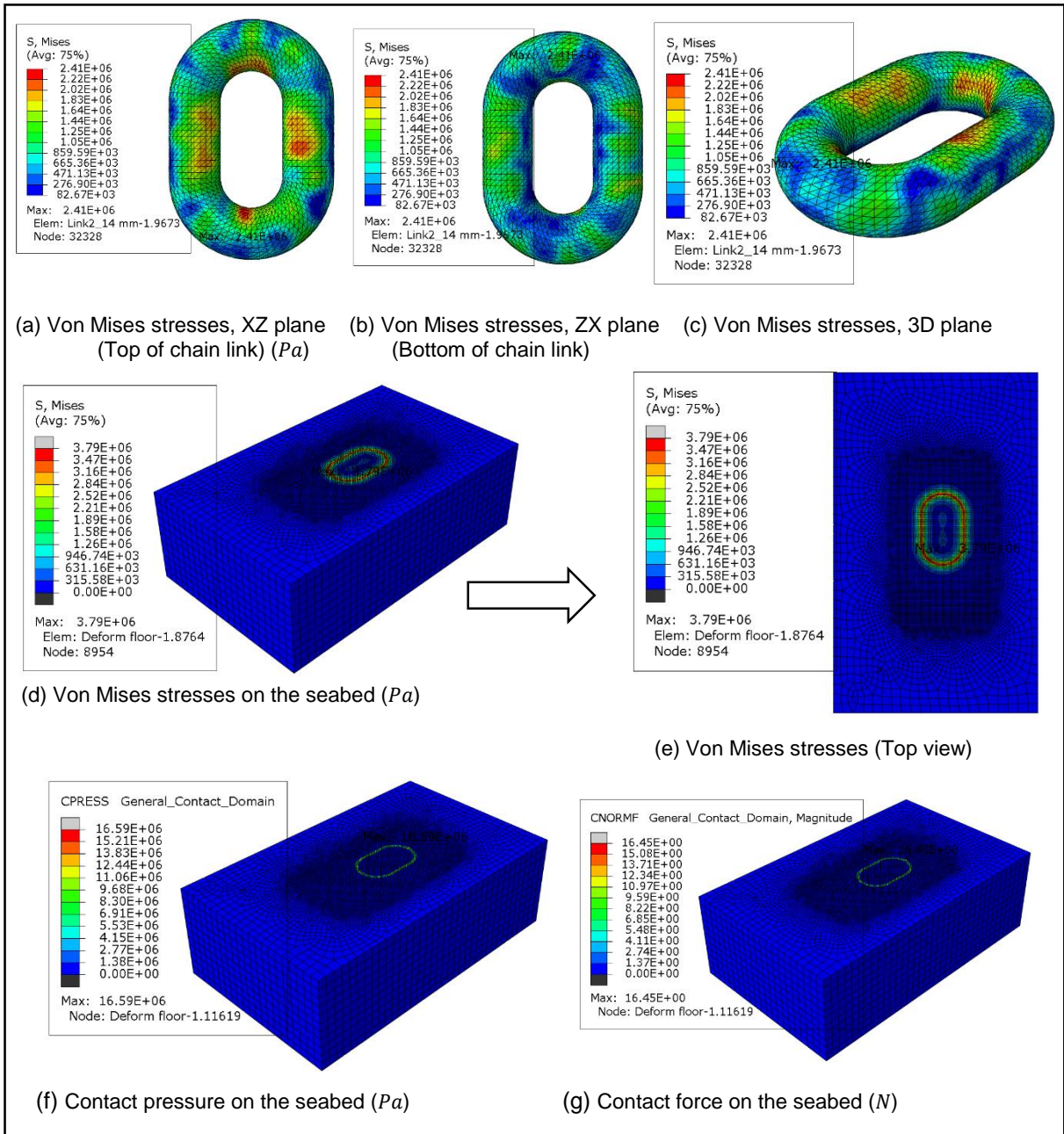


Figure 4.22: Chain link-seabed contact stresses, pressures and forces at 1 m/s for the 14 mm diameter chain

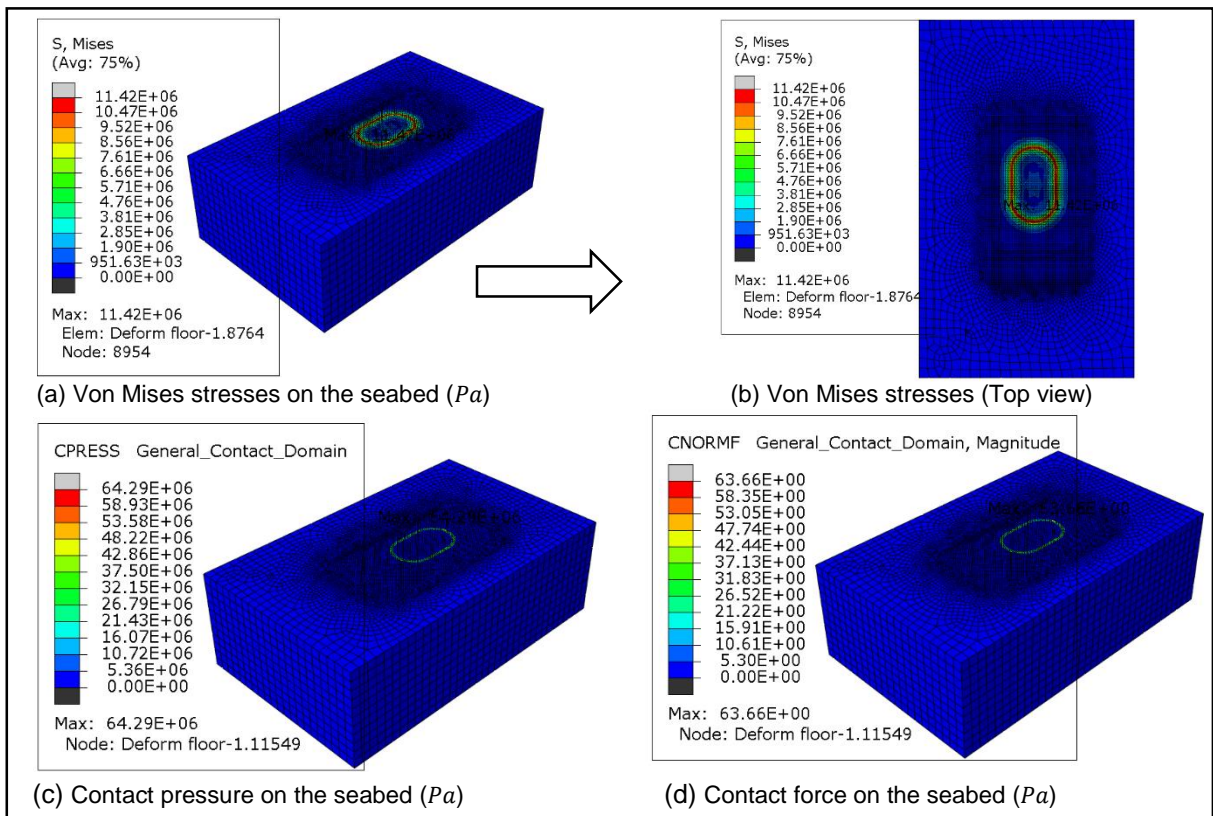


Figure 4.23: Chain link-seabed contact stresses, pressures and forces at 3 m/s for the 14 mm diameter chain

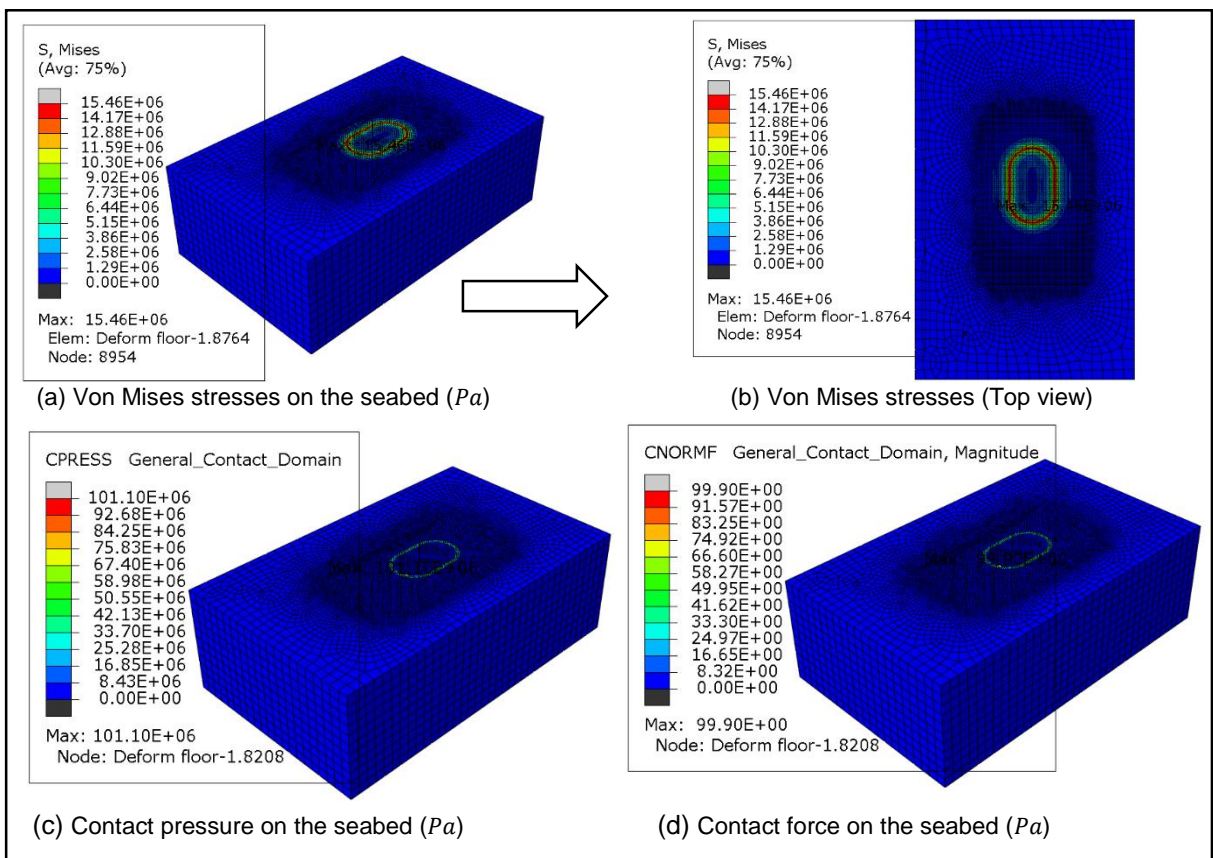


Figure 4.24: Chain link-seabed contact stresses, pressures and forces at 5 m/s for the 14 mm diameter chain

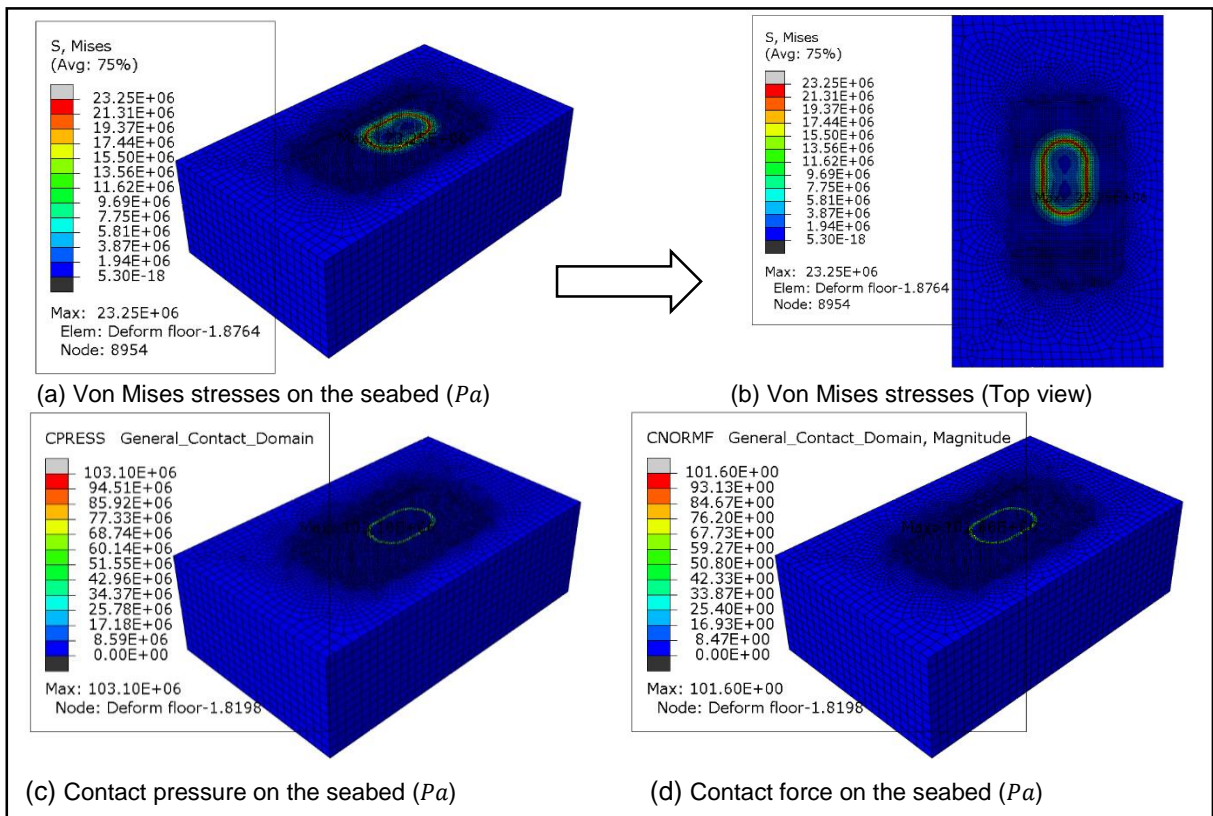


Figure 4.25: Chain link-seabed contact stresses, pressures and forces at 6 m/s for the 14 mm diameter chain

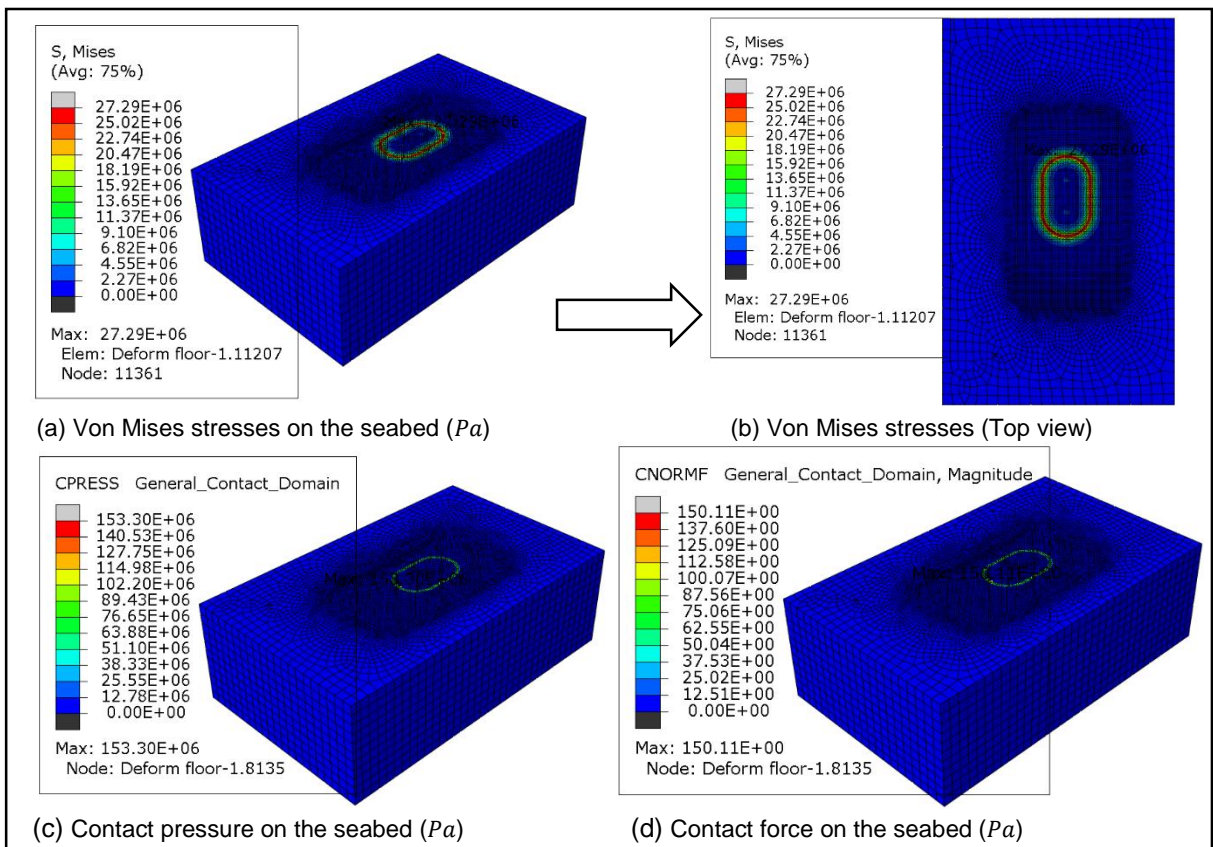


Figure 4.26: Chain link-seabed contact stresses, pressures and forces at 8 m/s for the 14 mm diameter chain

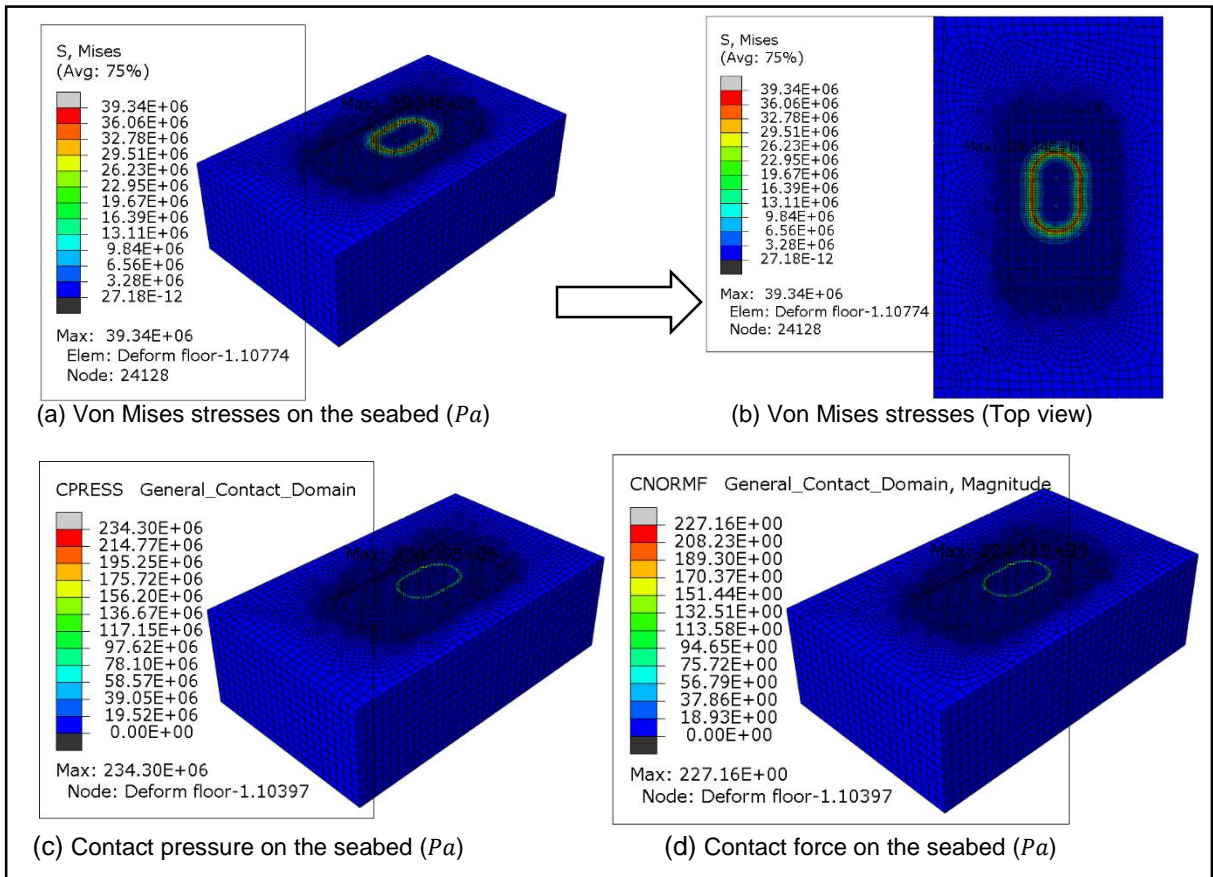


Figure 4.27: Chain link-seabed contact stresses, pressures and forces at 10 m/s for the 14 mm diameter chain

4.1.6.4. Summary of velocity versus contact force graphs and equations

The next Figure 4.28, Figure 4.29 and Figure 4.30 show the velocity plot versus the seabed contact force. As mentioned before, seabed impact velocities of 1, 3, 5, 6, 8 and 10 m/s were analysed by evaluating the 20, 16 and 14 mm diameter chain sizes. The highest seabed contact pressure were observed to occur when the 20 mm diameter was used, this result is what is expected as larger diameter chains have more contact area than smaller chain sizes.

The relationship between the 20 mm chain impact velocity and the seabed contact can be described by a cubic function, obtained by regression, as in the following equation:

Equation 4.1

$$F_{Chain\ link} = 1.2524v^3_{impact} + 17.716v^2_{impact} + 96.61v + 67.912 \dots\dots 20$$

mm chain velocity impact equation

This equation can further be used for predicting seabed contact pressures and forces for other velocity values of interest when the 20 mm diameter chain is used. Likewise, Figure 4.29 (16 mm chain link) and Figure 4.30 (14 mm chain link) have the cubic polynomial regression in the form the following equations:

Equation 4.2

$$F_{Chain\ link} = -0.19v^3_{impact} + 2.333v^2_{impact} + 9.0115v - 8.7346 \dots 16\ mm$$

chain velocity impact equation

Equation 4.3

$$F_{Chain\ link} = 0.4704v^3_{impact} + 6.8862v^2_{impact} + 42.112v - 23.479 \dots 14\ mm$$

chain velocity impact equation

In Figure 4.28, Equation 4.1 can be used for determining the contact force in Newton's and contact pressure in mega Pascal's. This is also true for Figure 4.29 and Figure 4.30.

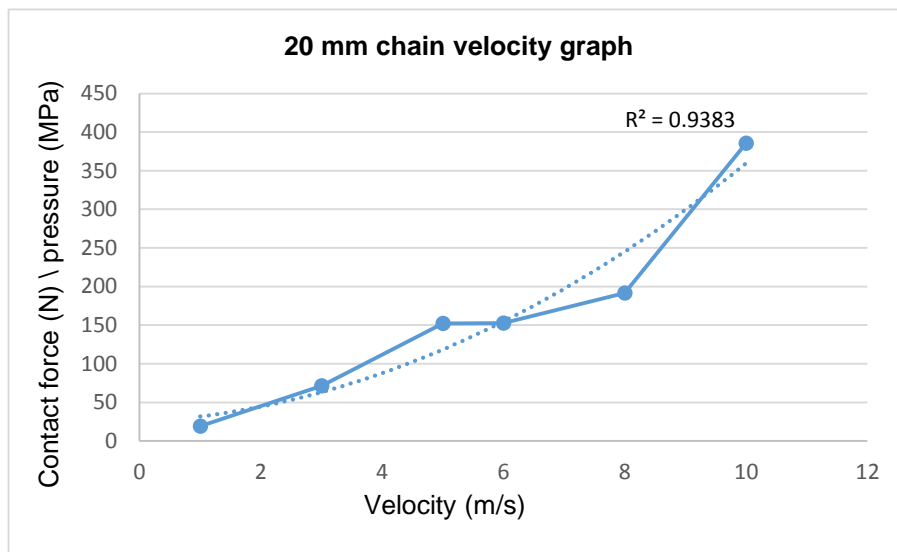


Figure 4.28: Seabed contact forces by the 20 mm chain

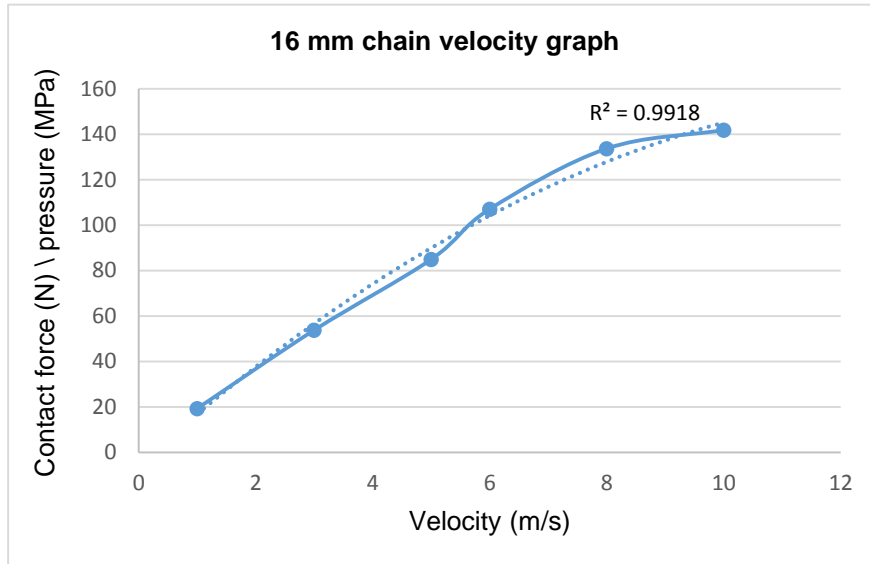


Figure 4.29: Seabed contact forces by the 16 mm chain

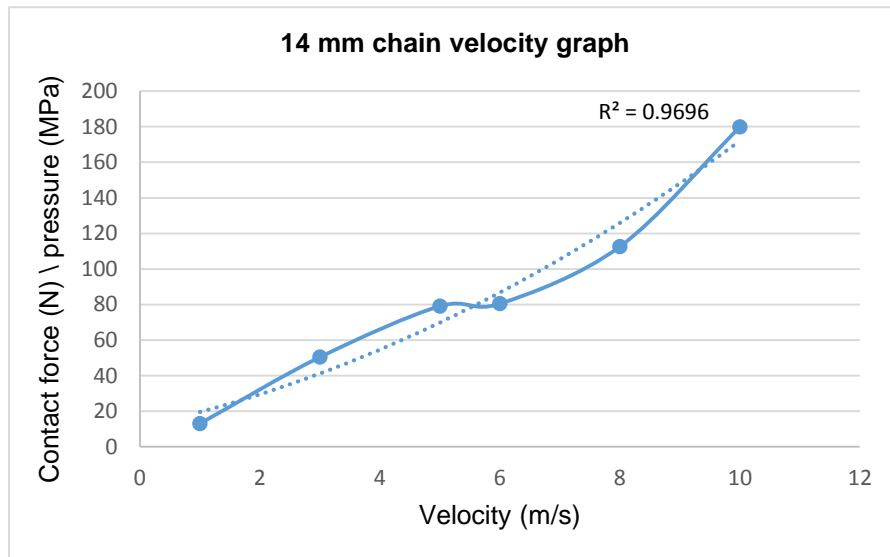


Figure 4.30: Seabed contact forces by the 14 mm chain

The reason we have chosen a cubic polynomial over a linear regression is the apparent point of inflection observed on some of the curves more clearly than others. The reason for the point of inflection is a more complex relationship between the velocity and impact pressure due to the changing surface area in contact as the cylindrical (through the thickness) chain link penetrates the substrate. The changing shape and corresponding surface area change results in a more complex change in pressure and frictional force than a simple linear relationship.

The 20 mm chain link produces the greatest seabed impact force, this was followed by the 16 mm diameter chain link. The 14 mm diameter chain link produced the least seabed impact force. The contact forces for the three chain sizes are all shown in Figure 4.31 below.

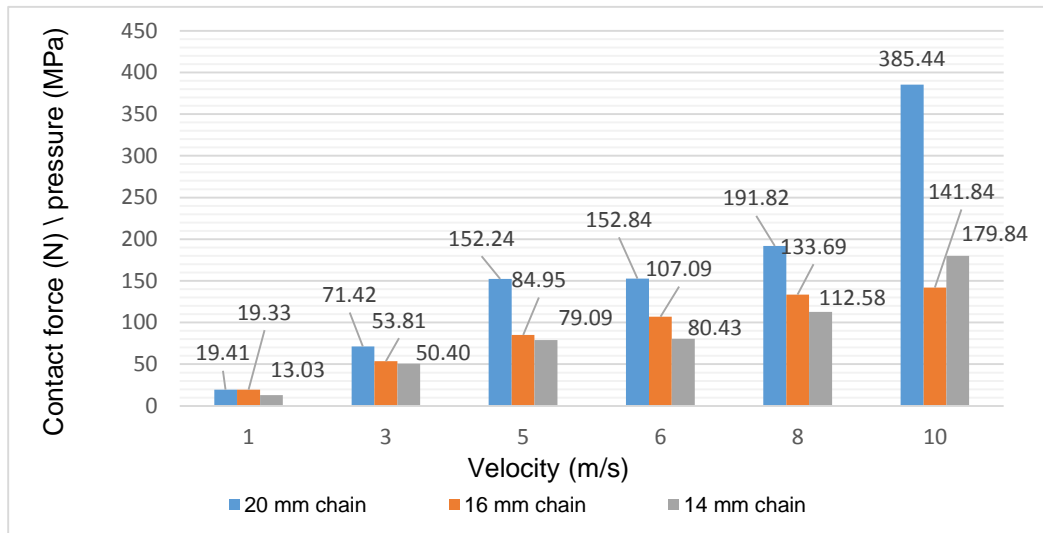


Figure 4.31: Chain link-seabed contact forces (showing the 20, 16 and 14 mm chain links)

4.1.7. Studless chain link seabed contact forces comparison with the slender rod method

Slender rod method is mostly used for simplifying the chain geometry in many offshore engineering numerical simulation codes (Garrett, 1982). The numerical simulation code (ANSYS AQWA) used in this work also uses this method. The mooring chain is represented by a circular section with a constant diameter. This method reduces computational effort required to solve the complex geometry of chain links.

The equivalent diameter of the rod is obtained by $1.8D$, where D is the nominal chain link diameter. In this case the equivalent diameter of the 20 mm chain is 36 mm diameter rod.

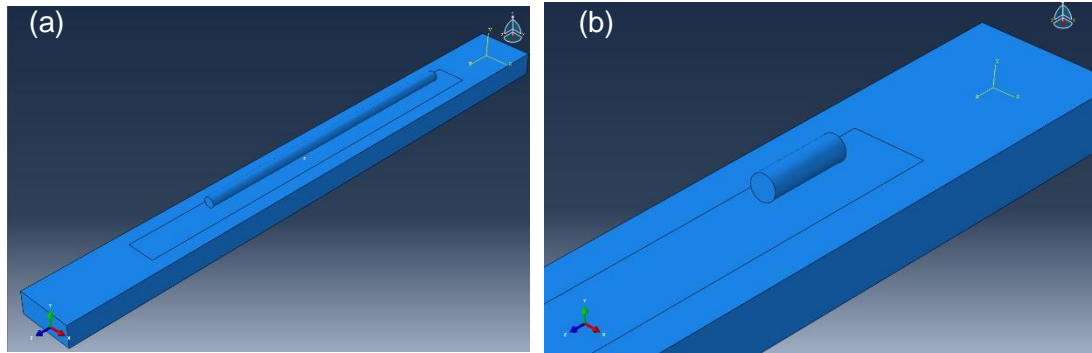


Figure 4.32: 36 mm diameter slender rod (a) 1 m long, (b) 0.12 m long

The next Figure 4.33 shows comparisons of the *ABAQUS* simulation results using 0.12 and 1 m slender rod with the studless chain link. Both slender rods were simulated at 8 m/s using the same simulation procedure as for the single chain link shown previously.

Figure 4.33 shows the following:

- The seabed contact pressure and force are the same for both the 0.12 and 1 m long rods. The maximum contact pressure on the 1 m slender rod is shown to be 323.67 MPa while the 0.12 m long rod is 324.72 MPa. The corresponding maximum contact forces are shown to be 316.31 and 317.19 N for the 1 m and 0.12 m slender rods respectively.
- The seabed contact pressure and force were also found to be similar when comparing the slender rod and the 20 mm studless chain calculated previously. These were found to be 247.81 MPa and 242.3 N contact pressure and force. The comparison between the 0.12 m rod and the 20 mm studless chain contact pressure was found to be 26.87%, while the contact force difference was 26.77%.

This comparison above shows that the slender rod method overestimates the contact pressure and force by about 27%. This difference may be due to the difference in the contact cross-sectional area of the slender rod and the surface contact area of the studless chain link.

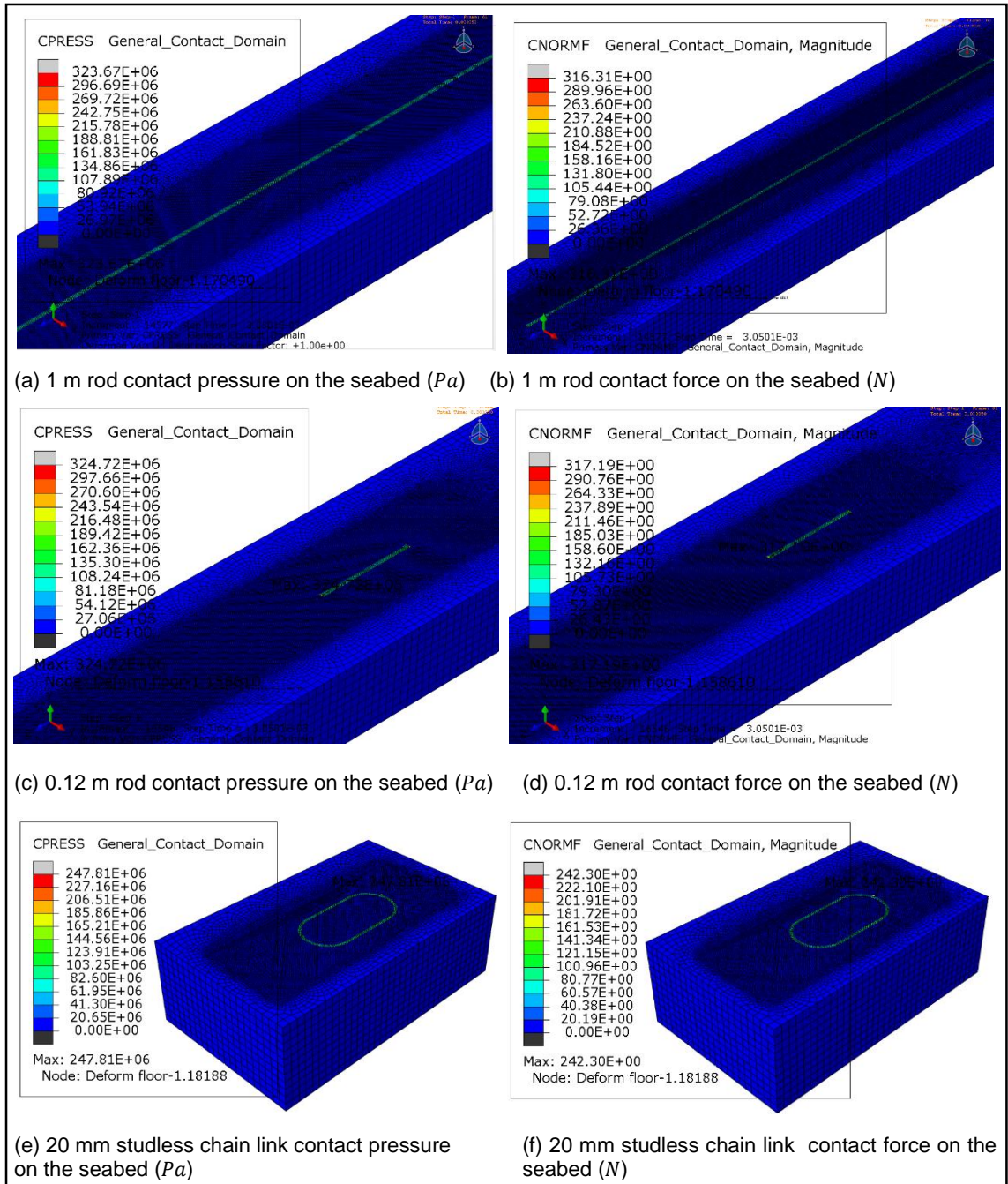


Figure 4.33: Contact pressure and force at 8 m/s on seabed using (a) & (b) 1 m rod, (c) & (d) 0.12 m rod and (e) & (f) studless chain link

4.2. ANSYS AQWA model description and setup

This section presents a description of the ANSYS AQWA modelling procedure in detail. It also presents the model setup with the input data used in this study.

4.2.1. ANSYS AQWA simulation procedure description

The simulation procedure in ANSYS AQWA for the moored vessel can be summarised by separating the model setup in four stages i.e. 1) Vessel construction, which is obtained from the constructed CAD model, 2) Input data, which is the pre-processing stage, 3) Simulation stage where the model input data are solved and 4) Result Analysis, where the moored vessel response is obtained. These stages are shown Figure 4.34.

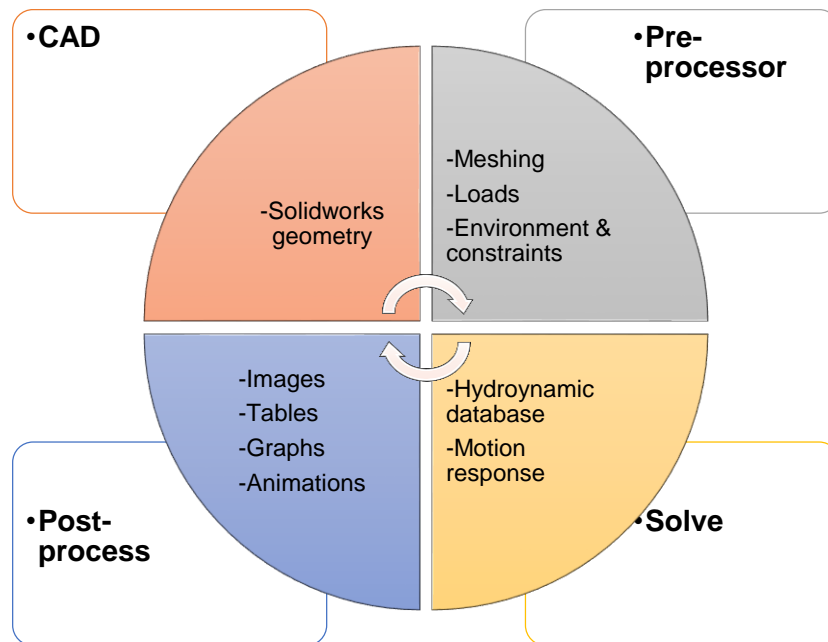


Figure 4.34: ANSYS AQWA Hydrodynamic Simulation Procedure

ANSYS AQWA Workbench interface is shown in Figure 4.35. It shows workflow defining a system of analysis. The Hydrodynamic Diffraction is the pre-processor stage where Hydrostatic Results of the vessel are determined. This stage comprises of defining the mass distribution of the imported CAD geometry and defining the mass distribution of the vessel. The Hydrodynamic Diffraction static results are then obtained which include the Centre of Gravity (CoG) Position of the vessel, Centre of Buoyancy (CoB) Position and Metacentric Heights which are the measurement of the initial static stability of a floating vessel.

The Static Response stage analyses the initial equilibrium position of the moored vessel. It determines the vessel starting position before the simulation is run. Both Hydrodynamic Diffraction and Static Response results are used as input data for the Time Domain response stage. The Time Domain Response is the dynamic analysis stage where sea conditions are applied i.e. ocean waves and currents. The wave can either be regular or irregular waves. This study selected irregular waves as they best represent the real world behaviour of ocean waves. The time-history of the vessel position, velocity, acceleration, structural forces and mooring forces results are obtained.

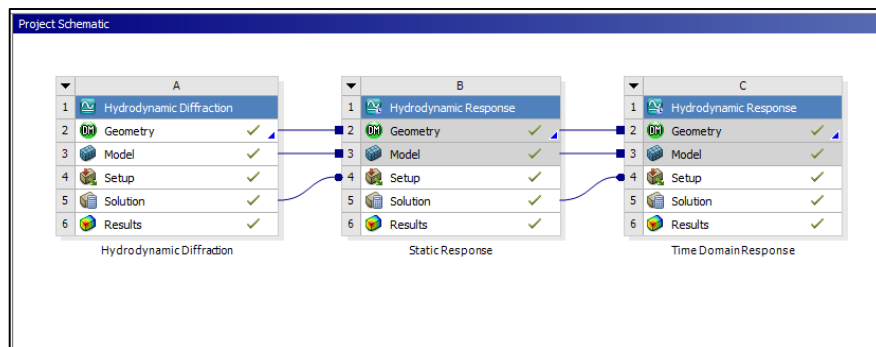


Figure 4.35: ANSYS AQWA Workbench project schematic

Figure 4.36 shows two sets of axes used in ANSYS AQWA. They are the FRA (Fixed Reference Axes) and the LSA (Local Set of Axes). The FRA is the Global Axis System. This system has its origin on the mean water surface with Z axis pointing upwards, X and Y on the mean water surface. The mean water surface is at Z=0. This axis system does not move at any stage of the ANSYS AQWA analysis.

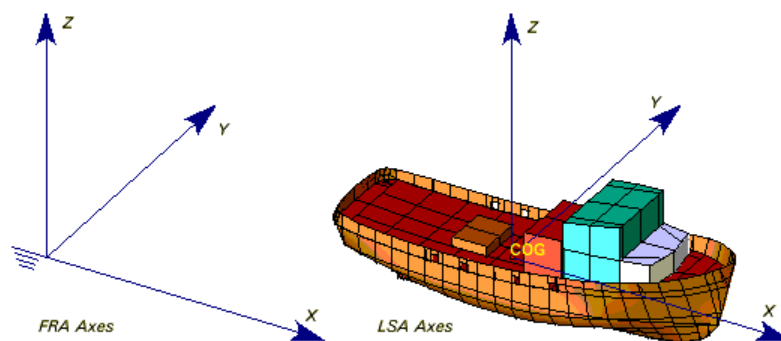


Figure 4.36: Axes Systems

(Adapted from ANSYS Aqwa Theory Manual, 2015)

The Local System Axis (LSA) has its origin at the CoG of the vessel, with X, Y and Z axes parallel to the FRA when the vessel is in its initial definition position. X is along the length of the vessel shown above, Y along the beam to port, and Z in the direction of the cross product of X and Y. This axis system moves with the vessel.

The following steps were followed when setting up a model in ANSYS AQWA:

- a) Geometry is attached – The CAD models of the both the 22 m and the 14 m vessels were constructed in Solidworks using surfaces; the models were then exported to ANSYS AQWA. (See Appendix C for 3D models).
- b) Surface body definition – This was done in ANSYS AQWA ‘Design modeller’ where the imported CAD geometry waterline was defined by splitting the geometry into Upper Hull and Lower Hull. ANSYS AQWA only process surface and line bodies, hence the CAD model was constructed in Solidworks using surface bodies instead of solid bodies. Surface bodies are areas that can be meshed to create diffracting (submerged lower hull) or non-diffracting elements (the exposed part of the vessel). Figure 4.37 shows Lower Hull of a vessel below the water line.

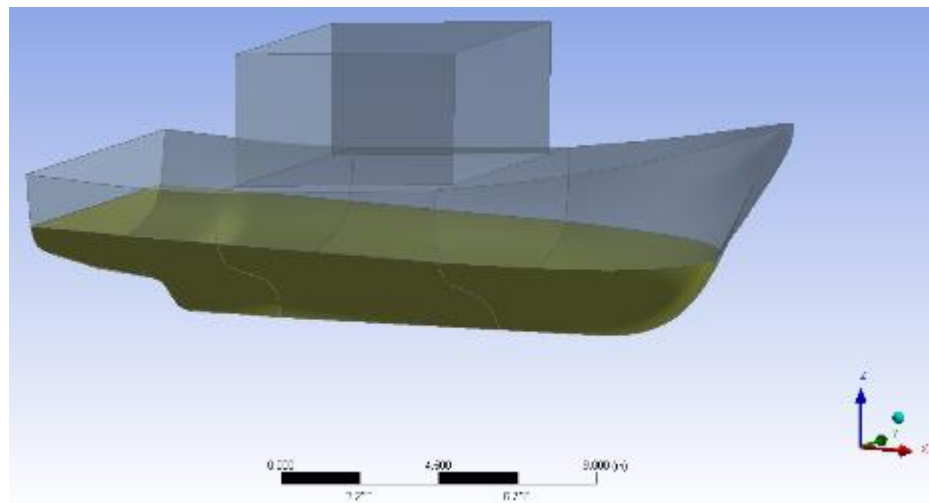


Figure 4.37: Fishing vessel cut at the waterline (vessel Lower Hull in yellow and Upper Hull in grey).

- c) Point mass definition - point mass is the mass inertia matrix that is defined via the Radius of Gyration of the vessel. It defines the centre of mass of the vessel in x , y and z coordinates. The mass distribution of the vessel (mass inertia matrix) is defined by $K_{xx} = 0.34 * width\ of\ the\ vessel$, $K_{yy} = 0.25 * length\ of\ the\ vessel$ and $K_{zz} = 2.6 *$

length of the vessel. The vessel mass is defined in *kg*. Figure 4.38 shows centre of mass of the vessel indicated by the green sphere.

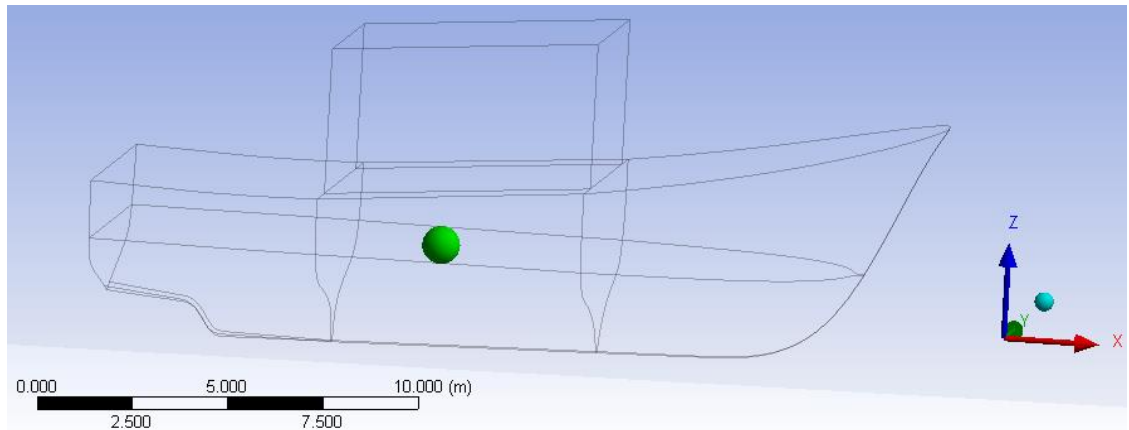


Figure 4.38: Vessel centre of mass

- d) Point Buoyancy – is defined by the submerged volume of the Lower Hull of the vessel.
- e) Definition of connections to the vessel – a non-linear catenary section is selected as it best represents the complex geometry of the mooring chain. The mooring chain is simplified as a cable with equivalent section properties. The catenary data is then defined after selecting non-linear catenary section option. This is where chain properties are defined i.e. mass/unit length, equivalent cross-sectional area and diameter, stiffness which is defined by EA (E is the elastic modulus and A the cross-sectional area) and drag coefficients of the chain.
- f) The model connection points where the mooring chain is connected are then defined; the vessel anchor which is located on the seabed is defined as a fixed point. This point is defined by x , y and z coordinates. The fairlead point is attached at the bow of the vessel and is also defined by x , y and z coordinates; this point moves relative to the vessel motions.
- g) Mesh – the vessel surface body was meshed in ANSYS AQWA Hydrodynamic Diffraction stage. Figure 4.39 shows the meshed 22 *m* vessel. The mesh is responsible for discretising the vessel into elements and nodes where loads are applied. ANSYS AQWA has a limit of 40 000 elements for the floating object, of these, 30 000 may be diffracting elements. The mooring chain has a limit of 250 elements, most studies use 100 elements for discretising the mooring line.

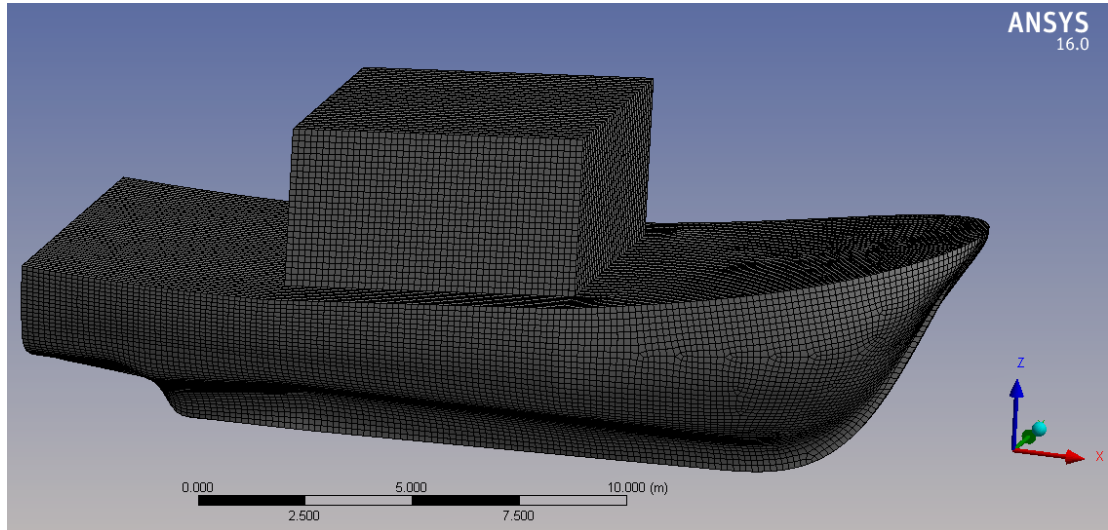


Figure 4.39: Meshed vessel (22 m vessel)

The table below shows the types of elements that are used in ANSYS AQWA and their description.

Table 4.4: Element types in ANSYS AQWA

Element type	Description	No of Nodes	Material Property	Geometric Property
QPPL	Quadrilateral Panel	4	None	None
TPPL	Triangular Panel	3	None	None
PMAS	Point Mass	1	Mass	Inertia
PBOY	Point Buoyancy	1	Displaced mass	None
TUBE	Tube	2	Density	Geometry
STUB	Slender Tube	3	Mas and inertia	Geometry
FPNT	Field Point	1	None	None
DISC	Circular Disc	2	None	Geometry

QPPL: This element generates pressure and hydrostatic forces only on the hull of the vessel. Quadrilateral pressure plate of zero thickness.

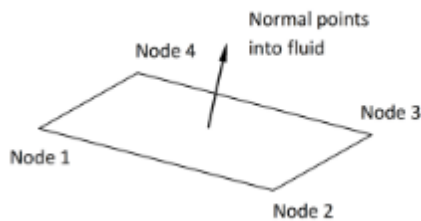


Figure 4.40: Quadrilateral Panel element (QPPL)

TPPL: This element generates pressure and hydrostatic forces only on the hull of the vessel. Triangular pressure plate of zero thickness.

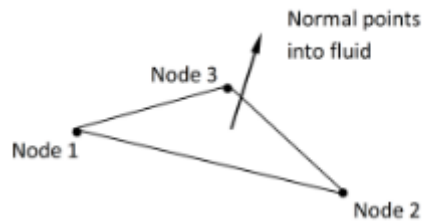


Figure 4.41: Triangular Panel element (TPPL)

PMAS: The PMAS element generates mass forces only. Point mass element having internal mass with the centre of mass coincident with a given node and specified values of second moments of mass inertia.

PBOY: The PBOY element generates hydrostatic displacement forces only on the hull of the vessel. This is an external point buoyancy element without mass.

DISC: The DISC element has a drag coefficient and added mass coefficient in its normal direction. When the mass is defined, it can be assigned geometry. This can be used to define the mooring line cross-section.

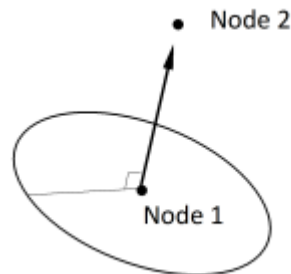


Figure 4.42: The DISC Element

TUBE: Tubular element with uniform circular cross-section and constant wall thickness. Forces on this element are calculated using Morison's equation.

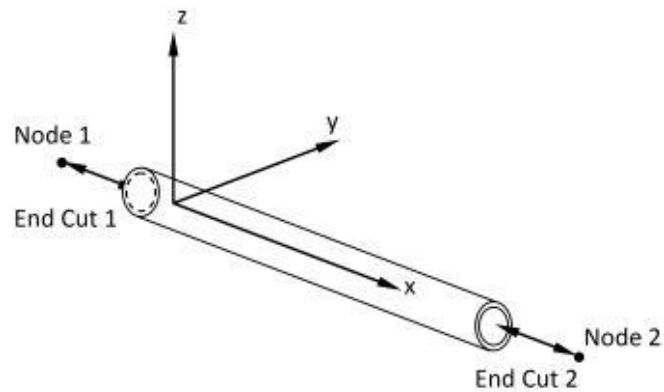


Figure 4.43: The TUBE Element

FPNT: The FPNT Element defines the external fluid field point element used to define the fairlead attachment point. This element gives the pressure head amplitude at a specified point in the external fluid domain. FPNT elements are defined in the local axes and move with the structure in which they are defined. The anchor is defined as a fixed point.

- h) Hydrodynamic Diffraction – this stage allows the user to obtain hydrostatic results of the vessel using wave frequencies and directions. Various parameters can be evaluated which include Diffraction and Radiation forces on the vessel, structural damping, Response Amplitude Operators (RAOAs), hull pressure and motions, Centre of Gravity (CoG) Position globally, Surge, Sway, Heave, Roll, Pitch, and Yaw, the Centre of Buoyancy (CoB) Position of the vessel, Out of Balance Forces/Weight and Small Angle Stability Parameters such as Metacentric Heights (GMX/GMY) and Metacentric Heights (GMX/GMY).
- i) Static Response – the static response analysis calculates the equilibrium configuration of the vessel and forms the basis for the dynamic analysis stage (Time Domain Response) of the moored vessel.
- j) Time Domain Response – the ‘Irregular Wave Response’ setting is selected in order to apply the Irregular wave type on this stage. The current profile is also defined. The time-history of the vessel’s position, velocity, acceleration, structural forces and mooring forces are obtained in this stage. ANSYS AQWA has several predefined wave models for representing various sea conditions.

4.2.2. ANSYS AQWA model setup

Figure 4.44 below shows an example of the 22 m vessel single-point mooring system in ANSYS AQWA environment. The dark blue arrow indicates the wave applied in the X –direction, and the purple lines show the current direction and speed. The current is shown to be defined at the origin. The yellow round object is a clump weight of negligible mass used as a reference point for tracking the motion of the chain.

Figure 4.44 also shows the coordinate system that will be used to present results. The X –direction represents the horizontal displacement (surge), taken as positive forwards; Y - lateral (sway), positive to the port side, and Z -the vertical displacement (heave), positive upwards. The displacements of the vessel are calculated from its centre of gravity. The 22 m vessel geometry was meshed using 29 566 fine elements.

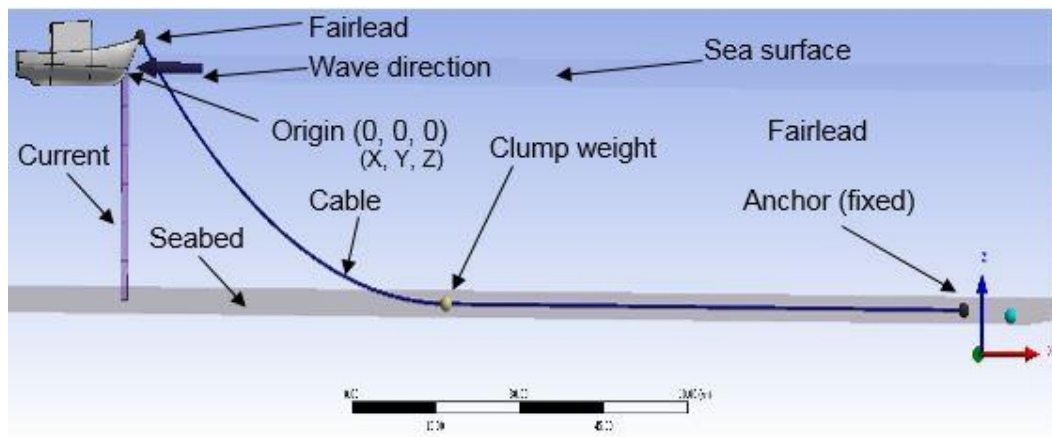


Figure 4.44: Single-point moored 22 m vessel

Table 4.5 shows properties of the 22 m vessel ‘Point Mass’ for defining the distribution of the centre of mass. (The detailed dimensions of the 22 m vessel can be found in Appendix C). The vessel parameters calculation are show in Appendix F.

Table 4.5: 22 m vessel properties

Parameter	Value	Units
Vessel dimensions	22 (Length) x 8.7 (width) x 4.45 (depth)	<i>m</i>
K_{xx}	2.72	<i>m</i>
K_{yy}	5.5	<i>m</i>
K_{zz}	5.72	<i>m</i>
Mass	123 000	<i>kg</i>

The 22 m vessel connection points are shown in Table 4.6 below.

Table 4.6: Single-point mooring anchor coordinates for the 22 m vessel

Name	Coordinates		
	x (m)	y (m)	z (m)
Anchor 1	150	-100	-30
Fairlead 1	0	0	4

Figure 4.45 below shows an example the 14 m vessel single-point mooring system in ANSYS AQWA environment. The vessel geometry was meshed using 15 983 fine elements. (The detailed dimensions of the 14 m vessel can also be found in Appendix C).

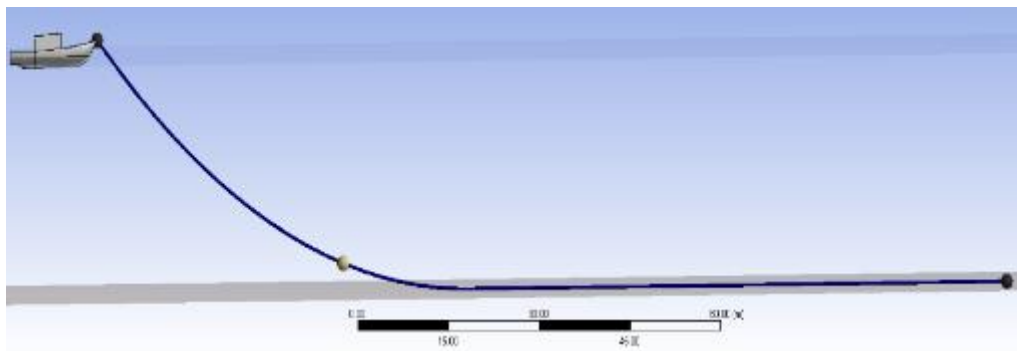


Figure 4.45: Single-point moored 14 m vessel

Table 4.7 below shows the 14 m vessel properties for defining the distribution of the centre of mass. The vessel parameters calculation are show in Appendix F.

Table 4.7: 14 m vessel properties

Parameter	Value	Units
Vessel dimensions	14 (Length) x 5 (width) x 2.2 (depth)	m
K_{xx}	1.7	m
K_{yy}	3.5	m
K_{zz}	3.64	m
Mass	35 000	kg

The 14 m vessel connection points are shown in Table 4.8 below.

Table 4.8: Single-point mooring anchor coordinates for the 14 m vessel

Name	Coordinates		
	x (m)	y (m)	z (m)
Anchor 1	150	-100	-30
Fairlead 1	0	0	2

The following Table 4.9 shows the mechanical properties of the 20, 16 and 14 mm diameter chain sizes. The mooring chain drag coefficients were obtained from the ‘Offshore Standard ‘DNV-OS-E301’ document which recommends a normal drag coefficient of 2.4 and axial drag coefficient of 1.15 for the studless chain without marine growth (DNV, 2010).

The ANSYS AQWA computational model assumes that the mooring chain is a line with a constant circular section, the equivalent chain properties were derived based on derivations from OrcaFlex shown in Table 4.9. (OrcaFlex is a dynamic analysis tool for offshore marine systems). The chain link bending stiffness has been set to zero assuming that the links are subjected to very small moments (OrcaFlex, 2010). The vessel parameters calculation are show in Appendix F. Appendix A shows the mechanical properties of the type chain used.

Table 4.9: Mooring chains mechanical properties

The properties of an equivalent Cable connection				
Chain diameter (D), mm	OrcaFlex derivation	20	16	14
Equivalent Diameter, (m)	1.8D	0.036	0.029	0.025
Mass/unit length (kg/m)	19.9 D ²	7.96	5.09	3.9
Equivalent Cross-Sectional Area (m ²)	-	6.28E-04	4.02E-04	3.08E-04
Stiffness, EA	0.85 × 10 ⁸ D ²	3.42E+07	2.19E+07	1.67E+07
Minimum break load (N)	-	2.51E+05	1.61E+05	1.23E+05
Added Mass Coefficient	-	1	1	1
Transverse Drag Coefficient	-	2.4	2.4	2.4
Longitudinal Coefficient	-	1.15	1.15	1.15
Chain length (m)		160	160	160
Chain No. elements		250	250	250

The minimum breaking load of the mooring chain was obtained from the manufacture’s catalogue which can be found in Appendix A. The minimum breaking load describes failure condition of the chain. The failure condition is defined by Equation 4.1.

Equation 4.1

$$F_{Chain\ max\ tension} > F_{Minimum\ break\ load}$$

If the tension on the mooring line exceeds the minimum breaking load, the chain will fail or break. This condition was monitored to check whether the chains fails for the analyses in this study.

Table 4.10 below shows the ocean environment conditions selected for all the types of analysis in this study. The Pierson-Moskowitz Irregular wave spectrum was selected for modelling ocean waves. This wave type is considered as a developed sea state and is a good approximation of variable and complex ocean waves. Wave height and period were varied in some analysis; therefore, they were left out of the table. These will be specified for each type analysis in this study.

Table 4.10: Ocean environment data

Parameter	Value	Units
Water Density	1025	kg/m^3
Ocean Depth	30	m
Wave Type	Pierson-Moskowitz (Irregular wave)	-
Direction of spectrum	180	°
Current speed (Uniform)	1	m/s

The simulation duration of 1200 s (20 minutes) and a time step of 0.1 s were used, this was to ensure the dynamics of the mooring line impacting the seabed is well captured. (The sea depth was obtained from skippers during site visit).

4.3. ANSYS AQWA model simulation results

The section presents the ANSYS AQWA model results. Firstly, the ANSYS AQWA model velocity is correlated to the measured underwater chain velocity. Secondly, the effect of varying wave height and period mooring line impact on the seabed is investigated. Thirdly, three mooring line configurations are studied for investigating their effect on the seabed. Lastly, three mooring chain sizes are varied for studying their effect on the seabed. The section also presents comparisons between the effects of the single-point versus the two-point mooring systems.

4.3.1. ANSYS AQWA model correlation with underwater chain velocity

The ANSYS AQWA model was calibrated by correlating it with the underwater chain velocity obtained in Chapter 3.4. The calibration was done by varying the wave height and period while other parameters were kept constant (this effect is fully investigated in Chapter 4.3.2). Four points along the mooring line which constantly made contact with the seabed during the simulation were tracked. The video analysis procedure described in Chapter 3.4 for tracking points in contact was used. This correlation between the underwater video analysis velocity and ANSYS AQWA model velocity can also be used for estimating realistic sea conditions.

For this analysis, both the 14 and 22 m vessels were simulated. Figure 4.46 and Figure 4.47 shows the mooring line profiles of both vessels which were anchored using the 20 mm diameter chain. The mooring line motion in the ANSYS AQWA model was observed to behave similarly to the mooring line motion observed from the underwater video footage.

The simulated single-point mooring system on the 22 m vessel has been stored on the following: <https://www.youtube.com/watch?v=IYRUDWr3ZT4&t=13s>.

The simulated single-point mooring system on the 14 m vessel has been stored on the following: <https://www.youtube.com/watch?v=rpVwcQ7WbSc>.

In Figure 4.46, the mooring line profile and tension with a time stamp are shown for 22 m single-point moored vessel for the simulation of 1200 s. The vertical (in Z direction) and horizontal (in X direction) components of tension are shown. The lateral (in the Y -direction) tension values has been left out as they were found insignificant. Figure 4.47 also shows the same results on the 14 m vessel.

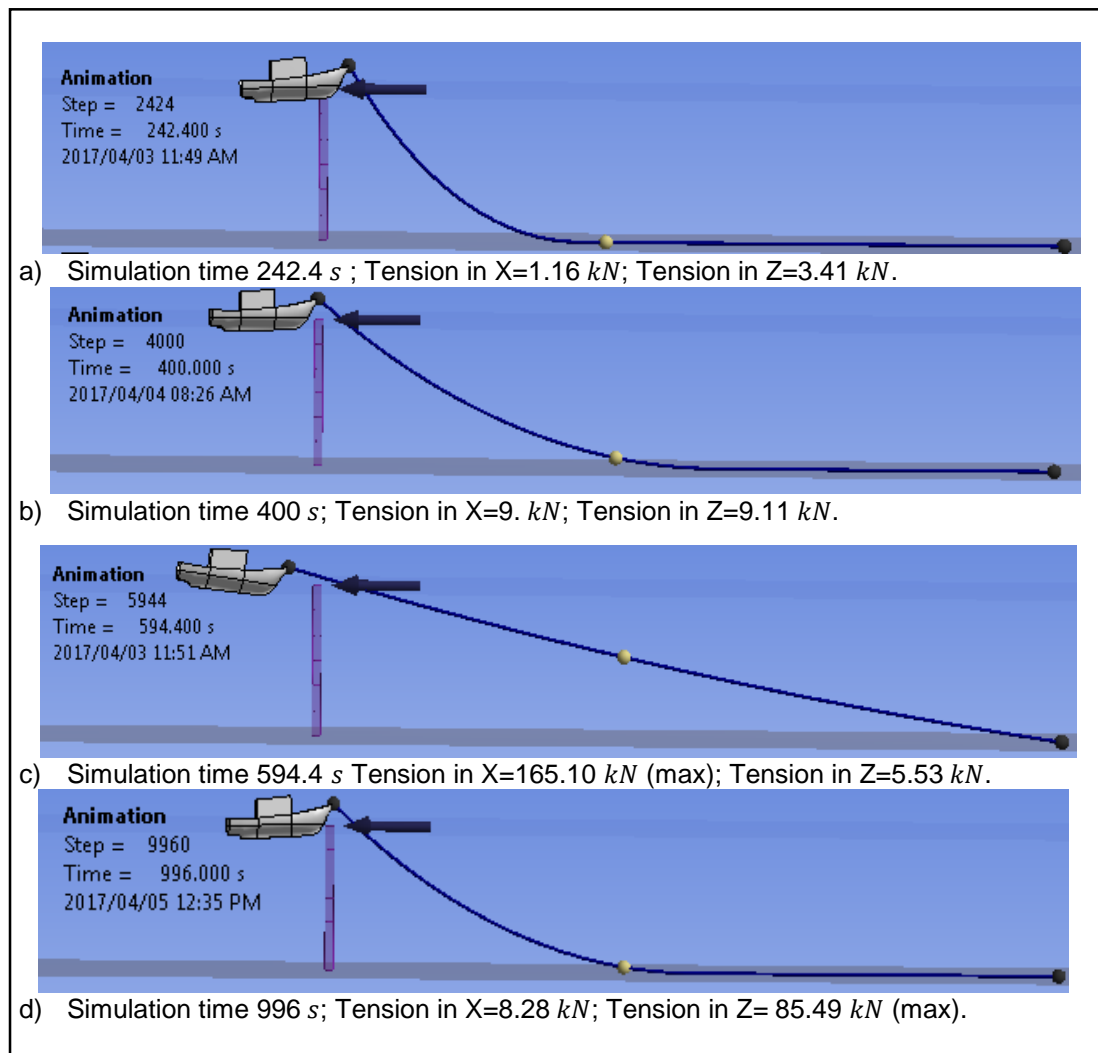


Figure 4.46: Mooring line profile of the 22 m vessel single-point for 1200 s simulation duration

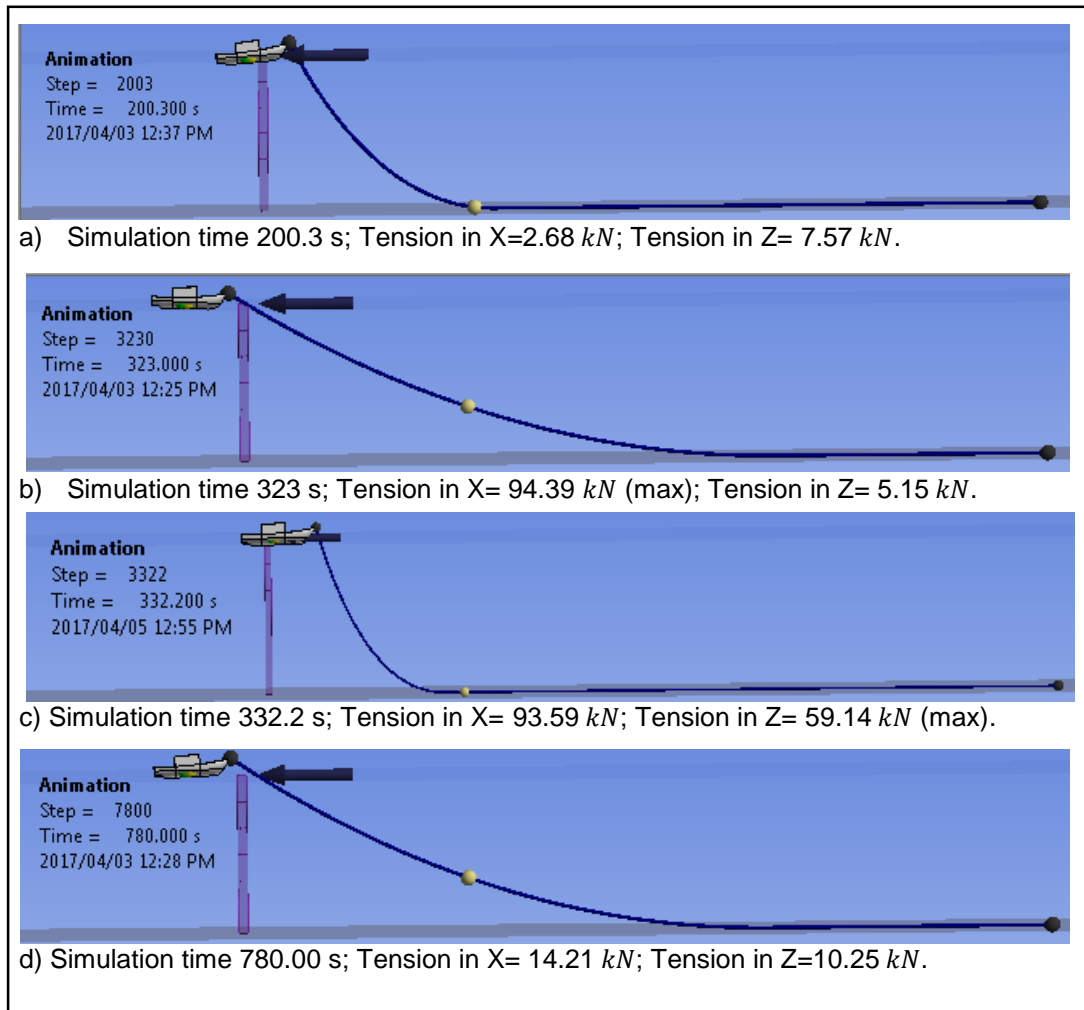


Figure 4.47: Mooring line profile of the 14 m vessel single-point for 1200 s simulation duration

The observation from these two figures above shows the 22 m moored vessel mooring chain fully stretching, while the 14 m moored vessel does not fully stretch. In this study, the 22 m vessel was used for correlating the underwater video analysis results for estimating the possible ocean conditions. The 14 m vessel has not been used for making correlations as it showed slack mooring line with considerable amount of mooring line lying dormant on the seabed.

The next Figure 4.48 illustrates an example of the *Tracker* video analysis performed to determine the mooring chain velocity in ANSYS AQWA. One clump weight is shown as an example where the motion was tracked. However, four clump weights were used as reference points for tracking.

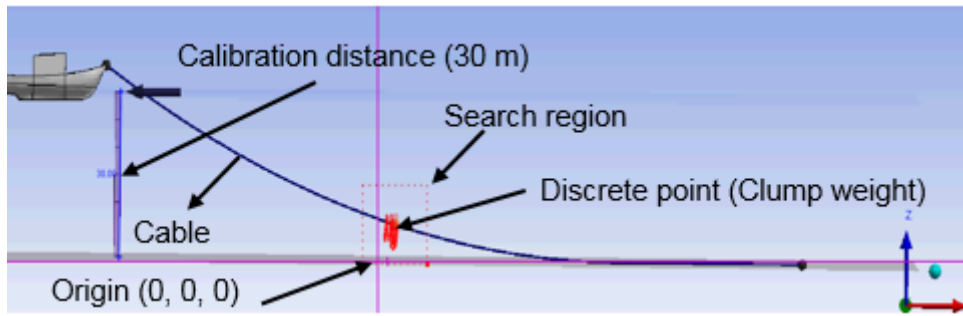


Figure 4.48: ANSYS AQWA video analysis using *Tracker*

Table 4.11 shows the results of the four points tracked in *ANSYS AQWA*. These results showed good correction compared to the underwater video analysis results previously shown in Figure 3.8. In this study, the contact velocity was obtained by finding the average between the maximum and minimum velocities for each point. The table shows the average seabed contact velocity of about 6.4 m/s.

Table 4.11: Wave conditions used for motion correlation

Wave condition 5: Wave height= 2.5 m; Wave period= 7 s			
	Velocity (m/s)		
Velocity points	Max	Min	Mean
Point 1	8.04	4.75	6.40
Point 2	7.93	4.43	6.18
Point 3	7.09	4.32	5.71
Point 4	3.00	2.30	2.65

4.3.2. Effect of wave height and period on the 22 m single-point moored vessel

The effect of varying the wave height and period results are shown in Table 4.12. These results were conducted on the 22 m long single-point moored vessel with a 20 mm diameter chain. The ocean depth, current and the mooring line length were kept constant. Table 4.13 shows the corresponding seabed pressure and force due to the impact velocity at various contact points (at the touch-down point) along the mooring line.

Table 4.12: Effect of wave height and period results

Wave condition 1: Wave height= 1 m; Wave period= 7 s				
Parameter	Max	Min	Mean	STD
Resultant Tension (kN)	23.93	1.30	5.07	1.72
Laid Length (m)	118.61	79.06	103.00	7.79
Anchor Uplift force (N)	3.06	0.003	0.17	0.28
Wave condition 2: Wave height= 1 m; Wave period= 10 s				
Parameter	Max	Min	Mean	STD
Resultant Tension (kN)	22.08	1.84	4.63	1.23
Laid Length (m)	113.82	88.19	103.51	5.28
Anchor Uplift force (N)	0.33	0.001	0.03	0.05
Wave condition 3: Wave height= 2 m; Wave period= 7 s				
Parameter	Max	Min	Mean	STD
Resultant Tension (kN)	106.96	-4.52	10.85	10.13
Laid Length (m)	111.43	4.63	75.48	19.06
Anchor Uplift force (kN)	11.59	-0.08	0.04	0.44
Wave condition 4: Wave height= 2 m; Wave period= 10 s				
Parameter	Max	Min	Mean	STD
Resultant Tension (kN)	61.98	-1.69	7.17	5.26
Laid Length (m)	107.62	29.98	87.40	12.66
Anchor Uplift force (N)	580.09	0.01	4.26	25.46
Wave condition 5: Wave height= 2.5 m; Wave period= 7 s				
Parameter	Max	Min	Mean	STD
Resultant Tension (kN)	174.13	-6.26	15.33	19.15
Laid Length (m)	110.23	4.02	63.11	23.30
Anchor Uplift force (kN)	18.58	-0.75	0.21	1.07

Note that the negative tension values in the table above indicate cable slack on the mooring line. Thus, all negative values for the tension and anchor uplift forces are taken as zero.

Due to the ANSYS AQWA software output file limitation of the lack of the time-history of velocities along the mooring line (mooring line nodes). A maximum of four points were selected for tracking the maximum and minimum impact velocities. These are shown in the table below. The contact pressure was found by using Equation 4.1 obtained from ABAQUS simulations.

Table 4.13: Seabed contact Pressure and Force due to various contact points velocities

Wave condition 1: Wave height= 1 m; Wave period= 7 s				
Parameter	Velocity (m/s)			Mean contact pressure / force (MPa / N)
	Max	Min	Mean	
Point 1	No contact	No contact	No contact	-
Point 2	2.68	1.05	1.87	42.48
Point 3	1.04	0.50	0.77	29.61
Point 4	No motion	No motion	No motion	-
Wave condition 2: Wave height= 1 m; Wave period= 10 s				
Parameter	Velocity (m/s)			Mean contact pressure / force (MPa / N)
	Max	Min	Mean	
Point 1	No contact	No contact	No contact	-
Point 2	1.79	1.14	1.47	36.96
Point 3	0.81	0.780	0.80	29.82
Point 4	No motion	No motion	No motion	-
Wave condition 3: Wave height= 2 m; Wave period= 7 s				
Parameter	Velocity (m/s)			Mean contact pressure / force (MPa / N)
	Max	Min	Mean	
Point 1	6.27	3.71	4.99	118.03
Point 2	6.19	3.46	4.82	112.51
Point 3	5.53	3.37	4.45	100.91
Point 4	1.34	0.50	0.92	30.95
Wave condition 4: Wave height= 2 m; Wave period= 10 s				
Parameter	Velocity (m/s)			Mean contact pressure / force (MPa / N)
	Max	Min	Mean	
Point 1	No contact	No contact	No contact	-
Point 2	4.92	3.69	4.31	96.59
Point 3	3.06	1.50	2.28	49.20
Point 4	No motion	No motion	No motion	-
Wave condition 5: Wave height= 2.5 m; Wave period= 7 s				
Parameter	Velocity (m/s)			Mean contact pressure / force (MPa / N)
	Max	Min	Mean	
Point 1	8.04	4.75	6.40	170.86
Point 2	7.93	4.43	6.18	162.03
Point 3	7.09	4.32	5.71	143.49
Point 4	3.00	2.30	2.65	56.06

The outcomes of the comparison in Table 4.12 showed that wave condition 5 had the highest mooring line length interacting with the seabed with the highest impact pressure. This mooring line length more frequently lifts up and drops back down on the seabed than during all the other wave conditions evaluated.

The effect of varying the wave height and period showed that the mooring line profile is greatly influenced by the decrease in wave period and an increase in wave height. This consequently increased the interaction of mooring line laid length with the seabed. The corresponding mooring line impact pressure and force on the seabed also increased when the wave height was increased with a decreased wave period. This also increased the tension at the fairlead as well as anchor uplift forces.

The increase in wave period from 7 to 10 s resulted in more slack of the mooring line profile; while the decrease in wave period from 10 to 7 s resulted in both slack and taut mooring line profiles when the wave height was doubled from 1 to 2 m. The increase in the slack of the mooring line profile resulted in a portion of the mooring line laid length on the seabed inactive. Figure 4.49 and Figure 4.50 shows the slack mooring line profiles with a large portion of the mooring line length lying dormant on the seabed for wave condition 1 and 2.

The comparison between wave conditions 1 and 2 shows the effect of the wave period when the wave height is kept constant. Figure 4.49 and Figure 4.50 demonstrates this effect on the mooring line profile showing both mooring line profiles which are almost identical. However, wave condition 1 showed slightly higher maximum tension which was 8.04% more than the tension in wave condition 2. The mooring line laid length on the seabed of these wave conditions was found to be the least when all five wave conditions were compared. Wave condition 1 also shows a slight increase of the mooring line interaction with seabed compared to wave condition 2 (see Figure 4.55). This outcome shows that short wave periods reduces slack on the mooring line profile and increases mooring line seabed interaction.

The mooring line impact pressure on the seabed due to wave condition 1 and 2 was found to be the least in all five wave conditions investigated. This can be seen in Table 4.13 which showed the maximum mooring line impact pressure of 42.48 and 36.96 MPa for wave conditions 1 and 2 respectively.

The mooring line length which interacts with the seabed dramatically increased when the wave height was doubled. This increase of the mooring line interaction with seabed was observed when comparing wave conditions 3 and 4. The comparison distinctively showed the effect of the wave period and height as was observed from the comparisons in wave conditions 1 and 2. Figure 4.51 and Figure 4.52 illustrates the mooring line profile of the two wave conditions mentioned. As can be seen, the wave period of 10 s resulted in more slack of the mooring line profile with more mooring line laid length lying on the seabed; while the wave period of 7 s (in Figure 4.51) shows both slack and taut mooring line profiles with a large portion of the mooring line interacting with the seabed.

Figure 4.51 also shows tension for each profile at a specific time. The mooring line touch-down point (TDP) was found to dynamically vary with time as stated in the literature. The mooring line length interacting with the seabed for wave condition 3 was found to be in the range of about 4.63 to 111.43 m, with the average length of about 75.48 m and a standard deviation (STD) of about 19.06 m. Wave condition 4, the mooring line length interacting with seabed was found to be in the range of about 29.98 to 107.62 m, with the average length of about 87.40 m and a standard deviation (STD) of about 12.66 m. As can be observed, wave condition 4 had the least mooring line laid length interaction on the seabed when compared to wave condition 3 which showed more frequent interaction (Figure 4.55).

The effect of increasing the wave height from 1 to 2 m with the wave period of 10 s showed an increase in the mooring line impact pressure on the seabed from 36.96 to 96.59 MPa. A decrease of the wave period from 10 to 7 s with the same increase of the wave height from 1 to 2 m showed an increase in the mooring line impact pressure on the seabed from 42.48 to 1118.03 MPa.

The slack mooring line profile was also found to be associated with reduced tension at the Fairlead. This tension was found to be 61.98 kN for wave condition 4 and 106.96 kN for wave condition 3 which showed an increase in tension. The corresponding anchor uplift forces were found to be directly proportional to the tension at the Fairlead. These forces were found to be 11.59 kN and 580.09 N for conditions 3 and 4 respectively.

Wave condition 5 (2.5 m wave height and 7 s wave period) showed the most interaction of the mooring line with the seabed. The mooring line laid length interacting with seabed

is shown to be in the range of about 4.02 to 110.23 m, with the average length of about 63.11 m and a standard deviation (STD) of about 23.30 m

Figure 4.55 show the time-history of mooring line laid length on the seabed. As can be seen, wave condition 5 shows the highest peaks followed by wave condition 3 (when the wave height is 2 m with 7 s wave period). This high interaction of the mooring line corresponds with slack and taut mooring line profiles shown in Figure 4.53. In this instance, the mooring line is observed to fully stretch and then becomes slack. This was phenomenon was observed to be repetitive over the simulation duration of 1 200 s.

The maximum mooring line impact pressure on the seabed in this wave condition was found to be 170.86 MPa which was found to be the highest in all wave conditions investigated.

The mooring line maximum tension at the Fairlead is also shown to be 174.13 kN. Figure 4.54 (b) show the time-history of tension at the Fairlead. High mooring line tension was found to have a linear relationship with the increase in wave height and a decrease in wave period.

The corresponding forces that act on the anchor which are termed 'Anchor uplift force' are also shown; the maximum force acting on the anchor of about 18.81 kN was found to be the highest in all wave conditions. Figure 4.56 (b) show the time-history of anchor uplift forces.

In summary, the mooring line impact pressure on the seabed was found to be influenced by the velocity of the chain link impact and its diameter. The impact pressure on a longer section of the mooring line was found to be the same if the impact chain links have the same impact velocity.

Results obtained in this section clearly show that an increase of the chain impact velocity causes an increase in impact pressure of the chain. This increase of the mooring chain link impact velocity was found to be associated with wave conditions 3 (when the wave height is 2 m with 7 s wave period) and 5 (when the wave height is 2.5 m with 7 s wave period).

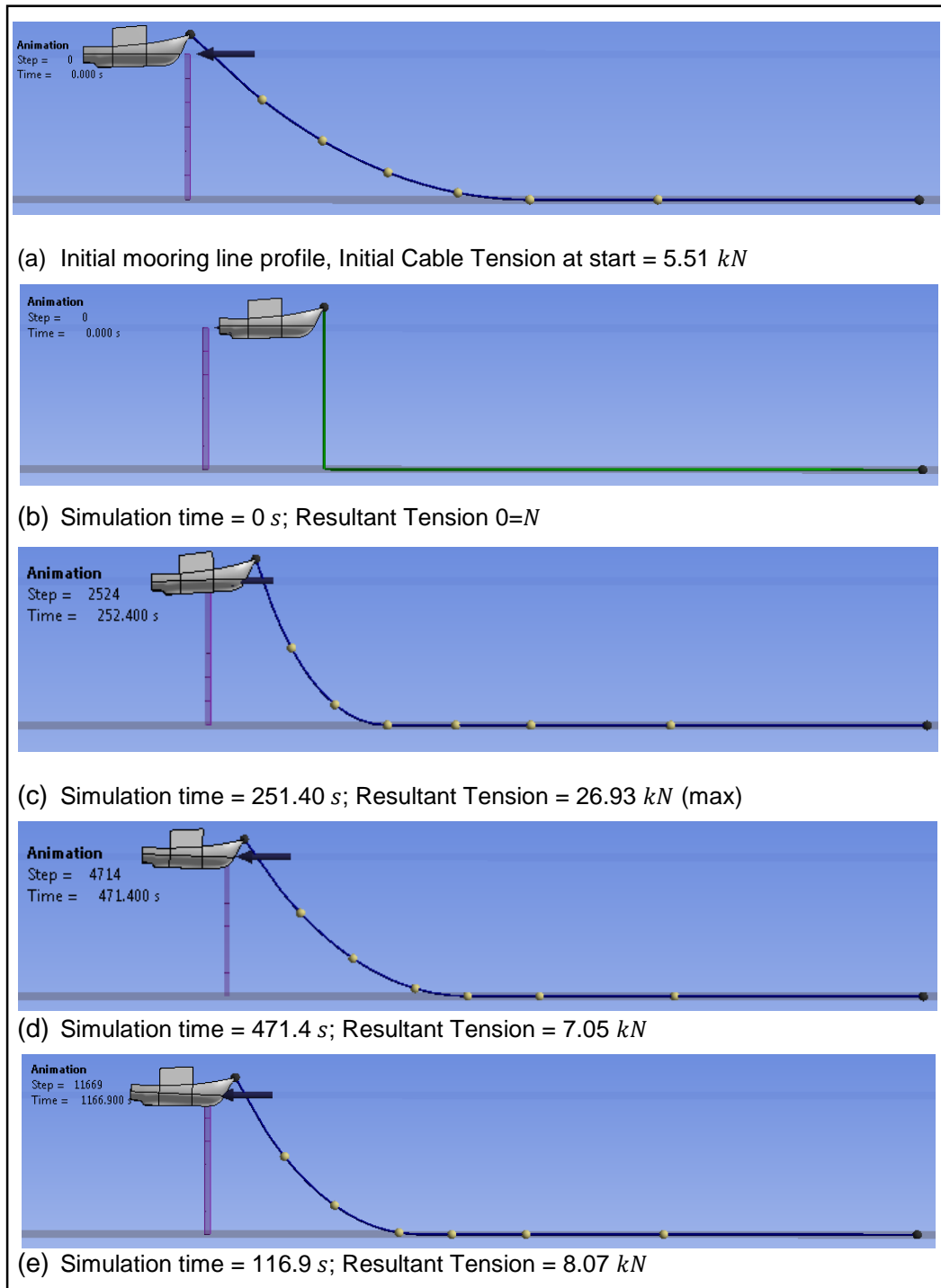


Figure 4.49: Mooring chain profile for 1 m and 7 s wave height and period

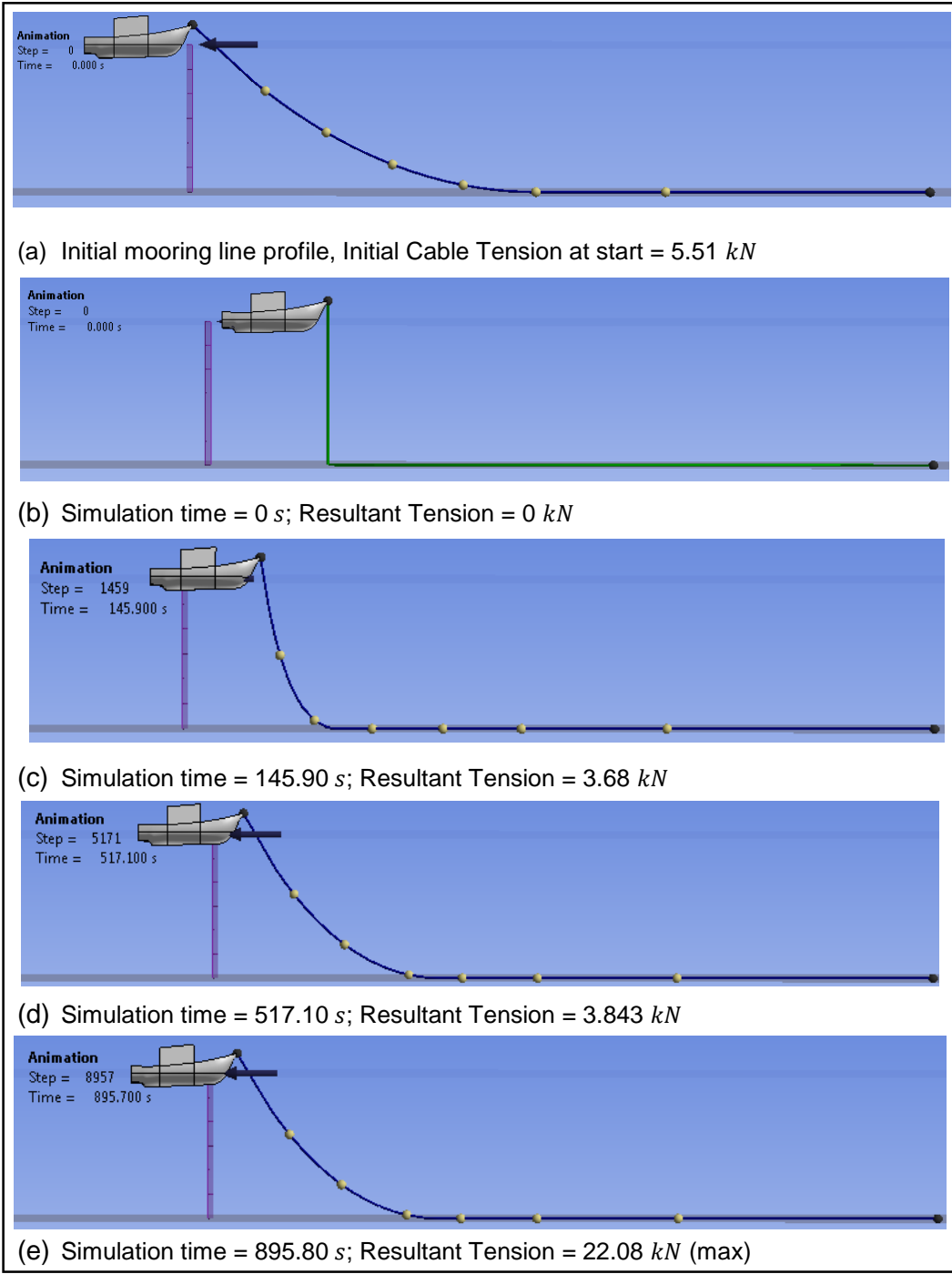


Figure 4.50: Mooring chain profile for 1 m and 10 s wave height and period

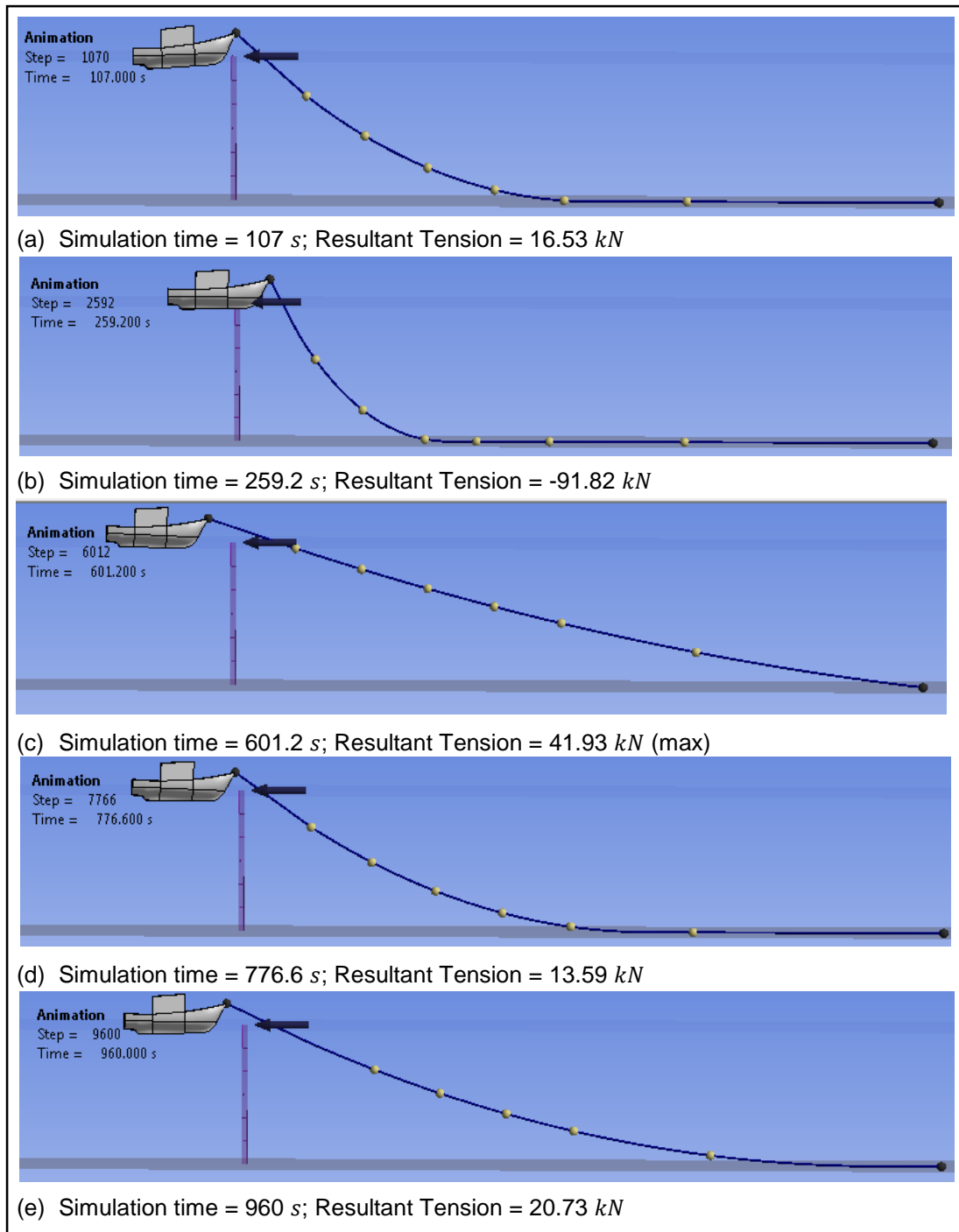


Figure 4.51: Mooring chain profile for 2 m and 7 s wave height and period

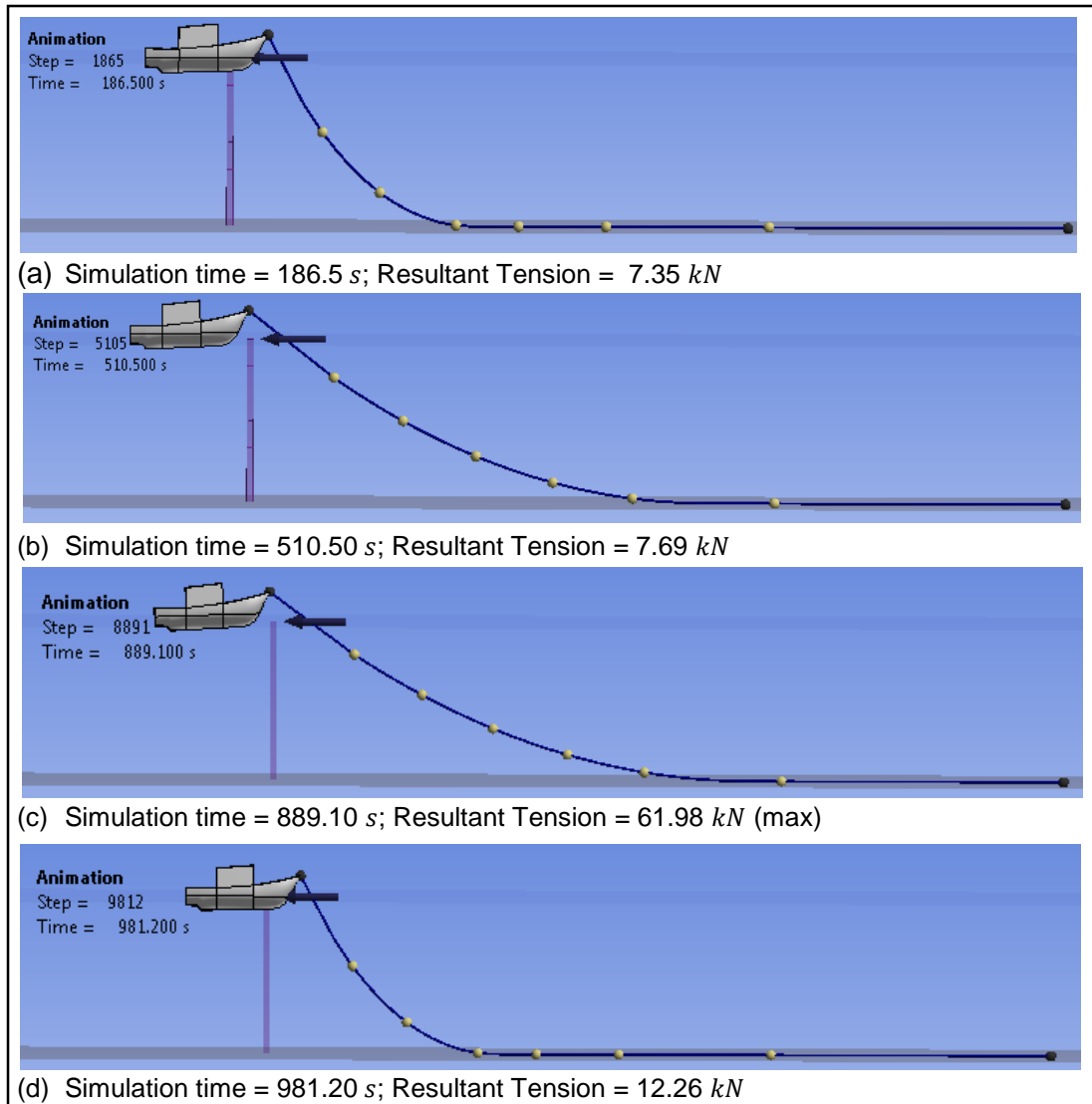


Figure 4.52: Mooring chain profile for 2 m and 10 s wave height and period

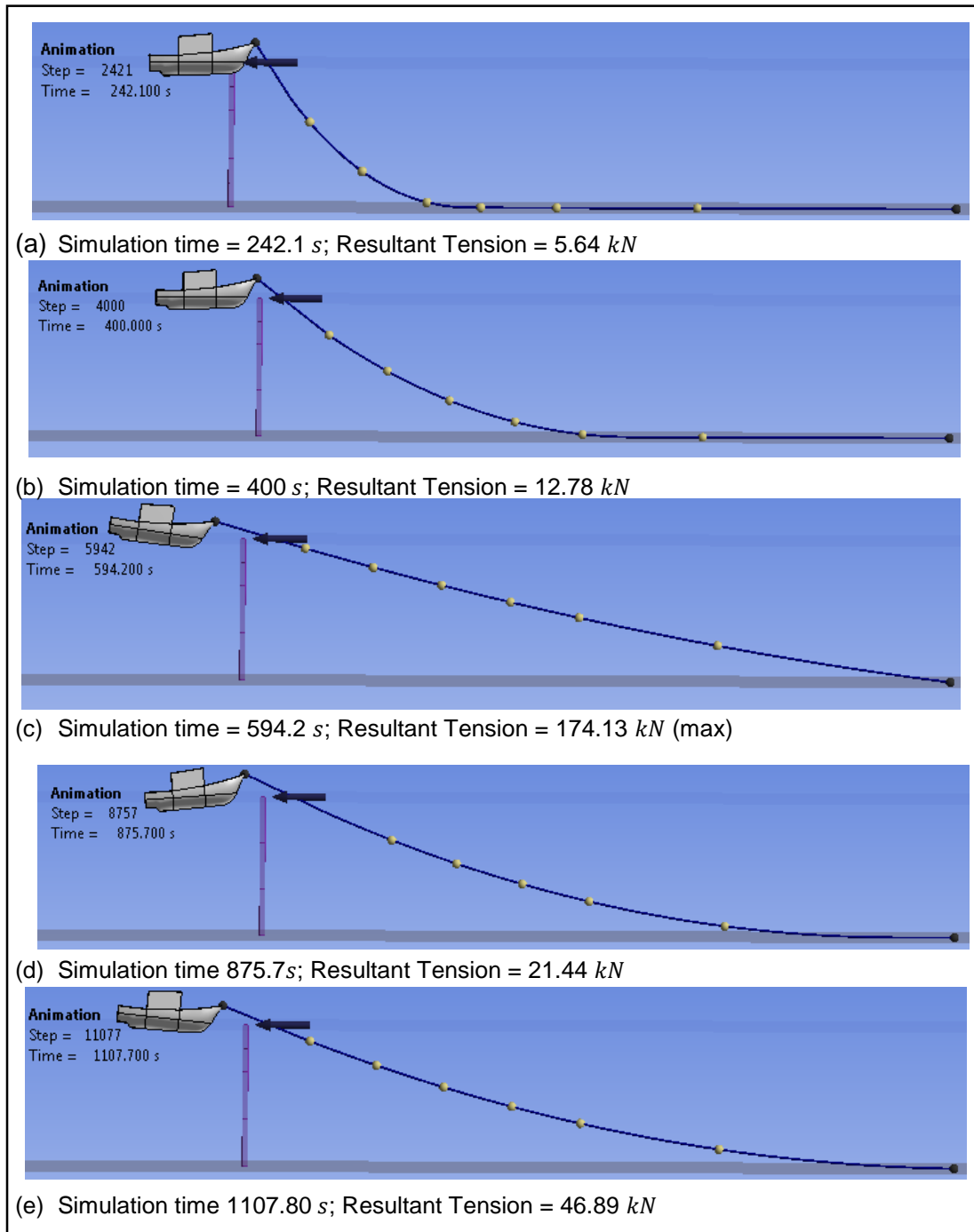
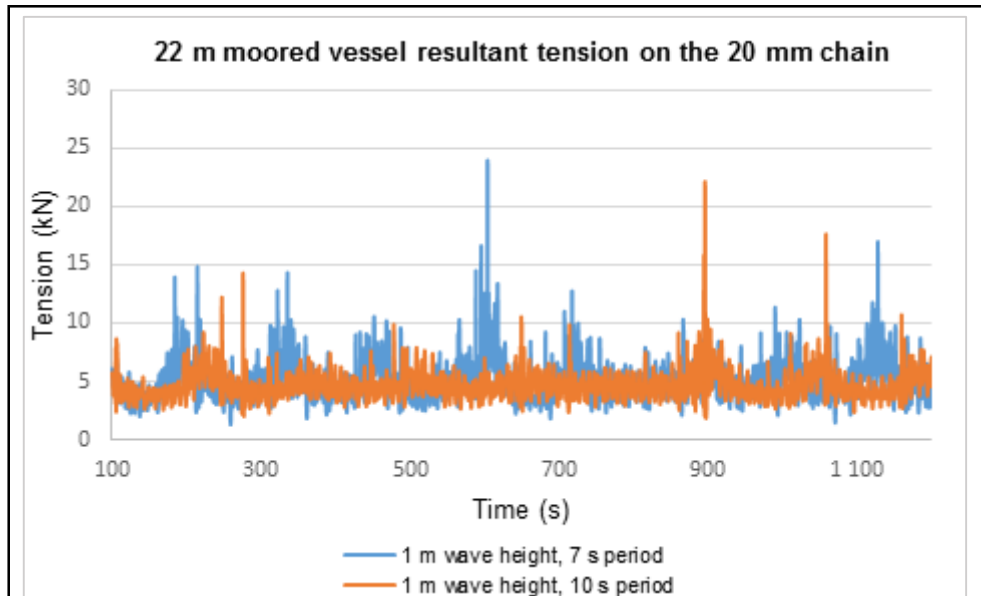
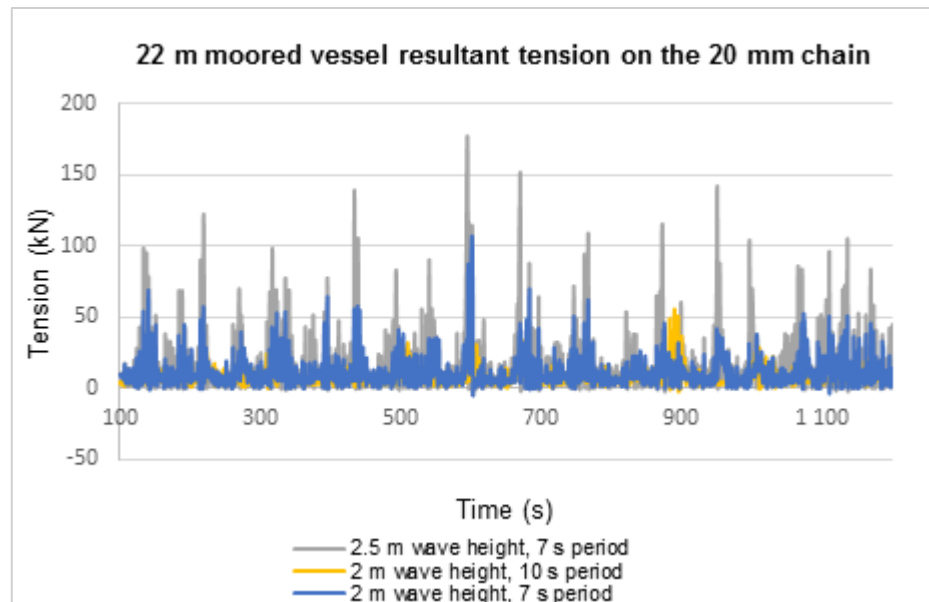


Figure 4.53: Mooring chain profile for 2.5 m and 7 s wave height and period



(a) Wave conditions at 1 m wave height when varying 7 and 10 s periods



(b) Wave conditions at 2.5 m wave height when varying 7 and 10 s periods

Figure 4.54: The effect of wave conditions on tension

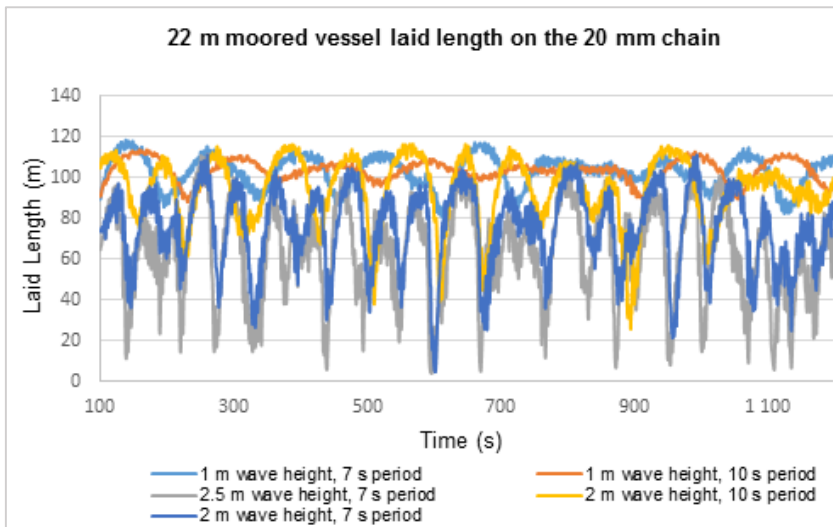
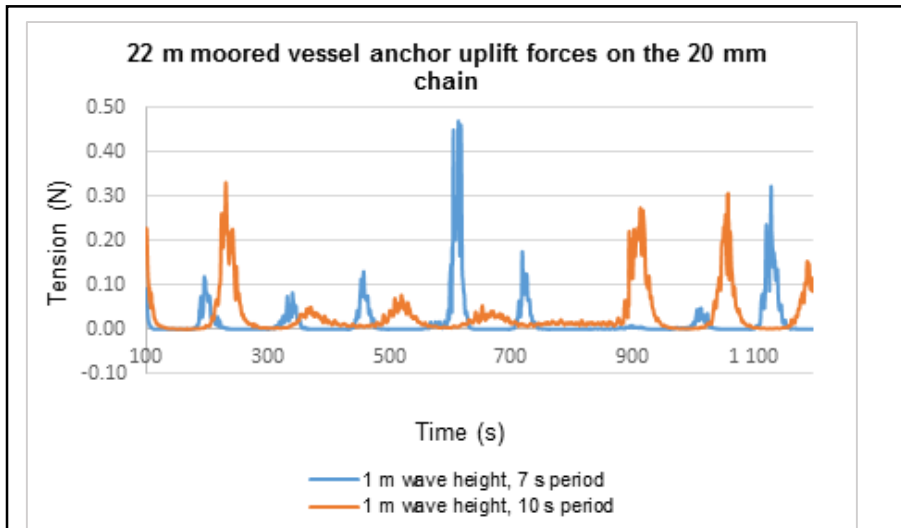
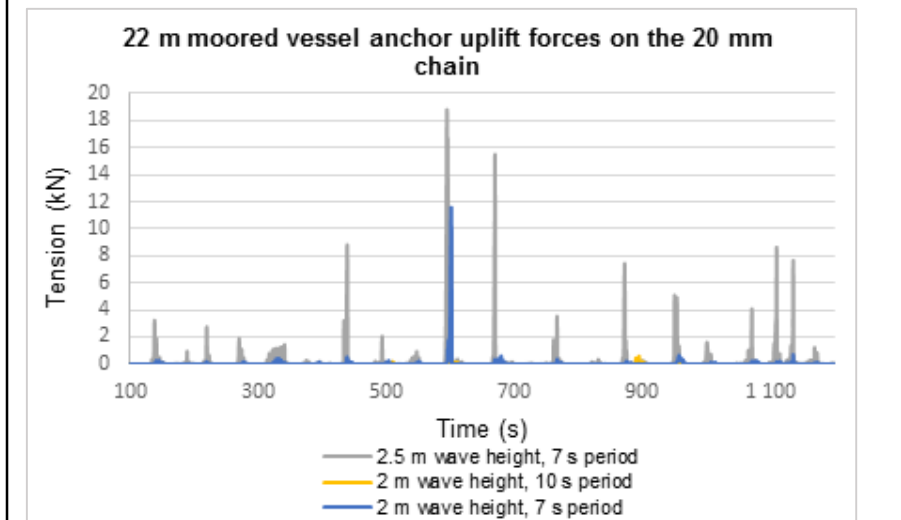


Figure 4.55: The effect of wave conditions on chain laid length



(a) Wave conditions at 1 m wave height when varying 7 and 10 s periods



(b) Wave conditions at 2.5 m wave height when varying 7 and 10 s periods

Figure 4.56: The effect of wave conditions on anchor uplift forces

4.3.3. Mooring system results using three configurations

The simulation results parameters that are of interest in this study are the vessel displacements, the mooring chain tension, the mooring chain length laid on the seabed, the anchor uplift forces and the seabed impact pressure and force. All these parameters varied with time and were evaluated for 1200 s. The following three anchor configurations were used in this study on both the 14 and 22 m vessels:

Configuration 1: Single-point mooring system with the anchor position in-line with the vessel and the incoming waves (shown in Figure 4.57). Table 4.6 & Table 4.8 has already provided anchor coordinates for the 22 and 14 m configurations.

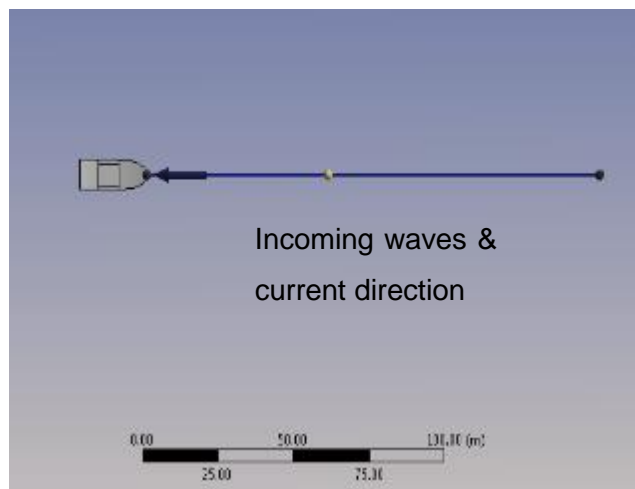


Figure 4.57: Configuration 1 - Single-point mooring system with anchor in line with waves and current (top view)

Configuration 2: Single-point mooring system with the anchor position at an angle with the vessel and incoming wave is shown in Figure 4.58.

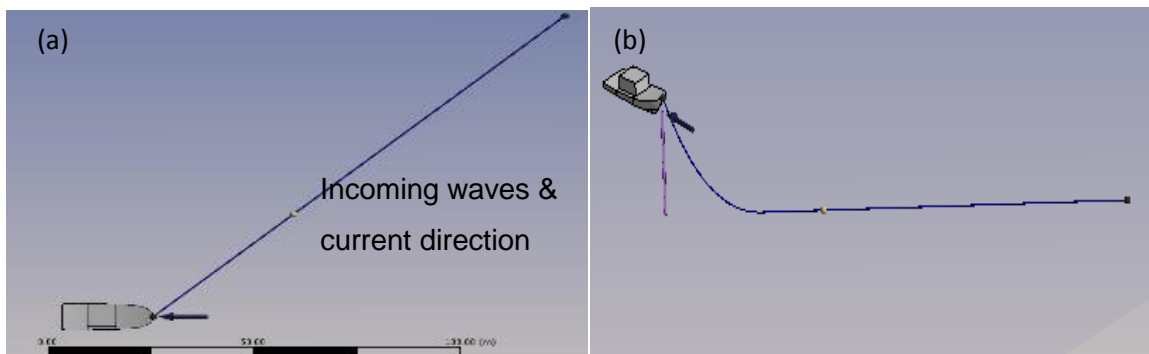


Figure 4.58: Configuration 2 - Single-point mooring system with anchor at an angle with incoming waves and current, (a) top view & (b) isometric view

The 22 m vessel anchor connection points are shown in Table 4.14 below.

Table 4.14: Single-point mooring with ‘Anchor 2’ coordinates for the 22 m vessel (anchor at angle)

Name	Position		
	x (m)	y (m)	z (m)
Anchor 2	100	100	-30
Fairlead 2	0.01	1	4

The 14 m vessel anchor connection points are shown in Table 4.15 below.

Table 4.15: Single-point mooring with Anchor 2 coordinates on the 14 m vessel

Name	Position		
	x (m)	y (m)	z (m)
Anchor 2	100	100	-30
Fairlead 2	0.01	1	2

Configuration 3: Two-point mooring system with ‘V’ shaped anchor is shown in Figure 4.59 below.

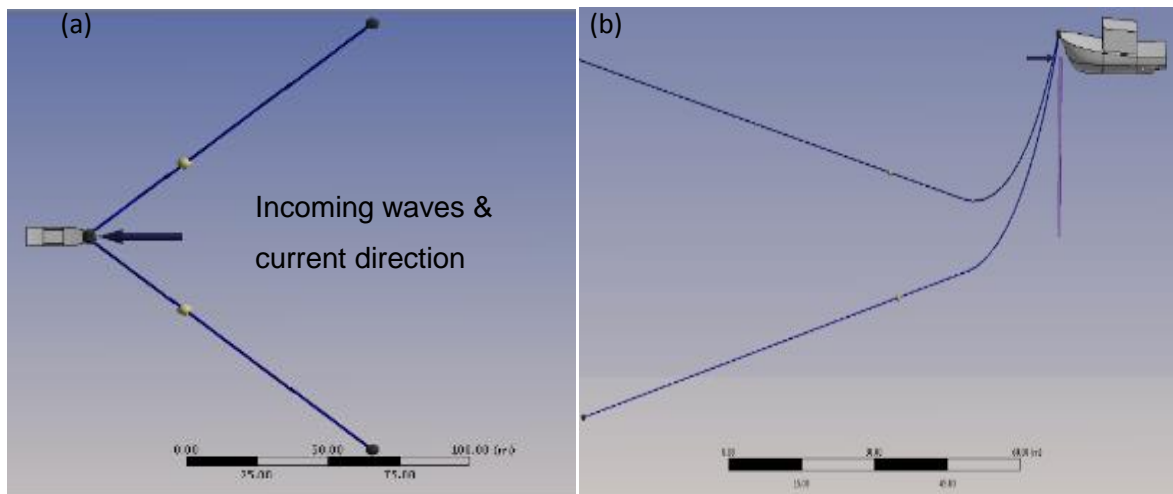


Figure 4.59: Configuration 3 - Two-point mooring system with ‘V’ shaped anchoring, (a) top view & (b) Isometric view

The 22 m vessel connection points with two anchors are shown in Table 4.16 below.

Table 4.16: Two-point mooring anchor coordinates on the 22 m vessel

Name	Position		
	x (m)	y (m)	z (m)
Anchor 1	100	-100	-30
Anchor 2	100	100	-30
Fairlead 1	0.01	-1	4
Fairlead 2	0.01	1	4

The 14 m vessel connection points with two anchors are shown in Table 4.17 below.

Table 4.17: Two-point mooring anchor coordinates on the 14 m vessel

Name	Position		
	x (m)	y (m)	z (m)
Anchor 1	100	-100	-30
Anchor 2	100	100	-30
Fairlead 1	0.01	-1	2
Fairlead 2	0.01	1	2

The above three configurations were simulated with the wave height of 2.5 m and wave period of 7 s.

The ANSYS AQWA model included sensitivity analysis for determining the best number of mooring line elements for discretisation. Since the program only allows 250 maximum elements, most studies use 100 elements to discretise the mooring line. The difference between using 100 and 250 elements was found to be 1.39%. This difference was found by comparing the mooring line maximum tension when using 100 and 250 elements.

The maximum horizontal tension of 167.4 kN was obtained when 100 elements were used, while the maximum horizontal tension force of 165.1 kN was obtained when 250 elements were used. This study used 250 elements for discretising the mooring line.

When the three configurations are solved numerically in ANSYS AQWA, the motion response for the 14 and 22 m vessels is obtained. The initial hydrostatic results showed

the 22 m vessel center of gravity of -13.24 m, while the 14 m vessel center of gravity was -8.61 m. The full hydrostatic results which include Hydrostatic Stiffness, the center of buoyancy and stability parameters can be found in Appendix D.

The next Figure 4.60 shows the horizontal displacements of both vessels using the three mooring line configurations mentioned above. The displacements are calculated at the CoG of the vessel.

When Figure 4.60 (a) & (c) are compared, the 14 m vessel in particular is shown to have less horizontal displacements than the 22 m vessel. Since both vessels were simulated under the same ocean conditions, this shows the effect of the mooring line on large and small vessels. In this case, the mooring line induces high motion damping on the 14 m vessel by counteracting the vessel motions due to the action of the wave and current loads. However, when the wave direction changes (Configuration 2 - anchor at an angle to the incoming wave) shown in Figure 4.60 (b), the 14 m vessel is observed to have higher horizontal displacements than the 22 m vessel.

Since the mooring chain (line) has its highest stiffness (resistance) in the longitudinal direction, this stiffness is low in its lateral direction (*Y*-direction). In this instance, in Configuration 2, the 14 m vessel experienced high horizontal displacements because of the low mooring line stiffness. The outcome from comparing results from Figure 4.60 (a) & (b) is that that the 20 mm mooring chain stiffness is low when the wave angle changes and becomes high when the wave angle and the anchor are in the same alignment. The 14 m vessel experienced low mooring chain stiffness in Configuration 2 and high mooring chain stiffness in Configuration 1. This shows that high mooring chain stiffness results in less vessel displacements which agree with literature.

When Figure 4.60 (a) horizontal displacements are closely observed – Configuration 1, this configuration shows the single-point mooring system on the 14 and 22 m vessels with the least horizontal displacements amongst the three mooring line configurations analysed. This is due to high mooring chain horizontal stiffness caused by the alignment of the anchor and vessel to the incoming waves. The 22 m vessel is shown to have slightly higher horizontal displacements than the 14 m vessel. The 22 m vessel was displaced within the distance range of between -7.18 and +7.27 m with the STD (Standard Deviation) of approximately 7.37, while the 14 m vessel was displaced within the distance range of between -10.01 and 4.418 m with the STD of 2.88.

Additionally, the 22 m vessel was observed to have a significant portion of the mooring line lifting off and dropping back down on the seabed compared to the 14 m vessel (in Configuration 1). The 14 m vessel was observed to have a significant amount mooring chain lying dormant on the seabed; only a small portion was observed to be lifting off and dropping on the seabed. Note that the displacement range is taken from the simulation time of 20 – 1200 s when the vessel's initial starting position was established.

A closer look at Figure 4.60 (b) shows the single-point 14 m moored vessel in Configuration 2 with the highest horizontal displacements in all three configurations; this was followed by the 22 m vessel with high horizontal displacements on the same configuration. The 22 m vessel was displaced within the distance range of between – 0.21 and +56.94 m with the STD of 7.37; while the 14 m vessel was displaced within the distance range of between –6.57 and +54.44 m with the STD of 12.26. The difference on the horizontal motion between the two vessels is shown by the great STD of approximately 12.16 m on the 14 m vessel. Note that this range is taken from the simulation time of 30 – 1200 s when the vessel's initial starting position was established.

Figure 4.60 (c) shows the horizontal displacements of the two-point moored 14 and 22 m vessels using Configuration 3. In this configuration, the horizontal displacements of both vessels were observed to be the second highest when the three configurations are compared. The 22 m vessel in particular, had higher horizontal displacements than the 14 m vessel. The 22 m vessel was displaced within the distance range of between – 8.16 and 18.16 m with Standard Deviation two times greater than the 14 m vessel's Standard Deviation; while the 14 m vessel was displaced within the distance range of between – 5.08 and 16.57 m with the STD of 3.02. Note that this range is taken from the simulation time of 25 – 1200 s when the vessel's initial starting position was established.

The outcome from analysing the horizontal motion of the three configurations, demonstrates that the anchor deployed at an angle to the incoming waves and the vessel will result in high horizontal displacements of the vessel, especially smaller vessels. This also implies that when the wave direction changes, the horizontal excursions of the vessel increase accordingly. The result in the high horizontal displacement of the both vessels is caused by low mooring chain stiffness due to the wave approaching at an angle. This is because chain mooring lines have their highest stiffness on their longitudinal axis.

The 14 m vessel showed to have less displacement because of the presence of the 20 mm mooring line when the two anchors were used. In practice, smaller vessels mostly use smaller chain sizes of 14 and 16 mm. This shows that when the two-mooring system is used, smaller vessels (14 m vessel for example) will result in less displacements when the 20 mm chain is used than large vessels (22 m vessel for example). This also shows that heavier weight chain imposes high motion resistance to the moored vessel, especially smaller vessels.

It is evident from the three mooring line configurations that the 14 m vessel has the least amount of mooring chain lifting off and dropping back down on the seabed. This suggests that the seabed footprint is high when larger vessels are used since they imposed high dynamic forces on the mooring chain. The comparisons in Figure 4.60 show that the two-point mooring system has better vessel motion restriction when the wave angle changes. This also suggests that if the wave direction slightly changes during fishing, the two-point moored vessels will have less vessel displacement than single-point moored vessels. However, the two-mooring system potentially increases the mooring line footprint of the seabed.

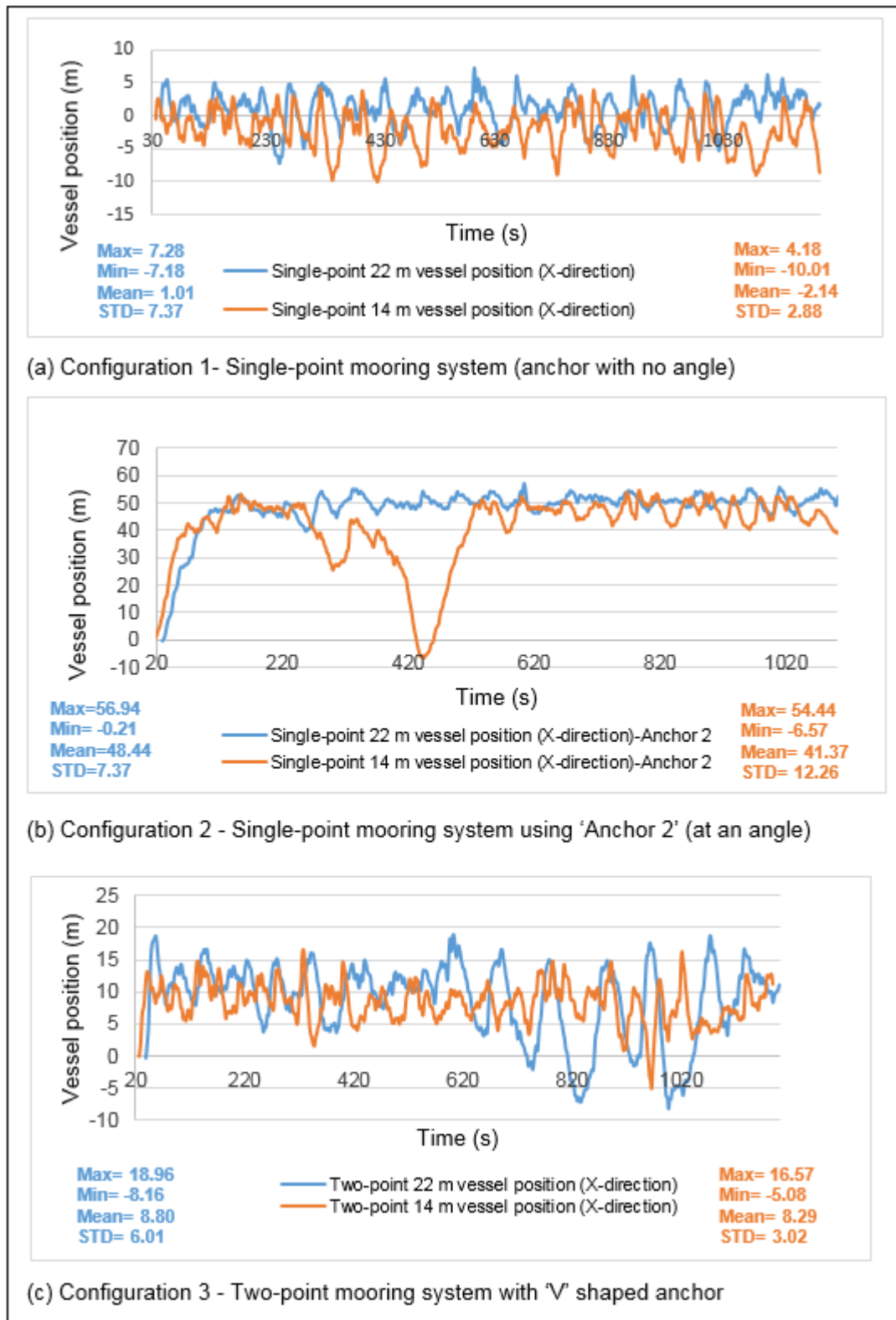


Figure 4.60: Horizontal displacements (X-direction) of the vessels in three configurations

The next Figure 4.61 shows lateral displacements (Y-direction) of the three mooring line configurations. Figure 4.61 (a) shows the single-point mooring system

(Configuration 1) with the least lateral displacements when compared to Configuration 1 and 2, the 14 m vessel, in this case, is shown to have slightly higher lateral displacements than the 22 m vessel. The 22 m vessel was displaced within the distance range of between -0.12 and 0.12 m with the STD of 0.04; while the 14 m vessel was displaced within the distance range of between -1.66 and 0.76 m with the STD of 0.46. Both vessels are shown to have very small lateral displacements which also indicated by their small Standard Deviation from their mean lateral displacement values.

Configuration 2 in Figure 4.61 (b), shows the highest lateral displacements of the 14 and 22 m vessels with the anchor at an angle to the incoming waves and the vessel. The 22 m vessel was displaced within the distance range of between 54.42 and 141.11 m with the STD of 15.54; while the 14 m vessel was displaced within the distance range of between 20.74 and 164.35 m with the STD of 26.62. This configuration was observed to have had a significant amount of the mooring chain sweeping on the seabed.

The 14 m vessel, in particular, showed high lateral displacements at the beginning. After about 450 s of the simulation time, both vessels are shown to have similar lateral displacements. This outcome is consistent with the observation made previously when the 'Anchor 2' coordinates were used (anchor at an angle), where the horizontal displacements of the single-point 14 m moored vessel were found to be the highest.

Lastly, Figure 4.61 (c), Configuration 3 - shows the lateral displacement of the two-point 14 and 22 m moored vessels. Higher lateral displacements on the 22 m vessel were observed than on the 14 m vessel which was similar to the observation illustrated in Figure 4.60 (c) previously. The 22 m vessel was displaced within the distance range of between -24.21 and 15.56 m with the STD of 9.23; while the 14 m vessel was displaced within the distance range of between -11.43 and 10.83 m with the STD of 2.95.

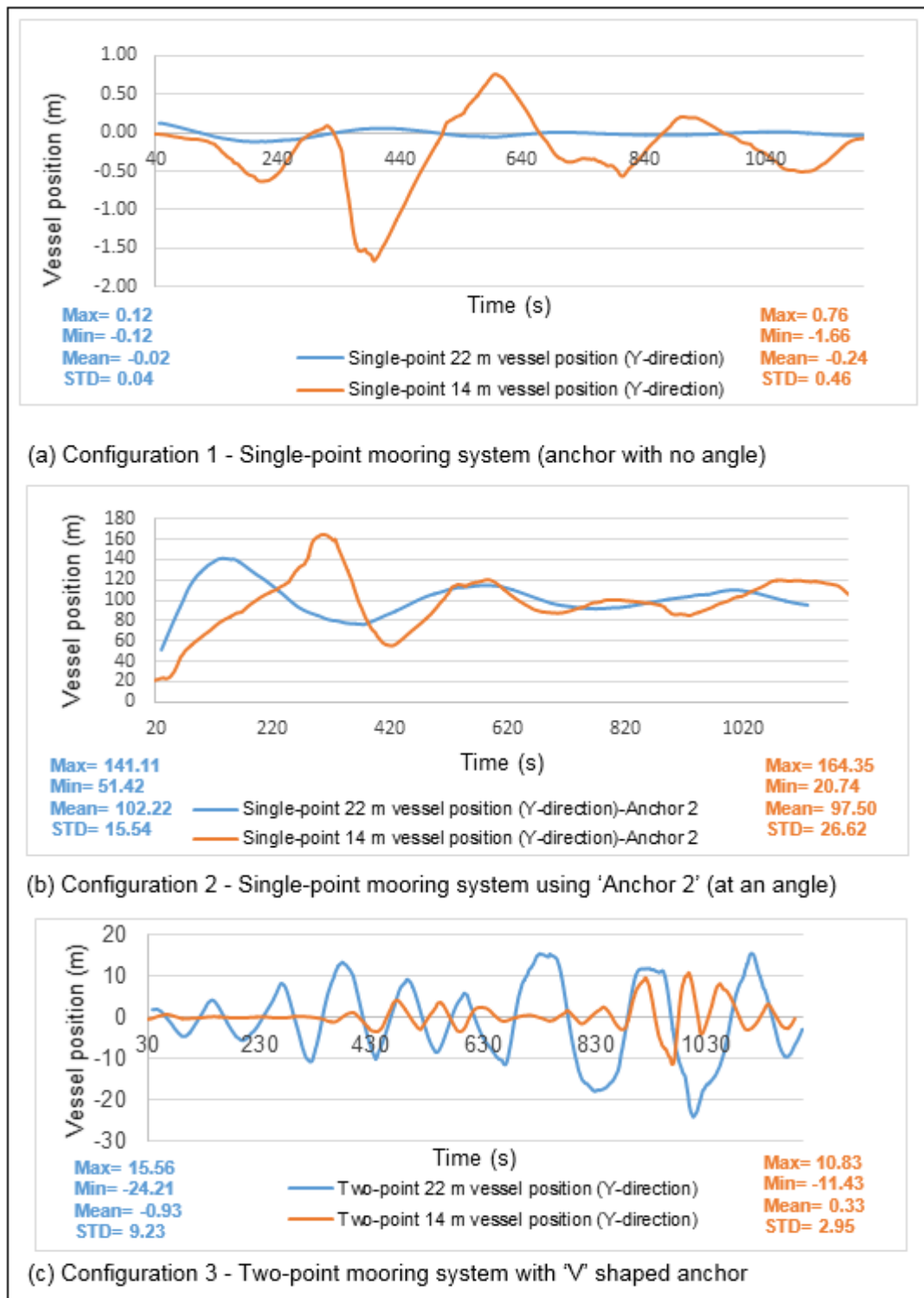


Figure 4.61: Lateral displacements (Y-direction) of the vessels in three configurations

Figure 4.62 shows the single-point moored vessels vertical displacements (Z-direction) of the three configurations. Figure 4.62 (a), Configuration 1, shows the 22 m vessel vertical displacements between the range of -0.46 and 2.36 m with the STD of 0.45; while the 14 m vessel was displaced within the distance range of between -0.41 and

1.64 m with the STD of 0.35. As can be seen, the 22 m vessel has higher vertical displacements than the 14 m vessel in all three configurations.

Figure 4.62 (b), Configuration 2, shows the 22 m vessel vertical displacements between the range of -0.41 and 2.14 m with the STD of 0.45; while the 14 m vessel was displaced within the distance range of between -0.36 and 1.80 m with the STD of 0.35. The 22 m vessel displacements, in this case, showed little variation when compared to the two configurations. This observation was also similar on the 14 m vessel vertical displacements.

Figure 4.62 (c), Configuration 3, the vertical displacements of the two-point 14 and 22 m moored vessels. The 22 m vessel vertical displacements are shown to be between the range of -0.34 and 2.39 m with the STD of 0.45; while the 14 m vessel was displaced within the distance range of between -0.38 and 1.74 m with the STD of 0.34.

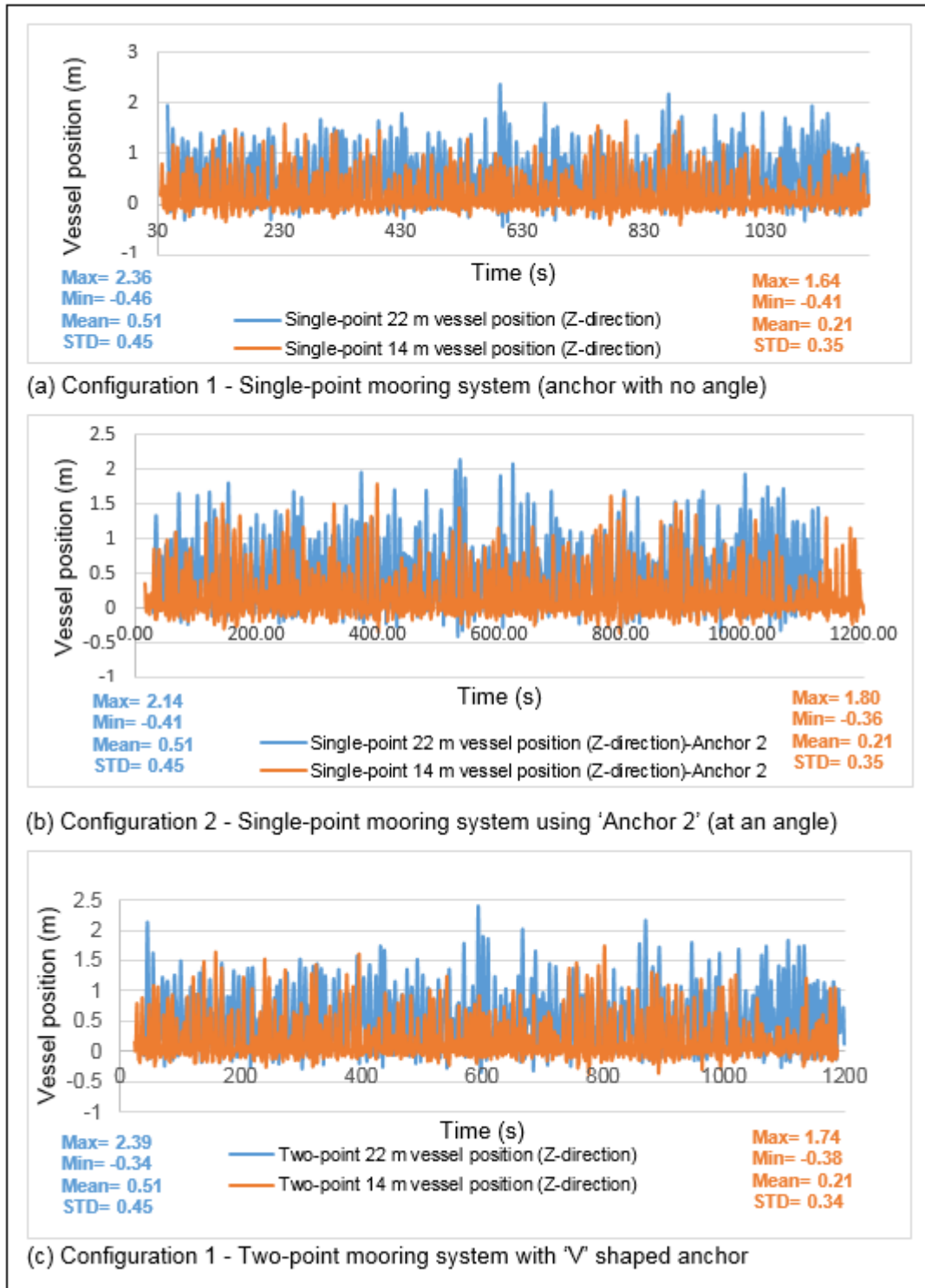


Figure 4.62: Vessel vertical displacements for all three configurations

Figure 4.65 shows the time-variation of mooring line laid length on the seabed for the three configurations. Figure 4.65 (a), Configuration 1, shows a comparison between the 22 and 14 m vessels laid length from 100 to 1200 s of the simulation time. The 22 m vessel mooring line is shown to have the most frequent contact on the seabed than the 14 m vessel. This comparison is further shown in Figure 4.63 (a) & (b) below using frequency distribution plot of the mooring line laid length for both vessels. This figure shows the most even distribution of the mooring chain on the 22 m vessel and was observed to have a substantial amount of the mooring chain lifting and dropping back on the seabed.

The 14 m vessel is shown to have an uneven distribution which implies that a large portion of the mooring chain is lying dormant on the seabed as also was observed from the simulation. The frequency distribution of the laid chain on the seabed overtime was stored in bins of 5 m intervals between the minimum and maximum laid length on the seabed. The 22 m vessel is shown to have about 75-80 meters frequently interacting with the seabed.

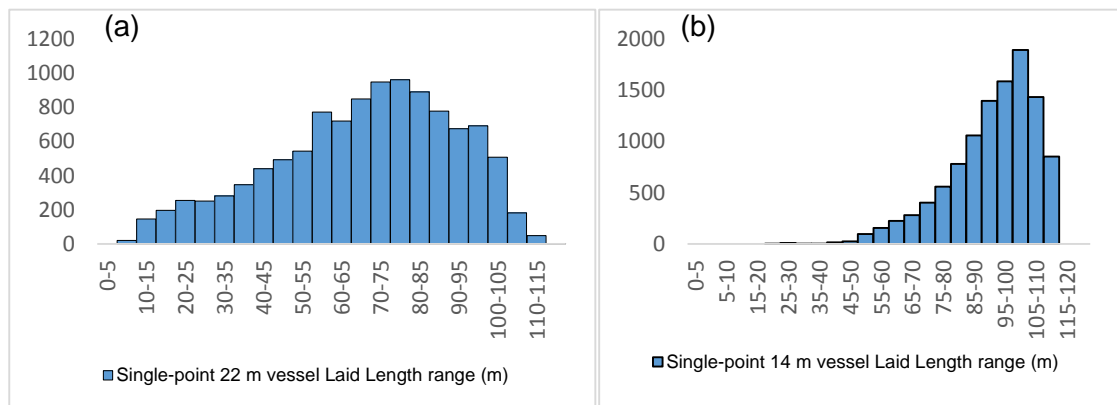


Figure 4.63: Frequency distribution of the mooring chain laid length on the seabed for Configuration 1

Figure 4.65 (b), Configuration 2, shows the comparison between the 22 and 14 m vessels laid length with a single-point mooring with the anchor at an angle. The frequency distribution plot of the mooring line laid length is shown in the next Figure 4.64. This figure also shows an even distribution of the mooring chain laid on the seabed on the 22 m vessel. The 14 m vessel, similar to the previous observation (Figure 4.65 (a)), was seen to have an uneven distribution which indicated that a large portion of the mooring line is lying dormant on the seabed.

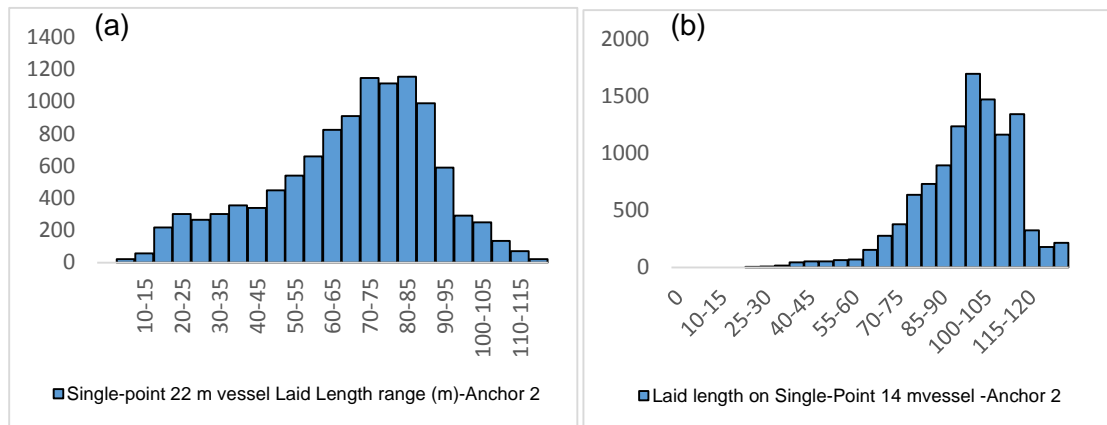
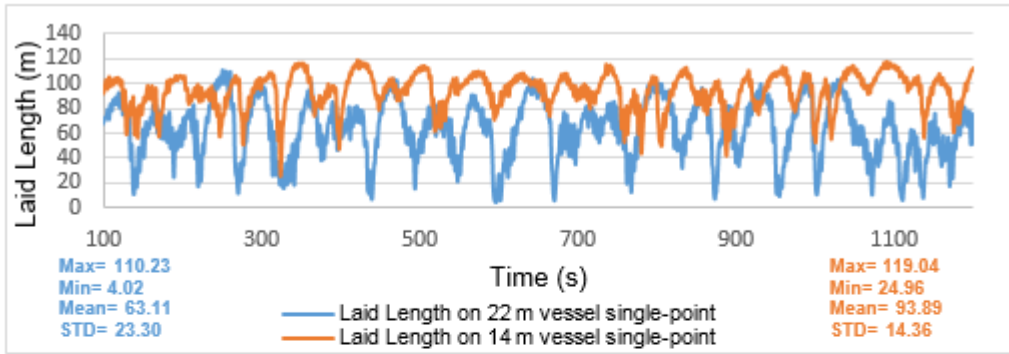
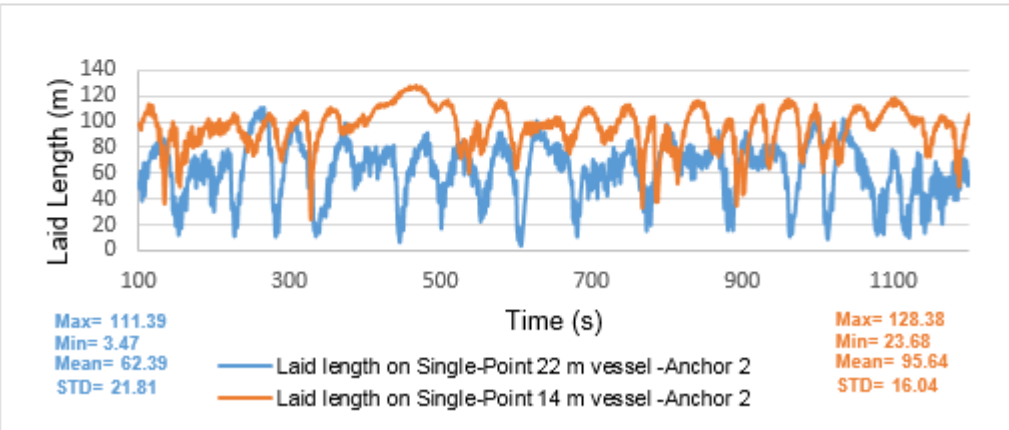


Figure 4.64: Frequency distribution of the mooring chain laid length on the seabed for Configuration 2

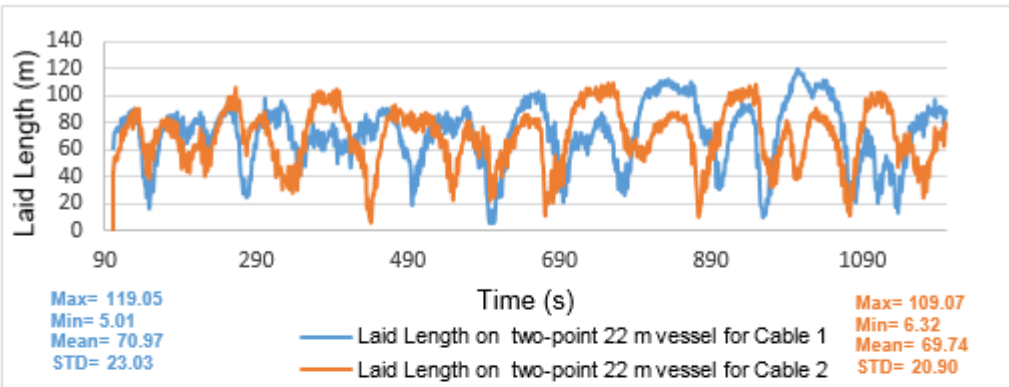
Figure 4.65 (c) & (d), Configuration 3, shows the laid length of the two-point moored 22 and 14 m vessels respectively; Cable 1 and Cable 2 are shown. The figure shows again that the 22 m vessel has more seabed footprint than the 14 m vessel (Both vessels using two-point mooring system). The amount of the laid length on the seabed of the two-point mooring system is shown to have a slight difference when compared to the other two configurations when considering the 22 m vessel only.



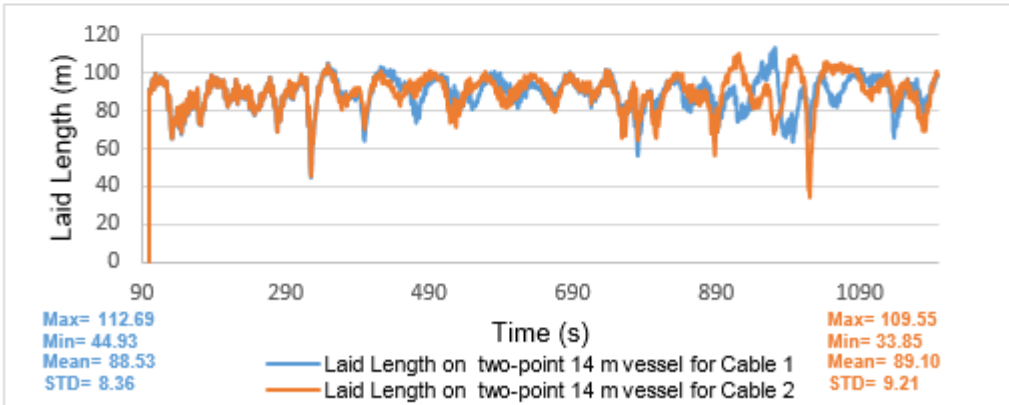
(a) Configuration 1 - Single-point mooring system (anchor with no angle)



(b) Configuration 2 - Single-point mooring system using 'Anchor 2' (at an angle)



(c) Configuration 3 - Laid length of the 22 m vessel two-point 'V' shaped anchor



(d) Configuration 3 - Laid length of the 14 m vessel two-point 'V' shaped anchor

Figure 4.65: Mooring chain laid length for all 3 configurations

Figure 4.66 below specifically compares the amount of the mooring chain laid on the seabed for the 22 m vessel in the three configurations. As can be seen, there is no significant difference in the trend for each configuration. This outcome suggest that the two-point mooring system will double the seabed footprint caused mooring line under these ocean conditions.

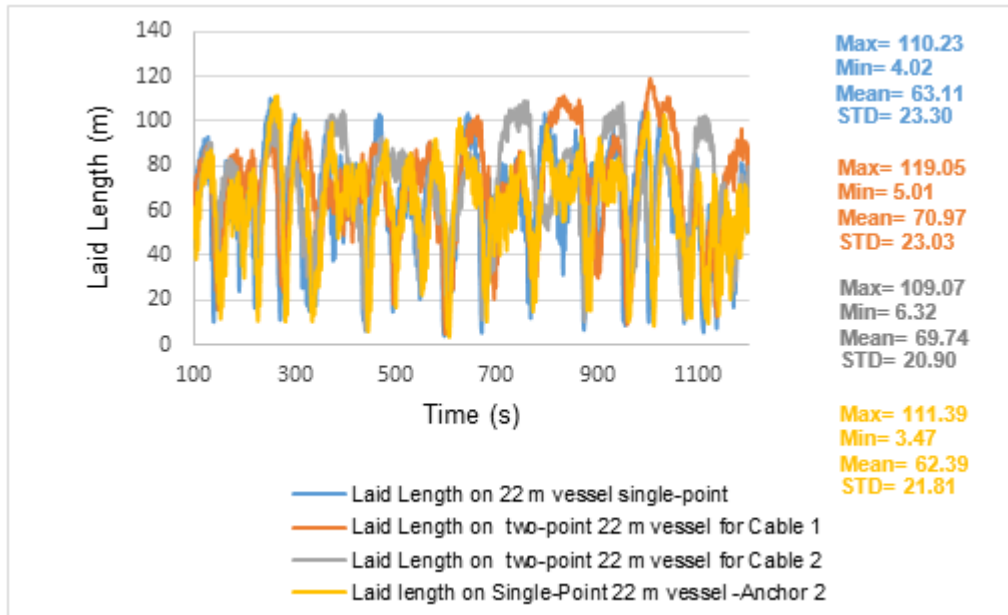


Figure 4.66: Mooring chain laid length for all three configurations on the 22 m vessel

Figure 4.67 shows the dynamic tension time-history for Configuration 1 and 2 in the XYZ directions of the single-point moored vessels with and without considering the wave angle. The results in Figure 4.67 (a) show the 22 m vessel with the maximum tension spike of 165.1 kN in the X -direction at the Fairlead. This tension spike manifested itself as a snap load, maybe as a result of tension discontinuity due to the vessel's motions under the influence of irregular waves and current loads. When the wave angle is considered, Figure 4.67 (b), Configuration 2, shows the highest tension spike at the Fairlead of 258.97 kN in the X -direction on the 22 m moored vessel, this was observed to be the highest tension spike in all of the three configurations.

The maximum tension in Figure 4.67 (a) satisfies Equation 4.1, where $F_{Chain\ max\ tension} < F_{Minimum\ break\ load}$ i.e. $165.1 < 251\ kN$. This relation indicates no failure when the mooring line tension was reached.

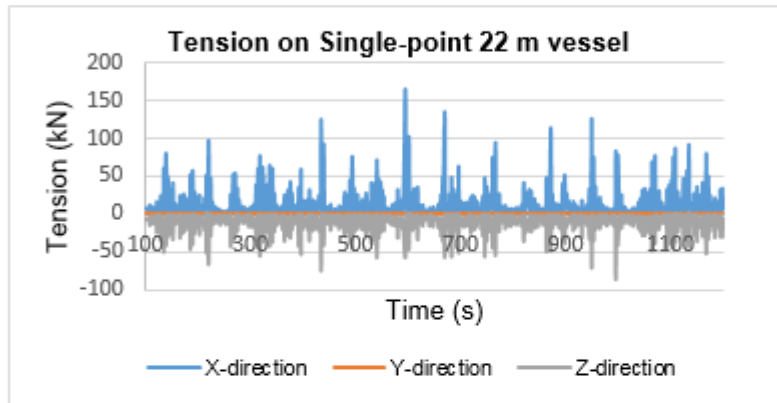
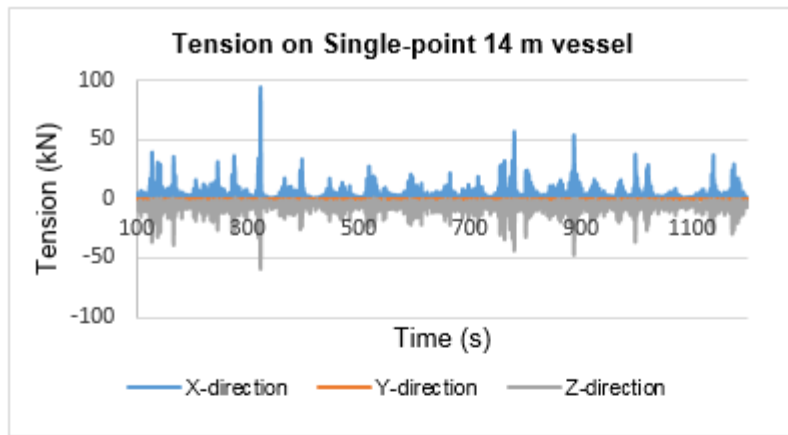
The maximum tension in Figure 4.67(b) does not satisfy Equation 4.1, where $F_{Chain\ max\ tension} > F_{Minimum\ break\ load}$ i.e. $258.97 > 251$ kN. This relation shows that the mooring line will fail when it reaches its maximum tension. However, in practice, the anchor chain will not fail but will instead drag on the seabed. This is because ANSYS AQWA assumes the anchor to be a fixed point whereas, in practice, the squid fishing industry uses anchors that are always retrieved from the seabed (drag embedded anchor). During anchor deployment, drag embedded anchors eventually lock into the seabed sand after dragging on the seabed; anchors locked to the seabed can be unlocked when the forces exerted upon them are greater than their holding capacity.

The maximum tension at the vessel's fairlead point was observed to be taking place when the vessel moves away from the anchor position due to the action of wave and current loads. It can be seen from Figure 4.67 that the maximum tension spike in Configuration 2 took place once-off and has a high discrepancy with other tension plots of below 100 kN. While on Configuration 1, the 22 m vessel showed low tension plot discrepancy between the maximum tension and other tension plots. Another observation is that both configurations showed a similar mean tension force of approximately 11 kN. Both graphs show tension fluctuation which represents loss and tension recovery as the vessel moves away and towards the anchor.

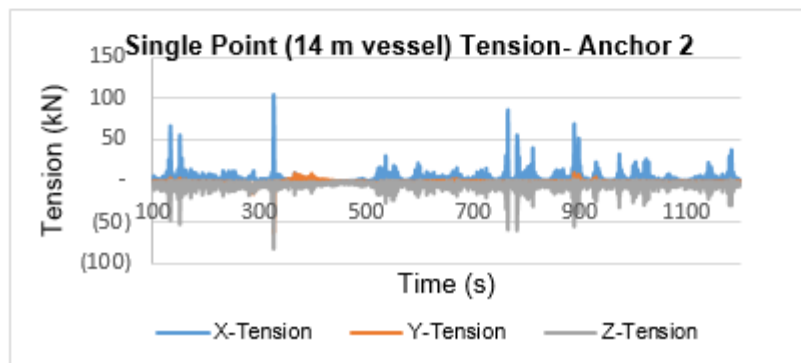
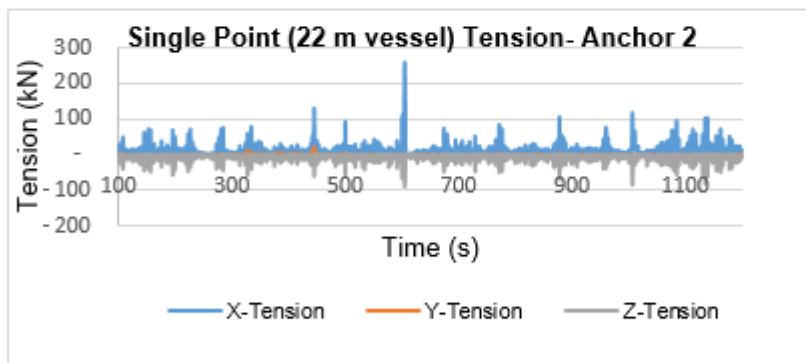
When the mooring chain reaches its maximum tension, it is also important to consider the forces exerted on the anchor, these forces are termed - anchor uplift forces. Figure 4.69 shows that in Configuration 1, when the mooring line on the 22 m vessel reaches its maximum tension, the anchor experiences the maximum uplift force of 18.58 kN; while in Configuration 2, Anchor 2 experiences the maximum uplift force of 36.65 kN. Since Klusman anchor type of between 100–250 kg is mostly used in the squid fishing industry, the weight that anchor exerts on the seabed is 2.5 kN.

This implies that anchor uplift force on Configuration 1 is 7 times greater than the anchor weight (with the assumption that the anchor is not embedded into the seabed); while in Configuration 2, the anchor uplift force is 14 times greater than the anchor weight. This finding suggests a high possibility of the anchor drag on the seabed in these wave conditions when the maximum tension is reached and potentially causes seabed anchor scour.

The 14 m vessel is shown to have low anchor uplift forces in the three configurations; the maximum anchor uplift of 6 kN is found in Configuration 2. This shows that a change in the wave direction influences the entire mooring chain causing it to sweep across the seabed and ultimately to drag the anchor.



(a) Configuration 1 - Single-point mooring system tension (anchor with no angle)



(b) Configuration 2 - Single-point mooring system using 'Anchor 2' (at an angle)

Figure 4.67: Tension time-history at Fairlead - Configuration 1 and 2

Figure 4.68, Configuration 3, shows the tension time-history in the *XYZ* directions of the two-point moored 14 and 22 m vessels. The 22 m vessel in particular, in this configuration, is shown to be experiencing high tension forces at the Fairlead, especially in the *X*-direction. The mooring chain maximum tension is shown to be 122.91 kN on the 22 m vessel which is experienced by Cable 1. Cable 2 is shown to have a maximum tension in the *Y*-direction (lateral direction) of 83.76 kN. This shows that the two anchor chains are experiencing different tension forces, especially Cable 1. When Cable 1 reaches its maximum tension, the Cable 2 was observed to be slack.

Cable 2 tension clearly shows that this anchor chain is sweeping across the seafloor. This was also observed in Figure 4.61 (c) where the vessel *Y*-direction maximum displacement was 15.56 m.

When the tension forces for 14 and 22 m vessels are compared, the 22 m vessel experiences high tension forces. This is due to high mooring chain stiffness which increases because of large forces generated by the 22 m vessel. A notable observation on these two vessels in the graph is that both show Cable 2 to have high lateral tension than the horizontal and vertical components, these are shown to be 44.19 kN and 83.76 kN on the 14 and 22 m vessels respectively. Cable 1 is shown to have high tension forces in the *X*-direction on both vessels of 32.18 kN and 122.91 kN respectively on the 14 and 22 m vessels. This confirms that the two-point mooring system causes better vessel motion restriction on both *X* and *Y* directions. However, this doubles seabed footprint caused by the two mooring chains as discussed before.

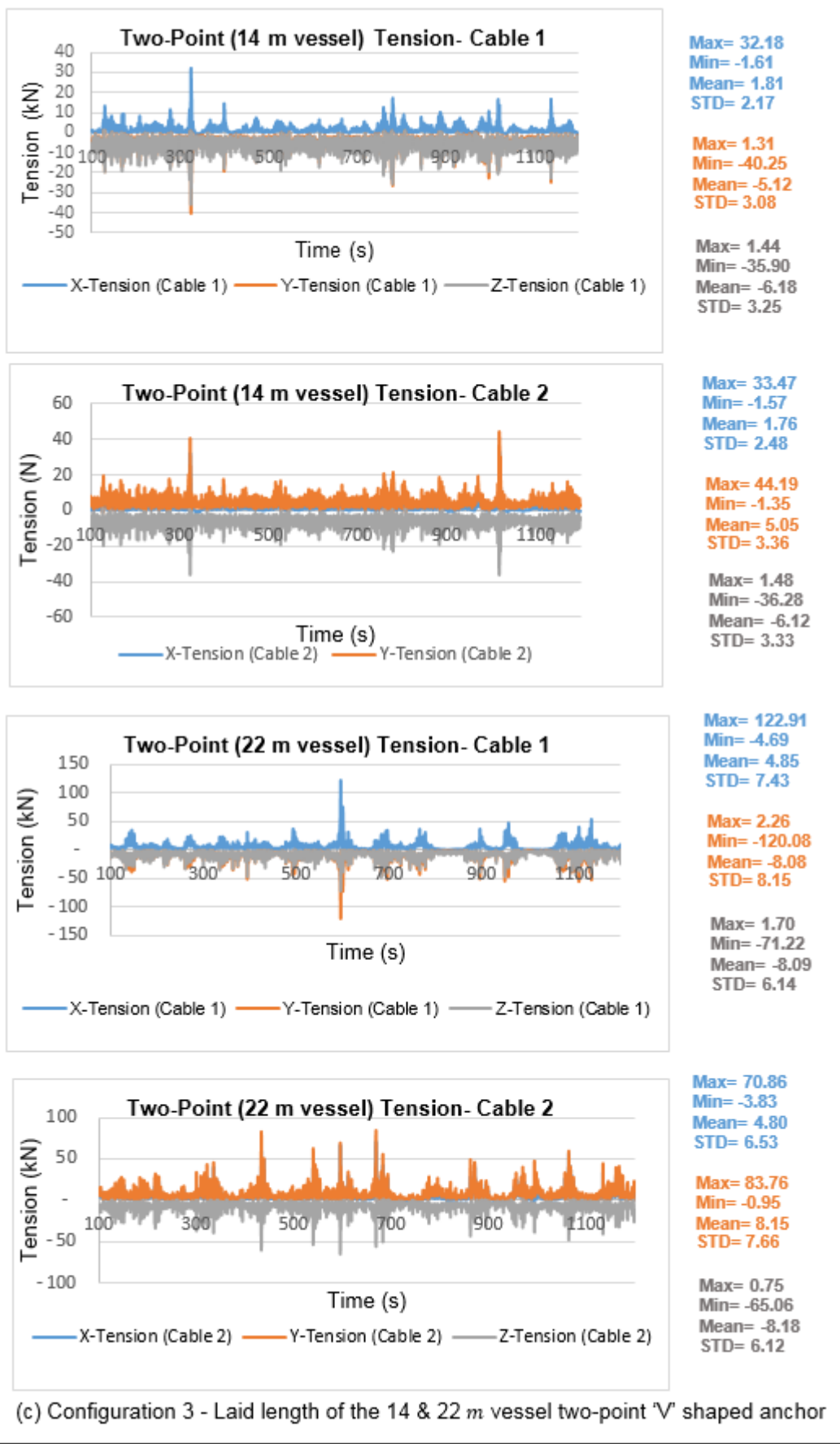


Figure 4.68: Tension time-history of the two-point mooring system – Configuration 3

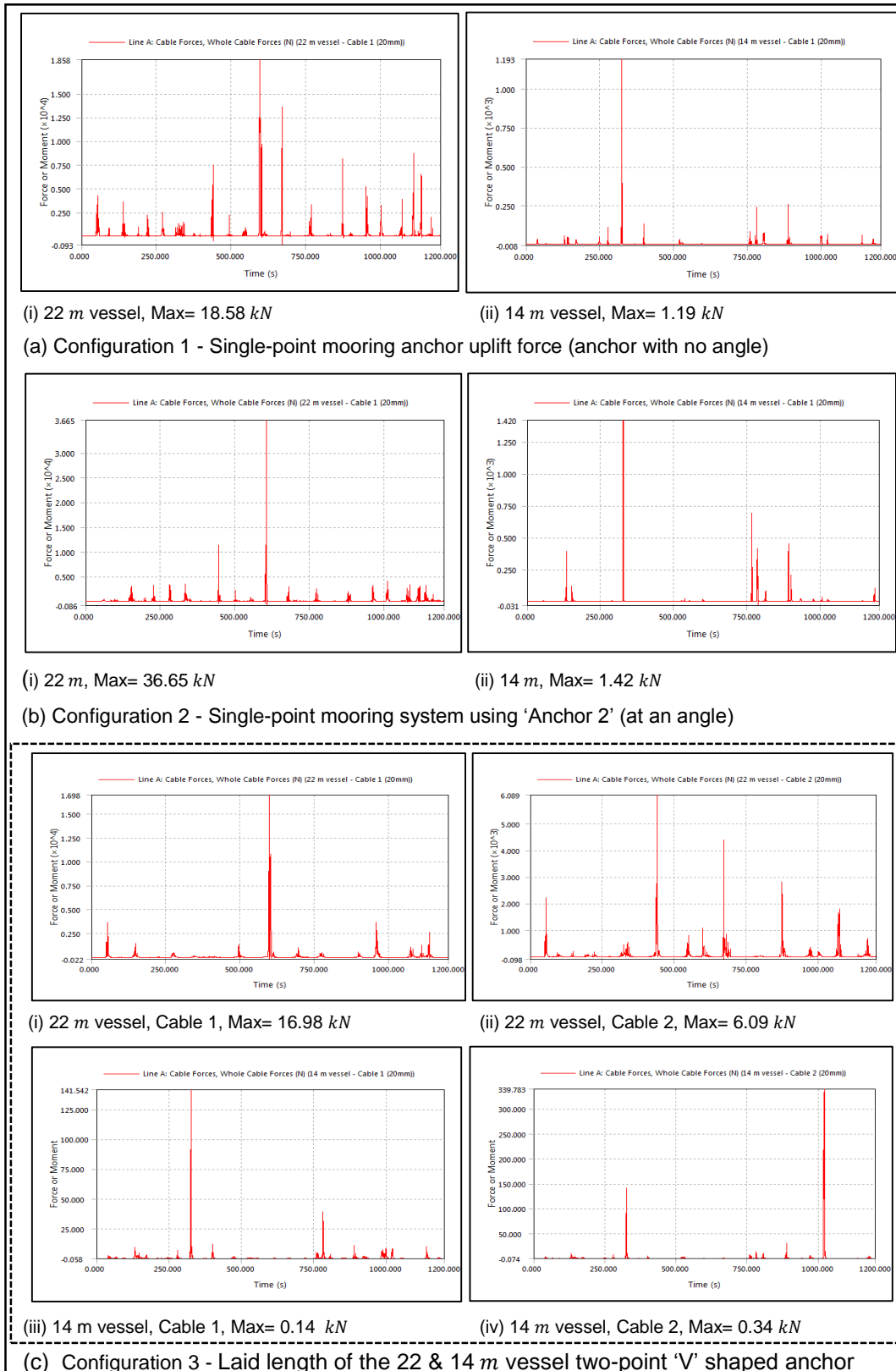


Figure 4.69: Anchor uplift forces for the all three Configurations

4.4. Summary of results: ANSYS AQWA and ABAQUS models

This section presents a summary of the result outcomes from the *ANSYS AQWA* and *ABAQUS* models using a single graphic. The graphic contains the *ANSYS AQWA* model result output parameters which are the resultant tension at the fairlead, the mooring chain laid length on the seabed and the anchor uplift forces. The *ABAQUS* model result output parameter presented is the chain link impact force on the seabed at different velocities.

In this analysis, the effect of chain diameters of 14, 16 and 20 mm is investigated; the wave height of 2.5 m and wave period of 7 s were used.

The purpose of this overview is to give a concise summary of the effect of the single-point moored vessel versus the two-point moored vessel when the 14 and 22 m vessel sizes are investigated by varying chain diameters of 14, 16 and 20 mm. The outcome from this analysis gives a brief comparison of the mooring system which causes the most footprint on the seabed.

The first graphic in Section 4.4.1 presents combined result outputs of the *ANSYS AQWA* and *ABAQUS* models on the 22 m single-point moored vessel. The second graphic presents the same outputs when the 14 m vessel is analysed. The last four graphics in Section 4.4.2 presents the aforementioned results when the two-point moored vessel are investigated.

The comparison between the single-point and two-point moored 14 and 22 m vessels using the 14, 16 and 20 mm diameter chain sizes in Section 4.4.1 and Section 4.4.2 is summarised by the following Table 4.18 and Table 4.19. These tables show maximum values of each parameter of the investigation.

Table 4.18: Result summary of the 22 m moored vessel

Parameter	20 mm chain		
	22 m vessel Single-point mooring system	22 m vessel Two-point mooring system	
	<i>Cable 1</i>	<i>Cable 1</i>	<i>Cable 2</i>
Resultant tension (kN)	174.13	186	123.15
Anchor uplift force (kN)	18.58	16.98	6.09
Laid length (m)	4.02-110.23	5.01-119.05	6.32-109.07
Parameter	16 mm chain		
	22 m vessel Single-point mooring system	22 m vessel Two-point mooring system	
	<i>Cable 1</i>	<i>Cable 1</i>	<i>Cable 2</i>
Resultant tension (kN)	195.92	141.23	191.82
Anchor uplift force (kN)	20.91	10.24	26.62
Laid length (m)	3.87-100.80	4.75-97.58	3.62-87.94
Parameter	14 mm chain		
	22 m vessel Single-point mooring system	22 m vessel Two-point mooring system	
	<i>Cable 1</i>	<i>Cable 1</i>	<i>Cable 2</i>
Resultant tension (kN)	188.59	173.28	115.2
Anchor uplift force (kN)	31.7	29.31	10.25
Laid length (m)	2.78-85.49	3.13-92.91	3.97-85.80

Table 4.18 above shows a summary of the result output of the single-point and the two-point mooring systems when the 22 m vessel is analysed; the chain diameters of 20, 16 and 14 mm were varied in the analysis. This analysis compares the resultant tension, anchor uplift forces and the mooring chain laid length on the seabed for both mooring systems.

The 22 m vessel anchored with the single-point mooring system was observed to fully stretch when the 20 mm diameter chain was used under ocean loads. This resulted in mooring chain maximum resultant tension of 174.13 kN. The tension on the two-point mooring system using the same chain diameter was found to be 186 kN for Cable 1 and 123.15 kN for Cable 2. The corresponding anchor uplift forces were found to be 18.58 kN for the single-point mooring system; the two-point mooring system anchor uplift forces were 16.98 for Anchor 1 and 6.09 kN for Anchor 2. Although the two anchors were placed symmetrically to the incoming wave and current loads, one anchor was observed to have higher anchor uplift forces than the other anchor. This outcome may be due to the nonlinear effects of the mooring chain and irregular sea waves which causes a nonlinear response of the vessel movements.

The corresponding mooring chain laid length on the seabed of the single-point mooring system was found to be in the of range 4.02 to 110.23 m as shown in Figure 4.70 (b); while the two-point mooring system range was 5.01 to 119.05 m for Cable 1 and 6.32 to 109.07 m for Cable 2 as shown in Figure 4.72 (c). These values show a slight difference of the amount of the mooring chain laid on the seabed. This implies that the two-point mooring system doubles the mooring chain laid length on the seabed in this instance.

Similarly, when observing the 16 mm diameter chain, mooring chain laid length on the seabed on the single-point mooring system range was 3.87 to 100.80 m; while the two-point mooring system was 4.75 to 97.58 m for Cable 1 and 3.62 to 87.94 m for Cable 2. In both mooring systems, the mooring chain laid on the seabed is shown to be fluctuating between the minimum and maximum range values. The maximum range occurs when the mooring is almost fully stretching, while the minimum range occurs when the mooring chain is slack.

When observing the 14 mm diameter chain, mooring chain laid length on the seabed on the single-point mooring system range was 2.78 to 85.49 m; while the two-point mooring system range was 3.13 to 92.91 m for Cable 1 and 3.97 to 85.80 m for Cable 2.

The resultant tension increased from 174.13 to 195.92 kN when the chain diameter was changed from 20 mm to 16 mm; and decreased from 195.92 kN to 188.59 kN when the 14 mm chain diameter was used on the single-point mooring system. As can be seen, the tension only varied slightly with the change in chain diameter in these wave conditions.

The corresponding anchor uplift forces on the 16 mm chain were found to be 20.91 kN for the single-point mooring system; while the two-point mooring system anchor uplift forces were 10.24 for Anchor 1 and 26.62 kN for Anchor 2. The 14 mm anchor uplift forces on the single-point mooring system were found to be 31.7 kN; the two-point mooring system anchor uplift forces were 29.31 for Anchor 1 and 10.25 kN for Anchor 2.

Table 4.19: Result summary of the 14 m moored vessel

Parameter	20 mm chain		
	14 m vessel Single-point mooring system	14 m vessel Two-point mooring system	
	<i>Cable 1</i>	<i>Cable 1</i>	<i>Cable 2</i>
Resultant tension (kN)	111.08	62.8	65.89
Anchor uplift force (kN)	1.192	0.141	0.339
Laid length (m)	24.96-119.04	44.93-112.69	33.85-109.55
Parameter	16 mm chain		
	14 m vessel Single-point mooring system	14 m vessel Two-point mooring system	
	<i>Cable 1</i>	<i>Cable 1</i>	<i>Cable 2</i>
Resultant tension (kN)	105.25	60.06	81.29
Anchor uplift force (kN)	2.54	0.343	1.31
Laid length (m)	13.73-111.74	31.29-106.30	17.73-106.51
Parameter	14 mm chain		
	14 m vessel Single-point mooring system	14 m vessel Two-point mooring system	
	<i>Cable 1</i>	<i>Cable 1</i>	<i>Cable 2</i>
Resultant tension (kN)	103.48	59.39	86.25
Anchor uplift force (kN)	4.04	0.558	2.66
Laid length (m)	9.41-108.71	22-122.67	10.25-106.77

The following analysis compares the resultant tension, anchor uplift forces and the mooring line laid length on the seabed for both mooring systems using the 14 m vessel.

Table 4.19 above shows a summary of the single and two-point mooring systems when the chain diameters of 20, 16 and 14 mm were varied. When looking at the single-point mooring system moored with the 20 mm chain, the mooring chain is shown to experience the highest tension of 111.08 kN with the corresponding maximum anchor uplift force of 1.19 kN. The two-point mooring system is shown to experience less tension and maximum anchor uplift forces compared to the single-point mooring system (using the 20 mm chain); Cable 1 experienced the maximum tension of 62.8 kN with the maximum anchor uplift force of 0.14 kN, while Cable 2 experienced the maximum tension of 65.89 kN with corresponding maximum anchor uplift force of 0.34 kN.

The corresponding mooring chain laid length on the seabed on the two-point mooring system of each cable was found to have the lowest minimum and maximum range compared to the single-point mooring system. However, when both Cable 1 and 2 are taken into account; the two-point mooring system increases the mooring chain laid length on the seabed by 41.57% (using the 20 mm chain) compared to the single-point mooring system. The range for Cable 1 was found to be from 44.93 to 112.69 m; while Cable 2 was observed to have a range of 33.85 to 109.55 m. The single-point mooring system mooring line laid length on the seabed range was found to be 24.96 to 119.04 m.

The two-point mooring system increased the mooring chain laid length on the seabed by 50.25% when the 16 mm chain was used; while the 14 mm chain increase was 2.73%. The small increase of the 14 mm chain was due to its light weight compared to the 16 and 20 mm mooring chains; the light weight of the 14 mm mooring chain resulted in a large portion mooring chain length to lift-off and drop back down on the seabed since it had less capability to resist vessel movements.

A closer look in Figure 4.71 (b) and Figure 4.75 (b), shows the single-point and the two-point mooring systems (on the 14 m vessel) moored with the 14 mm diameter mooring chain with the highest mooring chain laid length on the seabed. This outcome demonstrates that smaller chain sizes frequently lifts off and drops back down on the seabed. Figure 4.71 (c) show the 14 mm diameter chain with the least contact forces compared to the 16 and 20 mm diameter chain contact forces. The contact forces are shown to be increasing with an increase of the impact velocity and diameter of a chain.

The corresponding anchor uplift forces of the three chain sizes are shown in Figure 4.71 (d) of the 14 m single-point moored vessel. The 14 mm diameter chain is shown to be experiencing the highest anchor uplift force of 4.48 kN while the 16 and 20 mm diameter chains experienced 2.54 and 1.19 kN anchor uplift forces respectively.

Figure 4.75 (b) and (c) shows the corresponding anchor uplift forces of the three chain sizes on the 14 m two-point moored vessel. The 14 mm chain showed the highest anchor uplift force of 2.66 kN compared to the 16 and 20 mm chain sizes. The 20 mm chain on the two-point moored 14 m vessel showed the least anchor uplift forces on both Anchor 1 and Anchor 2.

In summary, the 14 m vessel analysis shows the single-point mooring system with higher anchor uplift forces than the two-point mooring system when the three chain sizes were evaluated. This observation was also found to be the same when observing the resultant tension. The two-point mooring Cable 1 and 2 each experienced almost half the tension experienced by the single-point mooring system. Lastly, Cable 1 and 2, individually showed less mooring chain laid length on the seabed compared to the single-point mooring laid length. However, since the two-point mooring system uses two mooring chains, this increased the amount of mooring chain laid length interacting with the seabed.

The 14 m vessel showed less mooring chain length of approximately 80 m interacting with the seabed; most of the mooring line length laid inactive on the seabed. The 22 m vessel showed approximately 110 m of the mooring chain length constantly lifting off and dropping down on the seabed. This outcome was observed on both the single-point and two-point mooring systems.

4.4.1. Single-point mooring system result overview

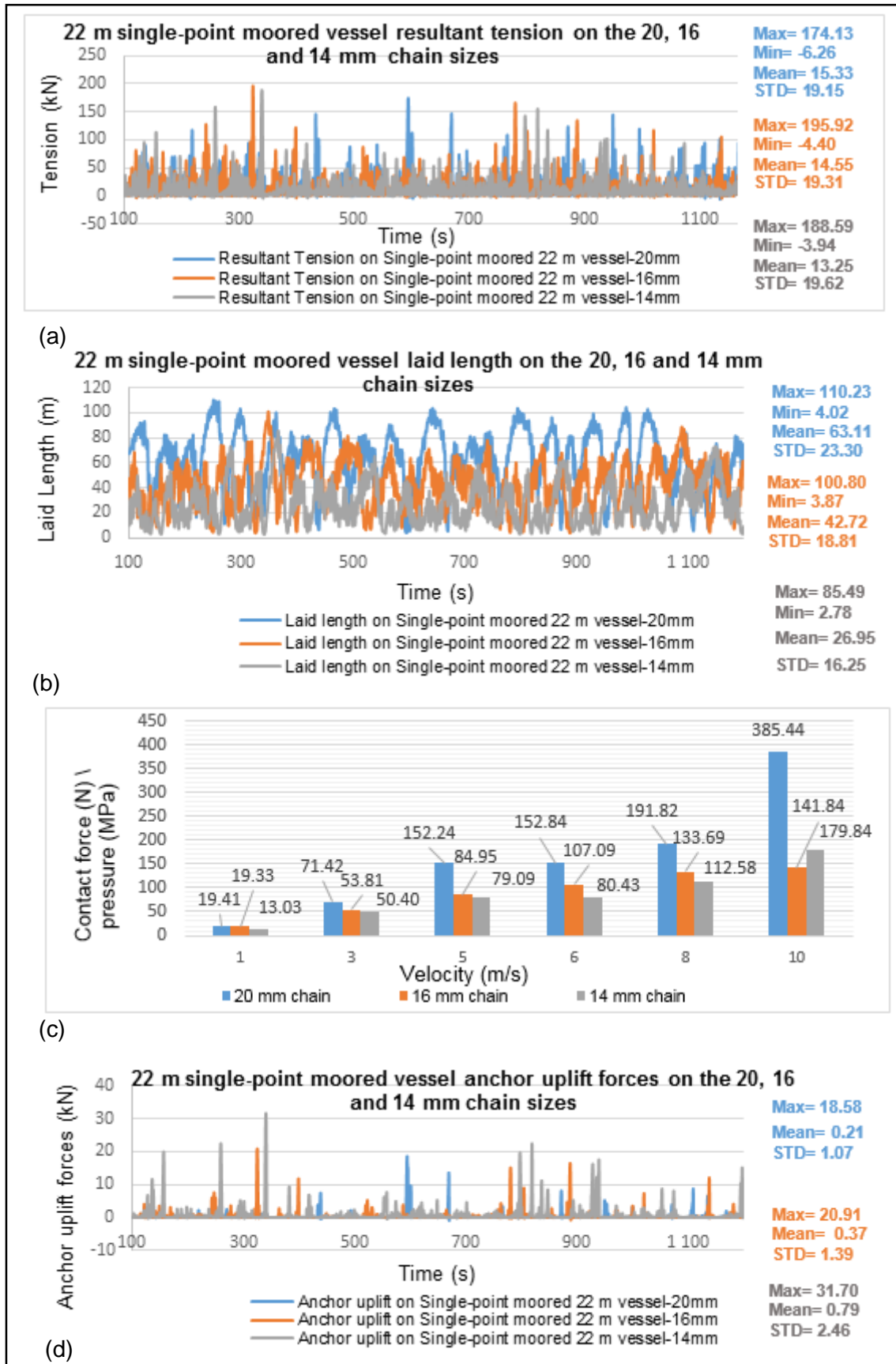


Figure 4.70: Single-point moored 22 m vessel overview (Tension (a), Laid chain length on the seabed (b), Mooring chain-seabed contact forces (c) & Anchor uplift forces (d))

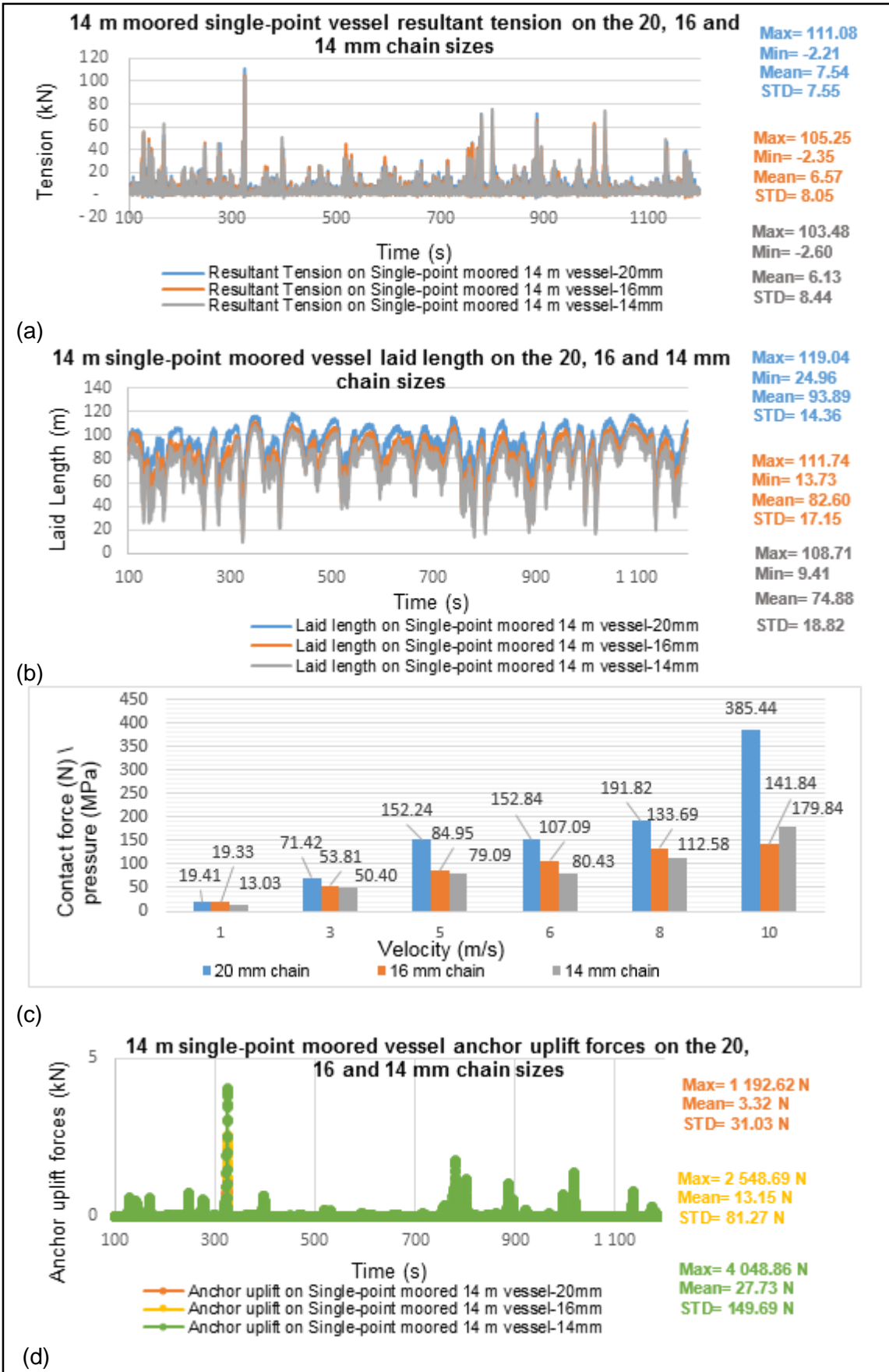


Figure 4.71: Single-point moored 14 m vessel overview (Tension (a), Laid chain length on the seabed (b), Mooring chain-seabed contact forces (c) & Anchor uplift forces (d))

4.4.2. Two-point mooring system result overview

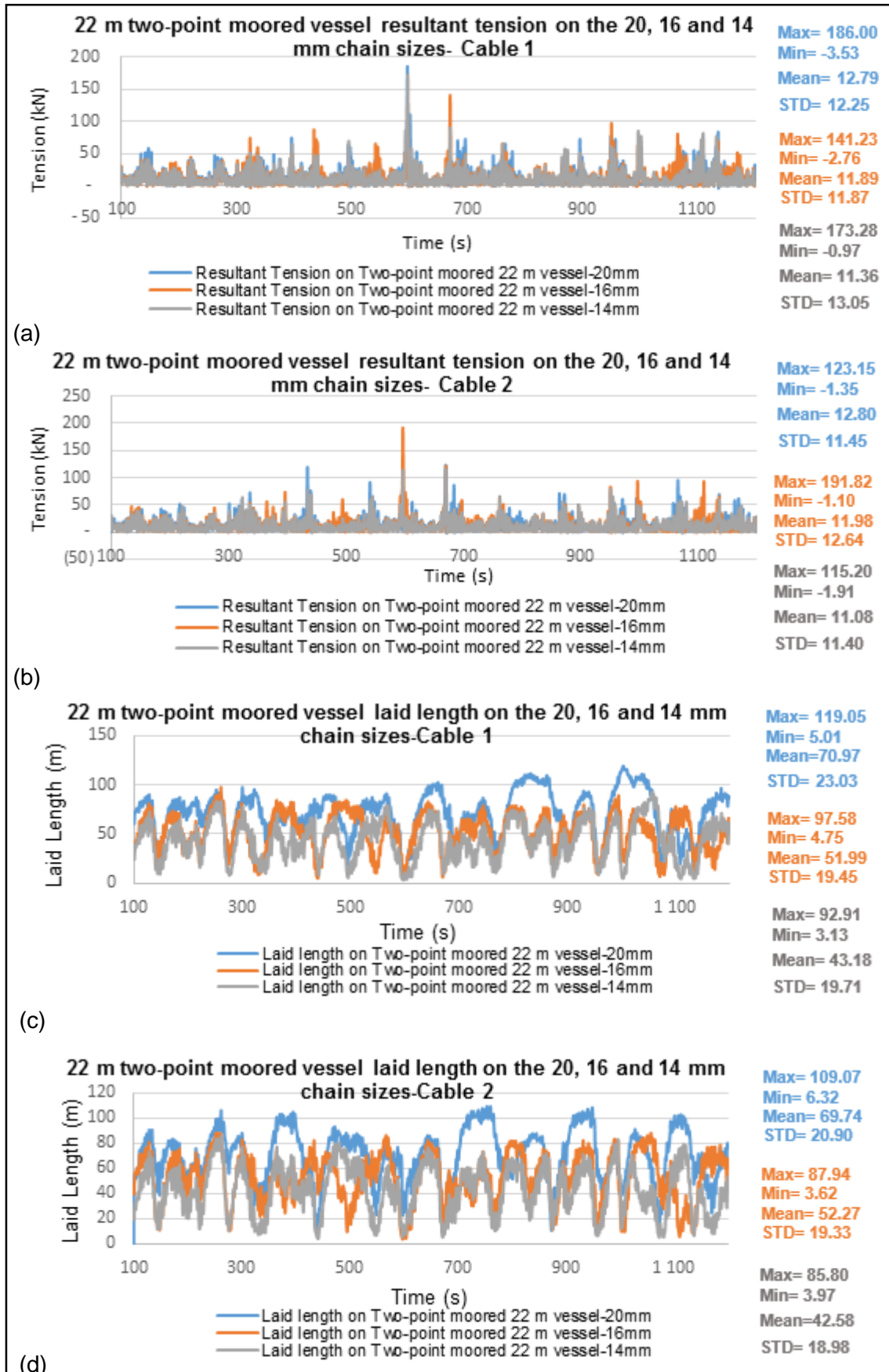


Figure 4.72: Two-point moored 22 m vessel overview (Tension on Cable 1 (a) & 2(b), Laid chain length on the seabed on Cable 1 (c) & 2(d))

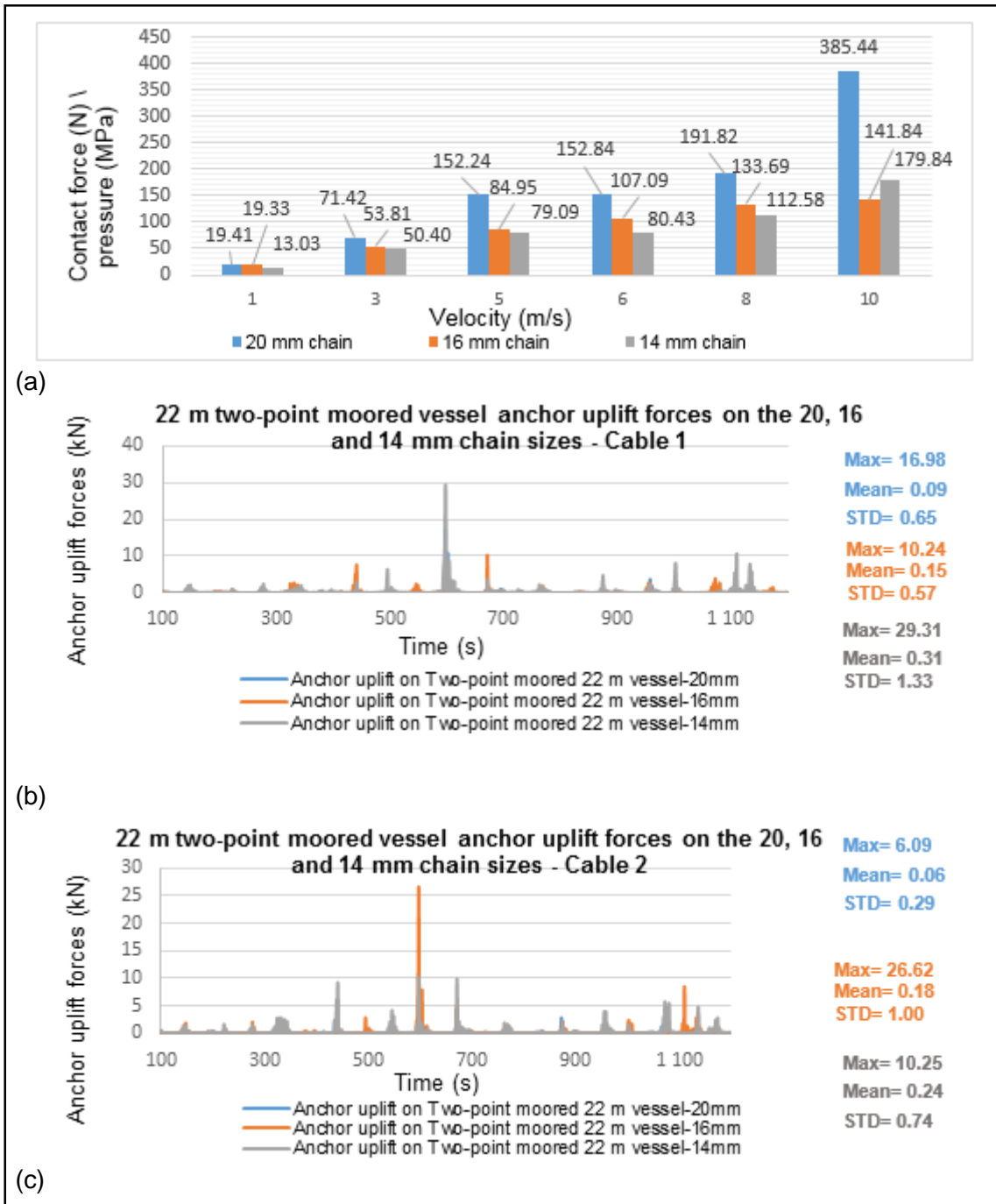


Figure 4.73: Two-point moored 22 m vessel overview (Mooring chain-seabed contact forces (a) and Anchor uplift forces on Cable 1 (b) & 2(c))

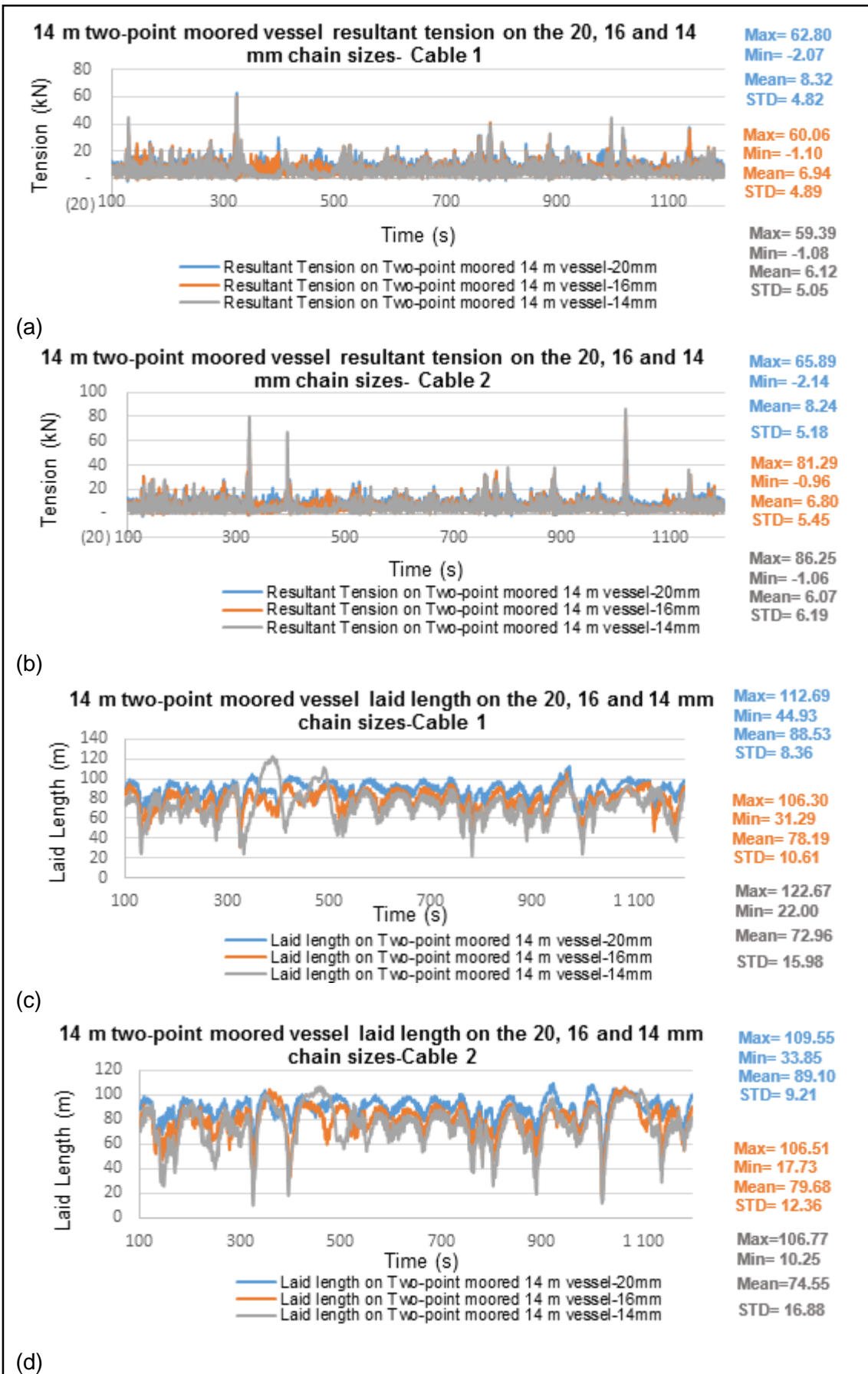


Figure 4.74: Two-point moored 14 m vessel overview (Tension on Cable 1 (a) & 2(b), Laid chain length on the seabed on Cable 1 (c) & 2(d))

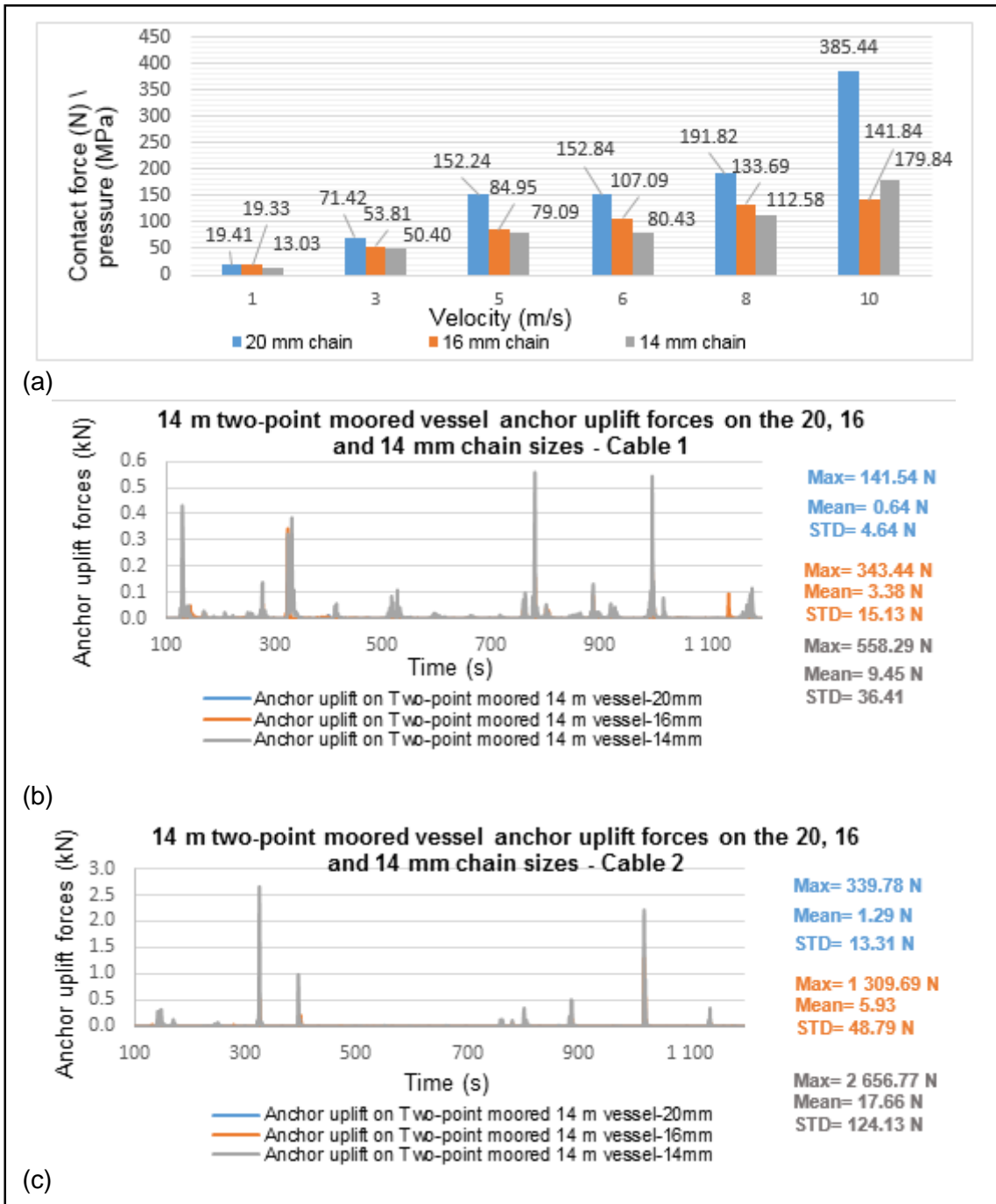


Figure 4.75: Two-point moored 14 m vessel overview (Mooring chain-seabed contact forces (a) and Anchor uplift forces on Cable 1 (b) & 2(c))

CHAPTER FIVE

5. Conclusion

The objective of this work has been to numerically analyse the effect of the single-point versus the two-point mooring systems on the seabed which are used for anchoring squid fishing vessels. This analysis is as result of an observation made by divers from the South African Department of Environmental Affairs who noticed an interaction between the mooring line and benthic squid egg beds. The mooring line which is made of steel chain was observed to impact the seabed with a noticeable velocity from the video footage obtained. This mooring line impact is suspected to possibly destroy benthic squid egg beds, which in consequence can be one of the causes of a decline in squid catches in South Africa.

In this study, two numerical models were developed for investigating the effects of the single-point and two-point mooring systems on the seabed. The primary model was developed using *ANSYS AQWA* which investigated the response of the two types of squid fishing vessels subjected to ocean loads. The secondary model was developed using *ABAQUS* finite element model, this model was used for simulating the mooring chain impact pressure and force on the seabed which is not available in *ANSYS AQWA*.

The mooring chain effect on the seabed due to varying the wave height and period was investigated using the 22 m vessel. Three mooring system configurations were also used on both the single-point and two-point mooring systems for analysing their effect on the seabed. The effect of the three chain sizes used in the squid fishing industry was also investigated using the 14 and 22 m fishing vessels by varying anchor chain diameters of 14, 16 and 20 mm.

The underwater video footage captured by marine divers was analysed using *Tracker* video analysis software to determine the actual impact velocity of the mooring chain on the seabed. The impact pressure on the seabed due to the obtained velocity was presented. The velocity from the video analysis was also used to calibrate the *ANSYS AQWA* model so that it correlates to realistic ocean conditions. From the results obtained in this study, the following conclusions are drawn:

1. The measured mooring chain impact velocity from *Tracker* was estimated to be 8 m/s with an average velocity of about 5 m/s.

2. The *ABAQUS* model developed by varying velocities of 1, 3, 5, 6, 8 and 10 m/s showed a linear relationship between the mooring chain impact velocity and pressure on the seabed. The mooring chain impact pressure on the seabed increased as the impact velocity of the chain increased. An increase in the diameter of the mooring chain also resulted in an increase in the impact pressure and forces on the seabed.
3. When looking at the obtained velocity of 8 m/s of the underwater chain impacting the seabed. The 20 mm diameter chain was found to cause the greatest seabed impact pressure and force of 191 MPa and 191.82 N respectively. The 16 mm diameter chain impact pressure and force on the seabed was found to be 133 MPa and 133.69 N respectively. The 14 mm diameter cause the least seabed impact pressure and force of 112 MPa and 112.58 N.
4. The effect of varying the wave height and period showed that a decrease in the wave height and an increase in the wave period increased the tension on the mooring line. This consequently resulted in a large portion of the mooring line lifting off and dropping back down on the seabed. The mooring line was observed to have both slack and taut profiles over the simulation duration.

This effect was clearly observed when the wave height was increased from 1 to 2 m while keeping the wave period of 7 s constant. The corresponding seabed impact pressure due to this effect showed a difference of 94.14% (from 42.48 to 118.03 MPa); while a difference in tension of 126.87% (from 23.93 to 106.96 kN) was obtained. However, when the wave height was increased from 1 to 2 m while keeping the wave period of 10 s constant; the mooring line resulted in more slack profile. This, in consequence, led to a significant amount of the mooring line lying dormant on the seabed. The corresponding seabed impact pressure difference of 89.29% (from 36.96 to 96.59 MPa) was obtained; while the difference in tension of 94.93% (from 22.08 to 61.98 kN) was obtained. It can then be said that when the wave height doubles, the impact pressure on the seabed also doubles. This effect was more apparent when the wave period of 7 s was present.

5. The outcomes of investigating the three mooring line configurations on both vessel sizes showed that the two-point mooring system doubles the mooring

line footprint on the seabed compared to the single-point mooring system. Each of the two mooring lines was observed to sweep across the seabed as the ocean waves passed across the moored vessel. However, the two-point mooring also showed less seabed footprint than the single-point mooring system when the wave direction changes.

The 14 m moored vessel was found to have less seabed footprint on the seabed, this was noticeable by a large portion of the mooring line which laid dormant on the seabed. On the contrary, the 22 m vessel mooring line was found to have a large portion which frequently interacted with the seabed. This outcome was observed when both vessels used the same mooring system configuration.

High tension values were found to be associated with frequent mooring line interaction with the seabed. The anchor uplift forces were also presented which can give more insight for further investigation such as the effect of anchor drag on the seabed.

6. The outcomes of investigating the effect of the three mooring chain sizes showed that the two-point mooring system increased the mooring line laid length on the seabed by 41.57% compared to the single-point mooring system when the 20 mm diameter was used. This increase was found to be 50.25% when the 16 mm diameter chain was used and 2.73% when the 14 mm diameter chain was used.

The 14 m vessel anchored with the 14 mm diameter chain using the single-point mooring system was found to have the most mooring line laid length on the seabed which frequently lifted up and down. The 22 m vessel in this case showed the 20 mm chain with the most frequent interaction on the seabed.

In summary, *ANSYS AQWA* can simulate the single-point and two-point mooring systems. However, the software is still limited as it does not include the seabed frictional effects and the contact force of the mooring line. *ABAQUS* finite element was used to account for the seabed contact forces, these forces were simulated based on the measured impact velocity of various points of contact along the mooring line. Results obtained in this study indicate that the two-point mooring doubles the mooring chain seabed contact length on the seabed. The 20 mm diameter chain was found to

cause up to 40% more damage than the 16 mm diameter chain in terms of impact pressure on the seabed. If the wave direction does not change, the two-point mooring system could cause more damage if one considers the greater footprint on the seabed as was shown in Figure 4.66 where one of the cables alone has 8% more laid length and there are two cables in contact so the damage will be slightly more than double the single point mooring. We can therefore, conclude, that the two point mooring system will cause more damage than a single point mooring system as the contact for each cable would have to have been halved for it to have caused the same damage and this is clearly not the case.

6. Recommendations and future work

Future improvements

- The quality of underwater video footage needs to be improved for more accurate analysis of the marked points along the mooring line.
- The video footage data can be improved through the following methods
 - The use of high-resolution camera, up 1000 frames per second and lighting is advised for more visibility. Use of underwater lights of about 9000 lumens without excessive glare.
 - Error tracking: inconsistency in detecting the centre point of the reflective marker (can use traffic reflective colour or reflective tape) in a recorded image, any given marker is composed of several pixels.
- Design related recommendations
 - Clump weights/buoys can be installed on the section of mooring line that interacts with the seabed in order reduce contact.

Software Limitations

For this application of *ANSYS AQWA*, some software limitations still exist. The main one is that the software does not consider the seabed impact or contact force with the associated seabed friction effects on the seabed.

Another limitation associated with the latter is that the software only outputs the time-history of the vessel nodes and elements; only two output nodes for the mooring line which are the anchor point (defined as fixed point) and the fairlead point where the mooring tension is calculated. The discretised mooring line nodes and elements are internally converted by the software to a two-dimensional load/extension database.

Lastly, another limitation is with regard to the fixed anchor assumption on the seabed for mooring the floating structure. In the squid industry, temporary anchors are used during fishing and retrieved from the seabed after fishing. These anchors have a high possibility of dragging on the seabed when the mooring line tension are high. The fixed anchor is more relevant for a permanent anchor on the seabed.

Future work

- Anchor drag impact on the seabed with the emphasis on anchor trajectory needs to be investigated.
- The use of improved high definition cameras is required for measurements with scientific accuracy.
- The chain motion should be also be studied 3-D for eliminating the assumptions from the 2-D video analysis.

REFERENCES

- Abadie, A., Lejeune, P., Pergent, G. & Gobert, S. 2016. From mechanical to chemical impact of anchoring in seagrasses: The premises of anthropogenic patch generation in *Posidonia oceanica* meadows. *Marine Pollution Bulletin*, 109(1): 61–71.
- ABAQUS. 2012. *Abaqus 6.12: Getting Started with Abaqus (Interactive Edition)*.
- ABC Moorings. 2015. Mooring Lines. <http://abc-moorings.weebly.com/mooring-lines.html> 2 April 2015.
- Allan, B. 2008. Solutions to simple boundary and initial value problems. *Applied Mechanics of Solids*. http://solidmechanics.org/text/Chapter4_1/Chapter4_1.htm 17 April 2017.
- ANSYS AQWA. 2015. *Aqwa Theory Manual*.
- Balzola, R. 1999. *Mooring Line Damping In Very Large Water Depths*. Massachusetts Institute of Technology.
- Belytschko, T., Ong, J.S.-J., Wing Kam Liu & Kennedy, J.M. 1984. Hourglass control in linear and nonlinear problems. *Computer Methods in Applied Mechanics and Engineering*, 43(3): 251–276.
- Bjørnsen, E. 2014. *Chains in Mooring Systems*. Master Thesis. Trondheim: Norwegian University of Science and Technology.
- Blignaut, J. 2012. Chokka industry in dire straits. *SABC News*: 1. <http://www.sabc.co.za/news/a/541d51804c0b3cfab72dfffa583a5af00/Chokka-industry-in-dire-straits-20120720> 18 February 2015.
- Boom, H.J.J. Van Den. 1985. Dynamic Behaviour of Mooring Lines. *Behaviour of Offshore Structures*: 359–368.
- Chrolenko, M.O. 2013. *Dynamic Analysis and Design of Mooring Lines*. Master Thesis. Trondheim: Norwegian University of Science and Technology.
- Collins, K.J., Suonpää, A.M. & Mallinson, J.J. 2010. The impacts of anchoring and mooring in seagrass, Studland Bay, Dorset, UK. *Underwater Technology*, 29(3): 117–123.

- Cummins, W. 1962. The impulse response function and ship motions. *Schiffstechnik*, 57(9): 101–109.
- Davis, A.R., Broad, A., Gullett, W., Reveley, J., Steele, C. & Schofield, C. 2016. Anchors away? The impacts of anchor scour by ocean-going vessels and potential response options. *Marine Policy*, 73: 1–7.
- Demers, M.C.A., Davis, A.R. & Knott, N.A. 2013. A comparison of the impact of 'seagrass-friendly' boat mooring systems on *Posidonia australis*. *Marine Environmental Research*, 83: 54–62.
- DNV. 2010. *Offshore Standard DNV-OS-E-301 - Position Mooring*.
- DNV. 2011. *Offshore Standard DNV-RP-H103 -Modelling And Analysis Of Marine Operations*.
- Ebbesen, C. 2013. *Analysis of Motions and Anchor Line Forces for Floating Production Units*. Norwegian University of Science and Technology.
- Eder, S. 2012. *ANSYS CFD for Naval Applications*.
- Francour, P., Ganteaume, A. & Poulain, M. 1999. Effects of boat anchoring in *Posidonia oceanica* seagrass beds in the Port- Cros National Park (north- western Mediterranean Sea). *Aquatic Conservation: Marine and Freshwater Ecosystems*, 9(4): 391–400.
- Garrett, D.L. 1982. Dynamic Analysis of Slender Rods. *Journal of Energy Resources Technology*, 104(4): 302–306.
- Ha, T.-P. 2011. *Frequency and Time Domain Motion and Mooring Analyses for a Fpso Operating in Deep Water*. PhD Thesis. Newcastle: Newcastle University.
- Haritos, N. 2007. Introduction to the Analysis and Design of Offshore Structures – An Overview. *Electronic Journal of Structural Engineering*, 7(Special Issue: Loading on Structures): 55–65.
- Hastings, K., Hesp, P. & Kendrick, G.A. 1995. Seagrass loss associated with boat moorings at Rottnest Island, Western Australia. *Ocean & Coastal Management*, 26(3): 225–246.

- Herbert, R.J.H., Crowe, T.P., Bray, S. & Sheader, M. 2009. Disturbance of intertidal soft sediment assemblages caused by swinging boat moorings. *Hydrobiologia*, 625(1): 105–116.
- Ibrahim, R.A. & Grace, I.M. 2010. Modeling of ship roll dynamics and its coupling with heave and pitch. *Mathematical Problems in Engineering*, 2010: 13–18.
- Jameel, M., Ahmad, S., Islam, A.B.M.S. & Jumaat, M.Z. 2011. Nonlinear Analysis of Fully Coupled Integrated Spar-Mooring Line System. *International Society of Offshore and Polar Engineers*, 8: 198–205.
- Ketchman, J. & Lou, Y. 1975. Application of the finite element method to towed cable dynamics. In *OCEAN 75 Conference*. IEEE: 98–107.
- Kim, Y.-B. 2003. *Dynamic analysis of multiple-body floating platforms coupled with mooring lines and risers*. Doctoral dissertation. Texas: Texas A&M University.
- Kininmonth, S., Lemm, S., Malone, C. & Hatley, T. 2014. Spatial vulnerability assessment of anchor damage within the Great Barrier Reef World Heritage Area, Australia. *Ocean & Coastal Management*, 100: 20–31.
- Krusche, P., Mia, N. & Hofmeyr, C.D. 2014. Squid exporters receive competition law exemption. *Cape Business News*: 1.
- Masciola, M., Jonkman, J. & Robertson, A. 2014. Extending the Capabilities of the Mooring Analysis Program: A Survey of Dynamic Mooring Line Theories for Integration Into FAST. In *Volume 9A: Ocean Renewable Energy*. ASME: 6.
- Mason, W. 2015. Incompressible Potential Flow Using Panel Methods. In *Applied Computational Aerodynamics Applied Computational Aerodynamics: A Modern Engineering Approach*. 4–1.
- Miedema, S.A., Kerkvliet, J., Strijbis, D., Jonkman, B. & Hatert, M.V. 2006. The digging and holding capacity of anchors. *Offshore (Conroe, TX)*.
- Milazzo, M., Badalamenti, F., Ceccherelli, G. & Chemello, R. 2004. Boat anchoring on *Posidonia oceanica* beds in a marine protected area (Italy, western Mediterranean): Effect

- of anchor types in different anchoring stages. *Journal of Experimental Marine Biology and Ecology*, 299(1): 51–62.
- OrcaFlex. 2010. *OrcaFlex Manual*.
- Paredes, G.M. & Taveira-Pinto, F. 2016. An experimental technique to track mooring cables in small scale models using image processing. *Ocean Engineering*, 111: 439–448.
- Pellegrino, S. & Ong, P.P.A. 2003. Modelling of Seabed Interaction in Frequency Domain Analysis of Mooring Cables. In *Proceedings of OMAE'03 22nd International Conference on Offshore Mechanics and Arctic Engineering*. 1–10.
- Rajasuriya, A., Olof, L. & Ohman, M.C. 2013. Disturbances on Coral Sri Lanka : A Case Study Reefs in. *Ambio*, 22(7): 474–480.
- Sarkar, A. & Eatock Taylor, R. 2002. Dynamics of mooring cables in random seas. *Journal of Fluids and Structures*, 16(2): 193–212.
- Sluijs, M.F. van & Blok, J. 1977. The Dynamic Behavior of Mooring Lines. *Offshore Technology Conference (OTC), Houston*.
- Taylor, R. & Valent, P. 1984. Design Guide for Drag Embedment Anchors. *Naval Civil Engineering Lab Port Hueneme CA*.
- The Editors of Encyclopædia Britannica. 2009. Agulhas Current | ocean current | Britannica.com. : 1. <https://global.britannica.com/place/Agulhas-Current> 6 March 2017.
- Vineesh, M. V, Sabu, N. V & Manju, P.M. 2014. Finite Element Analysis of Mooring Cable. *International Journal of Engineering Research and Applications (IJERA) ISSN*, (January): 13–18.
- Walker, D.I., Lukatelich, R.J., Bastyan, G. & McComb, A.J. 1989. Effect of boat moorings on seagrass beds near Perth, Western Australia. *Aquatic Botany*, 36(1): 69–77.
- Wang, L.Z., Guo, Z. & Yuan, F. 2010. Three-dimensional interaction between anchor chain and seabed. *Applied Ocean Research*, 32(4): 404–413.

World Wide Fund South Africa. 2011. South African Fisheries: The real facts and trends. *WWF South Africa*: 1. <http://www.wwf.org.za/?4900/fisheriesfactstrends> 18 February 2015.

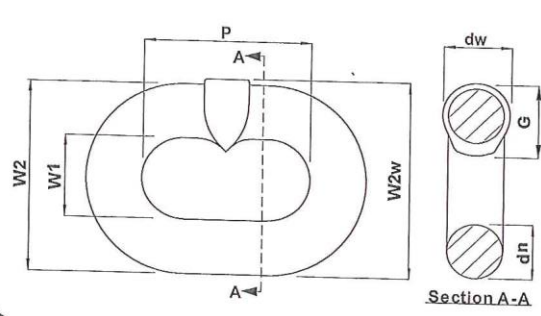
Yang, W.S. 2007. *Hydrodynamic Analysis of Mooring Lines Based on Optical Tracking Experiments*. PhD: Texas. Texas A&M University.

Yu, L. & Tan, J.H. 2006. Numerical investigation of seabed interaction in time domain analysis of mooring cables. *Journal of Hydrodynamics*, 18(4): 424–430.

APPENDIX/APPENDICES

APPENDIX A: Chain specification data

COMMODITY	Dimensions										Forces			Approx mass kg/m
	Diameter (dn)		Pitch (P)			W1	W2	W2w	dw	G	BF	MPF	WLL	
	nom	tol ±	nom	min	max	min	max	max	max	max	kN	kN	tonne	
CSL040	4.0	0.16	12.0	11.6	12.4	5.2	14.6	14.8	4.4	5.4	10.1	4.0	0.20	0.36
CSL056	5.6	0.22	16.8	16.3	17.3	7.3	20.4	20.7	6.2	7.6	19.7	7.9	0.40	0.70
CSL060	6.0	0.24	18.0	17.5	18.5	7.8	21.9	22.2	6.6	8.1	22.6	9.0	0.46	0.80
CSL063	6.3	0.25	18.9	18.3	19.5	8.2	23.0	23.3	6.9	8.5	24.9	10.0	0.51	0.88
CSL070	7.0	0.28	21.0	20.4	21.6	9.1	25.6	25.9	7.7	9.5	30.8	12.3	0.63	1.09
CSL080	8.0	0.32	24.0	23.3	24.7	10.4	29.2	29.6	8.8	10.8	40.2	16.1	0.82	1.43
CSL090	9.0	0.36	27.0	26.2	27.8	11.7	32.9	33.3	9.9	12.2	50.9	20.4	1.04	1.80
CSL100	10.0	0.40	30.0	29.1	30.9	13.0	36.5	37.0	11.0	13.5	62.8	25.1	1.28	2.23
CSL112	11.2	0.45	33.6	32.6	34.6	14.6	40.9	41.4	12.3	15.1	78.8	31.5	1.61	2.79
CSL130	13.0	0.52	39.0	37.8	40.2	16.9	47.5	48.1	14.3	17.6	106	42.5	2.16	3.77
CSL140	14.0	0.56	42.0	40.7	43.3	18.2	51.1	51.8	15.4	18.9	123	49.3	2.51	4.36
CSL160	16.0	0.64	48.0	46.6	49.4	20.8	58.4	59.2	17.6	21.6	161	64	3.28	5.71
CSL200	20.0	1.00	60.0	58.2	61.8	26.0	73.0	74.0	22.0	27.0	251	101	5.12	8.92
CSL220	22.0	1.10	66.0	64.0	68.0	28.6	80.3	81.4	24.2	29.7	304	122	6.20	10.8
CSL260	26.0	1.30	78.0	75.7	80.3	33.8	94.9	96.2	28.6	35.1	425	170	8.7	15.1
CSL280	28.0	1.40	84.0	81.5	86.5	36.4	102	104	30.8	N/A	493	197	10.0	17.4
CSL320	32.0	1.60	96.0	93.1	98.9	41.6	117	118	35.2	N/A	643	257	13.1	22.8
CSL360	36.0	1.80	108	105	111	46.8	131	133	39.6	N/A	814	326	16.6	28.9
CSL400	40.0	2.00	120	116	124	52.0	146	148	44.0	N/A	1005	402	20.5	35.7
CSL450	45.0	2.25	135	131	139	58.5	164	167	49.5	N/A	1272	509	25.9	45.1
CSL500	50.0	2.50	150	146	155	65.0	183	185	55.0	N/A	1571	628	32.0	55.6



Section A-A

NOTES

- 1- Dimensions in mm.
- 2- Forces: BF= Breaking Force (min)
MPF= Manufacturing Proof Force (min)
WLL= Working Load Limit (F.O.S. = 5:1)(max)
- 3- Mean stress at forces:
BF= 400 MPa
MPF= 160 MPa
WLL= 80 MPa
- 4- Dimensionally to SABS 189: 1993
- 5- Calibration to P(max) available on request
- 6- Chain Heat Treatment: not a specific requirement
- 7- Chain sizes greater than 26 mm with smooth weld only.
- 8- Larger chain sizes up to 70mm available on request
- 9- Chain markings = none
- 10- Elongation = 17% (min.)
- 11- When ordering describe item as follows:
e.g. 6.0mm Grade 4 Short Link Inswell chain.

McKINNON CHAIN (PTY) LTD
SPECIAL SHORT LINK CHAIN

Approved: Date: 30-Oct-98 Revision 1 DWG No: CAT 4901 - C

McKinnon Special Short Link Chain - SSL Chain

McKinnon special Short Link Chain is a high quality carbon-steel Short Link Chain for general purpose use.

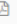
Special short link chain														
Commodity	Dimensions (mm)										Forces			Approx mass kg/m
	Diameter (dn)		Pitch (P)			W1	W2	w2w	dw	G	BF	MPF	WLL	
	nom	tol +/-	nom	min	max	min	max	max	max	max	kN	kN	tonne	
CSL130	13		39	37.8	40.2	16.9	47.5	48.1	14.3	17.6	106	42.5	2.16	3.77
CSL140	14		42	40.7	43.3	18.2	51.1	51.8	15.4	18.9	123	49.3	2.51	4.36
CSL160	16		48	46.6	49.4	20.8	58.8	59.2	17.6	21.6	161	64	3.28	5.71
CSL200	20		60	58.2	61.8	26	73	74	22	27	251	101	5.12	8.92

APPENDIX B: Steel and sand properties

Sand properties

Elastic Properties of Soils

Renier Cloete | 2003-01-14 | 2 Comments | in Reference Data

Download PDF 

Can you suggest values for elastic soil properties?

Many sources list elastic properties of various soil types. The data below is taken from *Foundation Analysis and Design (5th Edition)*, by J.E. Bowles, 1996 McGraw-Hill.

Poisson's ratio:

Clay, saturated: 0.4 to 0.5
Clay, unsaturated: 0.1 to 0.3
Sandy clay: 0.2 to 0.3
Silt: 0.3 to 0.35
Sand, gravelly sand: 0.1 to 1.0 (not elastic but 0.3 to 0.4 commonly used)
Rock: 0.1 to 0.3
Loess: 0.1 to 0.3

Poisson's ratio:

Most clay soils: 0.4 to 0.5
Saturated clay soils: 0.45 to 0.5
Cohesionless, medium and dense: 0.3 to 0.4
Cohesionless, loose to medium: 0.2 to 0.35

Young's modulus (MPa):

Clay:
Very soft: 2 to 15
Soft: 5 to 25
Medium: 15 to 50
Hard: 50 to 100
Sandy: 25 to 250
Glacial till:
Loose: 10 to 150
Dense: 150 to 720
Very dense: 500 to 1440
Loess: 15 to 60
Sand:
Silty: 5 to 20
Loose: 10 to 25
Dense: 50 to 81
Sand and gravel:
Loose: 50 to 150
Dense: 100 to 200
Shale: 150 to 5,000
Silt: 2 to 20

(<https://support.prokon.com/portal/kb/articles/elastic-properties-of-soils>)

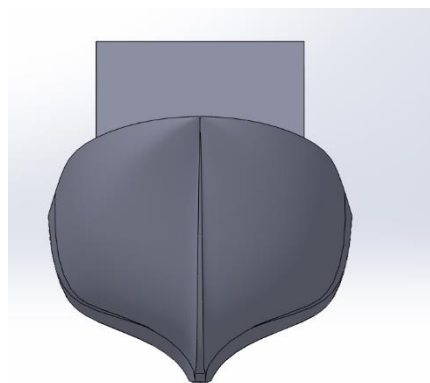
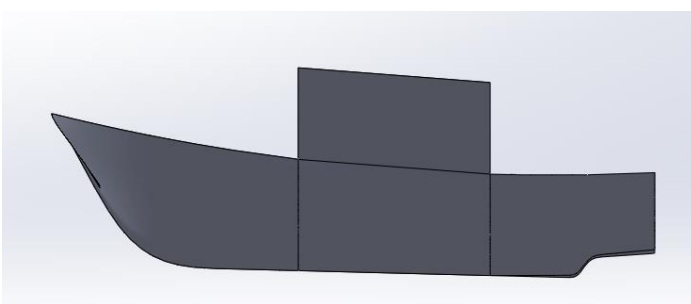
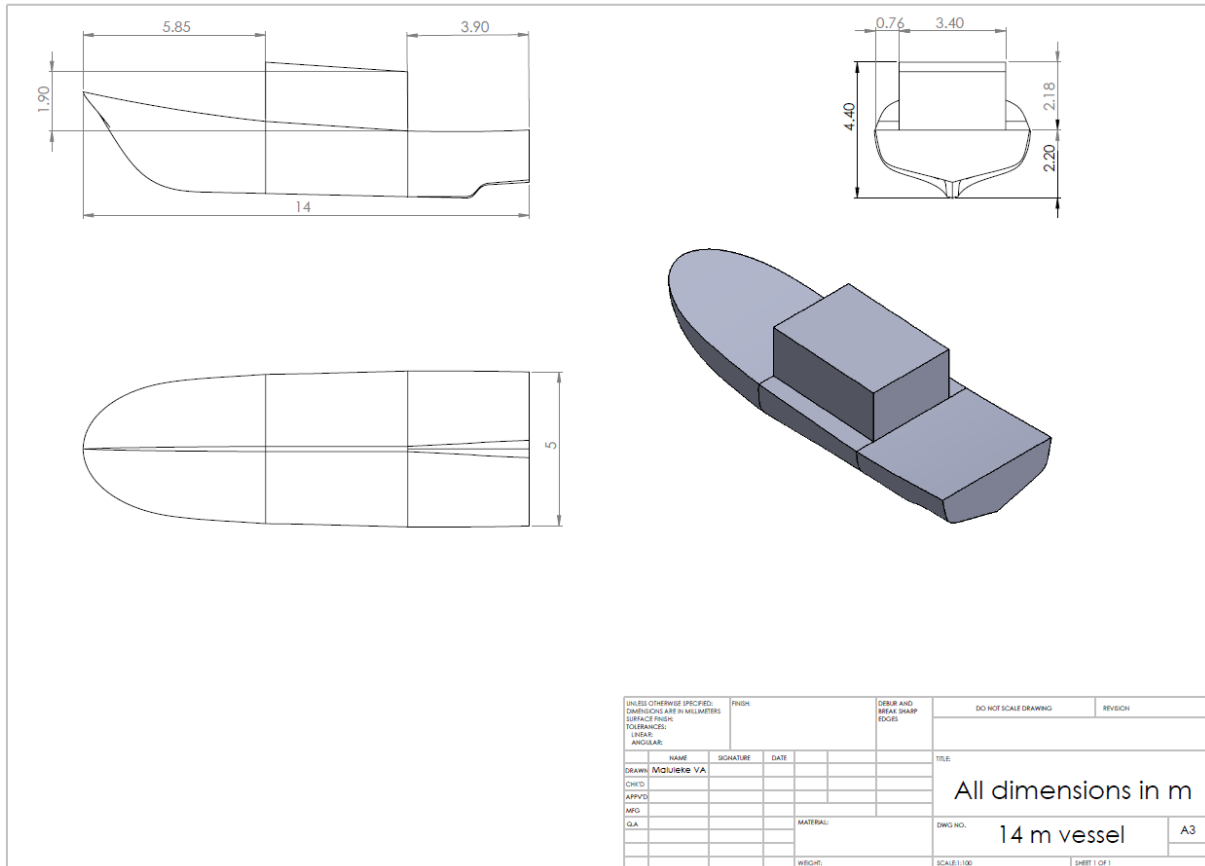
Steel properties

Material	Tensile Modulus (Young's Modulus, Modulus of Elasticity) - E -		Ultimate Tensile Strength - S _u - (10 ⁶ N/m ² , MPa)	Yield Strength - S _y - (10 ⁶ N/m ² , MPa)
	(10 ⁶ psi)	(10 ⁹ N/m ² , GPa)		
Steel, High Strength Alloy ASTM A-514			760	690
Steel, stainless AISI 302		180	860	502
Steel, Structural ASTM-A36		200	400	250
Tantalum	27			
Polytetrafluoroethylene (PTFE)		0.5		
Thorium	8.5			
Tin		47		
Titanium	16			
Titanium Alloy		105 - 120	900	730
Tooth enamel		83		
Tungsten (W)		400 - 410		
Tungsten Carbide (WC)		450 - 650		
Uranium	24	170		
Vanadium	19			
Wrought Iron		190 - 210		
Zinc	12			

(http://www.engineeringtoolbox.com/young-modulus-d_417.html)

APPENDIX C: Vessel drawings

14 m vessel drawing



22 m vessel drawing

Technical drawing of a 22 m vessel. The drawing includes three views: a side profile, a top-down view, and a 3D perspective view. Dimensions are provided in meters.

- Side Profile:** Total length 22 m. A section of length 9 m is shown with a height of 3.80 m. A section of length 6 m is shown at the rear.
- Top View:** Total width 8.70 m. A section of width 6 m is shown with a height of 1.33 m. A section of width 4.35 m is shown at the rear.
- 3D View:** Shows the vessel's hull and deck structure.

UNLESS OTHERWISE SPECIFIED, DIMENSIONS ARE IN MILLIMETERS		PRICE:	DRAW AND BREAK SHARP EDGES		DO NOT SCALE DRAWING	REVISION
DECIMALS FRACTIONS					All dimensions in m	
TOLERANCES:					TITLE	
± 0.15mm						
± 0.25mm						
± 0.50mm						
± 1.00mm						
± 1.50mm						
± 2.00mm						
± 3.00mm						
± 4.00mm						
± 5.00mm						
± 6.00mm						
± 7.00mm						
± 8.00mm						
± 9.00mm						
± 10.00mm						
± 12.00mm						
± 15.00mm						
± 20.00mm						
± 25.00mm						
± 30.00mm						
± 40.00mm						
± 50.00mm						
± 60.00mm						
± 70.00mm						
± 80.00mm						
± 90.00mm						
± 100.00mm						
± 120.00mm						
± 150.00mm						
± 200.00mm						
± 250.00mm						
± 300.00mm						
± 400.00mm						
± 500.00mm						
± 600.00mm						
± 700.00mm						
± 800.00mm						
± 900.00mm						
± 1000.00mm						
± 1200.00mm						
± 1500.00mm						
± 2000.00mm						
± 2500.00mm						
± 3000.00mm						
± 4000.00mm						
± 5000.00mm						
± 6000.00mm						
± 7000.00mm						
± 8000.00mm						
± 9000.00mm						
± 10000.00mm						
± 12000.00mm						
± 15000.00mm						
± 20000.00mm						
± 25000.00mm						
± 30000.00mm						
± 40000.00mm						
± 50000.00mm						
± 60000.00mm						
± 70000.00mm						
± 80000.00mm						
± 90000.00mm						
± 100000.00mm						
± 120000.00mm						
± 150000.00mm						
± 200000.00mm						
± 250000.00mm						
± 300000.00mm						
± 400000.00mm						
± 500000.00mm						
± 600000.00mm						
± 700000.00mm						
± 800000.00mm						
± 900000.00mm						
± 1000000.00mm						
± 1200000.00mm						
± 1500000.00mm						
± 2000000.00mm						
± 2500000.00mm						
± 3000000.00mm						
± 4000000.00mm						
± 5000000.00mm						
± 6000000.00mm						
± 7000000.00mm						
± 8000000.00mm						
± 9000000.00mm						
± 10000000.00mm						
± 12000000.00mm						
± 15000000.00mm						
± 20000000.00mm						
± 25000000.00mm						
± 30000000.00mm						
± 40000000.00mm						
± 50000000.00mm						
± 60000000.00mm						
± 70000000.00mm						
± 80000000.00mm						
± 90000000.00mm						
± 100000000.00mm						
± 120000000.00mm						
± 150000000.00mm						
± 200000000.00mm						
± 250000000.00mm						
± 300000000.00mm						
± 400000000.00mm						
± 500000000.00mm						
± 600000000.00mm						
± 700000000.00mm						
± 800000000.00mm						
± 900000000.00mm						
± 1000000000.00mm						
± 1200000000.00mm						
± 1500000000.00mm						
± 2000000000.00mm						
± 2500000000.00mm						
± 3000000000.00mm						
± 4000000000.00mm						
± 5000000000.00mm						
± 6000000000.00mm						
± 7000000000.00mm						
± 8000000000.00mm						
± 9000000000.00mm						
± 10000000000.00mm						
± 12000000000.00mm						
± 15000000000.00mm						
± 20000000000.00mm						
± 25000000000.00mm						
± 30000000000.00mm						
± 40000000000.00mm						
± 50000000000.00mm						
± 60000000000.00mm						
± 70000000000.00mm						
± 80000000000.00mm						
± 90000000000.00mm						
± 100000000000.00mm						
± 120000000000.00mm						
± 150000000000.00mm						
± 200000000000.00mm						
± 250000000000.00mm						
± 300000000000.00mm						
± 400000000000.00mm						
± 500000000000.00mm						
± 600000000000.00mm						
± 700000000000.00mm						
± 800000000000.00mm						
± 900000000000.00mm						
± 1000000000000.00mm						
± 1200000000000.00mm						
± 1500000000000.00mm						
± 2000000000000.00mm						
± 2500000000000.00mm						
± 3000000000000.00mm						
± 4000000000000.00mm						
± 5000000000000.00mm						
± 6000000000000.00mm						
± 7000000000000.00mm						
± 8000000000000.00mm						
± 9000000000000.00mm						
± 10000000000000.00mm						
± 12000000000000.00mm						
± 15000000000000.00mm						
± 20000000000000.00mm						
± 25000000000000.00mm						
± 30000000000000.00mm						
± 40000000000000.00mm						
± 50000000000000.00mm						
± 60000000000000.00mm						
± 70000000000000.00mm						
± 80000000000000.00mm						
± 90000000000000.00mm						
± 100000000000000.00mm						
± 120000000000000.00mm						
± 150000000000000.00mm						
± 200000000000000.00mm						
± 250000000000000.00mm						
± 300000000000000.00mm						
± 400000000000000.00mm						
± 500000000000000.00mm						
± 600000000000000.00mm						
± 700000000000000.00mm						
± 800000000000000.00mm						
± 900000000000000.00mm						
± 1000000000000000.00mm						
± 1200000000000000.00mm						
± 1500000000000000.00mm						
± 2000000000000000.00mm						
± 2500000000000000.00mm						
± 3000000000000000.00mm						
± 4000000000000000.00mm						
± 5000000000000000.00mm						
± 6000000000000000.00mm						
± 7000000000000000.00mm						
± 8000000000000000.00mm						
± 9000000000000000.00mm						
± 10000000000000000.00mm						
± 12000000000000000.00mm						
± 15000000000000000.00mm						
± 20000000000000000.00mm						
± 25000000000000000.00mm						
± 30000000000000000.00mm						
± 40000000000000000.00mm						
± 50000000000000000.00mm						
± 60000000000000000.00mm						
± 70000000000000000.00mm						
± 80000000000000000.00mm						
± 90000000000000000.00mm						
± 100000000000000000.00mm						
± 120000000000000000.00mm						
± 150000000000000000.00mm						
± 200000000000000000.00mm						
± 250000000000000000.00mm						
± 300000000000000000.00mm						
± 400000000000000000.00mm						
± 500000000000000000.00mm						
± 600000000000000000.00mm						
± 700000000000000000.00mm						
± 800000000000000000.00mm						
± 900000000000000000.00mm						
± 1000000000000000000.00mm						
± 1200000000000000000.00mm						
± 1500000000000000000.00mm						
± 2000000000000000000.00mm						
± 2500000000000000000.00mm						
± 3000000000000000000.00mm						
± 4000000000000000000.00mm						
± 5000000000000000000.00mm						
± 6000000000000000000.00mm						

14 m vessel hydrostatic results

Hydrostatic Results

Structure 14 m vessel

Hydrostatic Stiffness

Centre of Gravity (CoG) Position:	X: -8.6118422 m	Y: -1.4372e-5 m	Z: 0. m
	Z	RX	RY
Heave (Z):	545283.25 N/m	9.4518e-2 N/°	-2245.3723 N/°
Roll (RX):	5.4154811 N.m/m	13172.207 N.m/°	0.1523896 N.m/°
Pitch (RY):	-128650.36 N.m/m	0.1523895 N.m/°	114659.2 N.m/°

Hydrostatic Displacement Properties

Actual Volumetric Displacement:	66.770294 m³		
Equivalent Volumetric Displacement:	33.430294 m³		
Centre of Buoyancy (CoB) Position:	X: -8.1765099 m	Y: -6.9849e-6 m	Z: -0.1883904 m
Out of Balance Forces/Weight:	FX: -1.0395e-8	FY: -1.2263e-7	FZ: 0.9973009
Out of Balance Moments/Weight:	MX: 1.4494e-5 m	MY: -0.8694879 m	MZ: 1.7081e-7 m

Cut Water Plane Properties

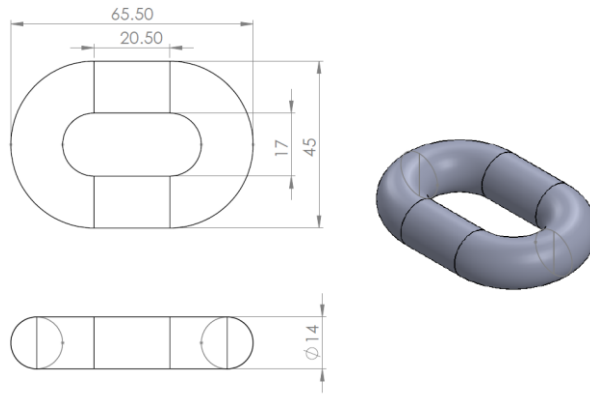
Cut Water Plane Area:	54.247238 m²		
Centre of Floatation:	X: -8.3759089 m	Y: -4.4405e-6 m	
Principal 2nd Moment of Area:	X: 87.661018 m⁴	Y: 663.12146 m⁴	
Angle Principal Axis makes with X(FRA):	9.9141e-5°		

Small Angle Stability Parameters

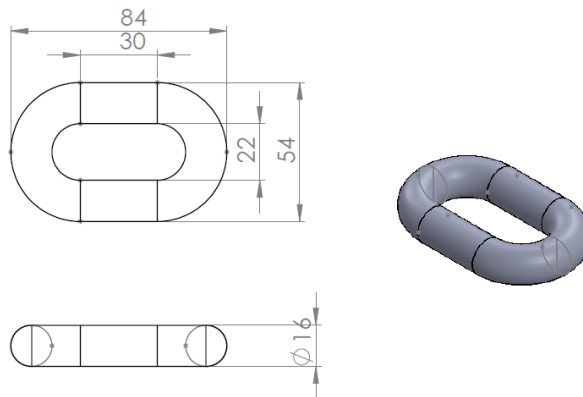
CoG to CoB (BG):	0.1883904 m		
Metacentric Heights (GMX/GMY):	1.1244842 m	9.7429934 m	
CoB to Metacentre (BMX/BMY):	1.3128746 m	9.9313841 m	
Restoring Moments about Principal Axes (MX/MY):	13172.207 N.m/°	114129.41 N.m/°	

APPENDIX E: Studless chain drawings

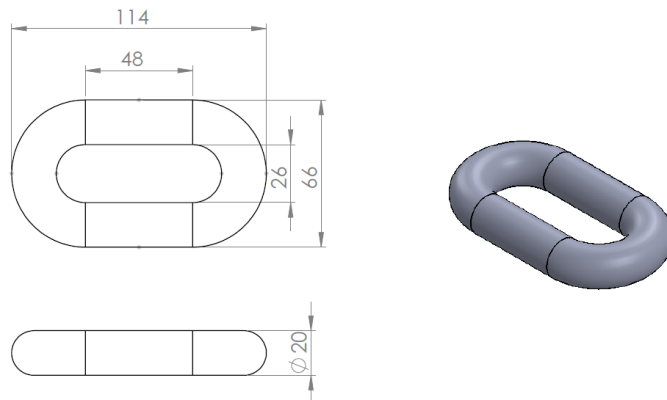
Dimensions in mm



E1: 14 mm studless chain link drawing



E2: 16 mm studless chain link drawing



E3: 20 mm studless chain link drawing

APPENDIX F: Calculations

22 m vessel calculations

Mass inertia calculations of the 22 m vessel, (see Appendix C for the vessel dimensions). The inertia values were defined via the Radius of Gyration.

$$K_{xx} = 0.34 * \text{width of the vessel}$$

$$K_{xx} = 0.34 * 8 = 2.72 \text{ m}$$

$$K_{yy} = 0.25 * \text{length of the vessel}$$

$$K_{yy} = 0.25 * 22 = 5.5 \text{ m}$$

$$K_{zz} = 2.6 * \text{length of the vessel}$$

$$K_{zz} = 2.6 * 22 = 5.72 \text{ m}$$

14 m vessel calculations

Mass inertia calculations of the 14 m vessel. The inertia values were defined via the Radius of Gyration.

$$K_{xx} = 0.34 * \text{width of the vessel}$$

$$K_{xx} = 0.34 * 5 = 1.7 \text{ m}$$

$$K_{yy} = 0.25 * \text{length of the vessel}$$

$$K_{yy} = 0.25 * 14 = 3.5 \text{ m}$$

$$K_{zz} = 2.6 * \text{length of the vessel}$$

$$K_{zz} = 2.6 * 14 = 3.64 \text{ m}$$

Chain properties calculation

Equivalent Area, axial stiffness, mass/unit length and equivalent diameter

The 20 mm steel chain

Equivalent cross-sectional area

The equivalent cross-sectional area of a chain link is obtained by combining the cross-sectional area of two chain link as:

$$A = 2 \times \frac{\pi}{4} D^2$$

$$\text{Area, } A = 2 \times \frac{\pi}{4} D^2 = \frac{\pi}{4} \times 0.02^2 = 6.28E - 04 \text{ m}^2$$

This leads to: $EA = 0.854 \times 10^8 D^2 \text{ kN}$ (for studless chain)

$$= 0.854 \times 10^8 0.02^2 \times 1000$$

$$= 3.42E + 07 \text{ N}$$

Mass/unit length is given by:

$$19.9D^2 = 19.9 \times 0.02^2 = 7.96 \text{ kg/m}$$

Equivalent Diameter for the studless chain is given by:

$$D_{\text{Equivalent}} = 1.8D = 1.8 \times 0.02 = 0.036 \text{ m}$$

The 16 mm steel chain

Equivalent cross-sectional area

$$\text{Area, } A = 2 \times \frac{\pi}{4} D^2 = \frac{\pi}{4} \times 0.016^2 = 4.02E - 04 \text{ m}^2$$

$EA = 0.854 \times 10^8 D^2 \text{ kN}$ (for studless chain)

$$= 0.854 \times 10^8 0.016^2 \times 1000$$

$$= 2.19E + 07 \text{ N}$$

Mass/unit length is given by:

$$19.9D^2 = 19.9 \times 0.016^2 = 5.09 \text{ kg/m}$$

Equivalent Diameter for the studless chain is given by:

$$D_{\text{Equivalent}} = 1.8D = 1.8 \times 0.016 = 0.029 \text{ m}$$

The 14 mm steel chain

Equivalent cross-sectional area

$$\text{Area, } A = \frac{\pi}{4} D^2 = 2 \times \frac{\pi}{4} \times 0.014^2 = 3.08E - 04 \text{ m}^2$$

$EA = 0.854 \times 10^8 D^2 \text{ kN}$ (For studless chain)

$$= 0.854 \times 10^8 0.02^2 \times 1000$$

$$= 1.67E + 07 \text{ N}$$

Mass/unit length is given by:

$$19.9D^2 = 19.9 \times 0.014^2 = 3.9 \text{ kg/m}$$

Equivalent Diameter for the studless chain is given by:

$$D_{\text{Equivalent}} = 1.8D = 1.8 \times 0.014 = 0.025 \text{ m}$$